

Part III

Magnetic fields in planetary nebulae

9

Magnetic field detection via dust polarisation

I present in this chapter a published article (Sabin et al. 2007) on the detection and role of magnetic fields in the shaping process of PNe.

9.1 Abstract

Magnetic fields are an important but largely unknown ingredient of planetary nebulae. They have been detected in oxygen-rich AGB and post-AGB stars, and may play a role in the shaping of their nebulae. Here we present SCUBA sub-millimeter polarimetric observations of four bipolar planetary nebulae and post-AGB stars, including two oxygen-rich and two carbon-rich nebulae, to determine the geometry of the magnetic field by dust alignment. Three of the four sources (NGC 7027, NGC 6537 and NGC 6302) present a well-defined toroidal magnetic field oriented along their equatorial torus or disk. NGC 6302 may also show field lines along the bipolar outflow. CRL 2688 shows a complex field structure, where part of the field aligns with the torus, whilst an other part approximately aligns with the polar outflow. It also presents marked asymmetries in its magnetic structure. NGC 7027 shows evidence for a disorganised field in the south-west corner, where the SCUBA data show an indication of

an outflow. The findings show a clear correlation between field orientation and nebular structure.

9.2 Introduction

Whether magnetic fields play a role in the shaping of planetary nebulae (PNe) is an open question. Most of the post-AGB nebulae appear elliptical, bipolar or even multipolar (Balick and Frank 2002). These morphologies are amplified by the interaction between a slow AGB wind with a faster post-AGB wind. However, this amplification still requires an initial asymmetry in the slow wind. This initial shaping has been mainly attributed to two possible phenomena: binarity and magnetic fields.

In the binary model, a close companion affects the mass-losing AGB star via common envelope evolution (De Marco and Moe 2006), mass transfer and/or tidal forces, and may lead to the formation of an accretion disk around the companion star. The binary orbit provides a source of angular momentum which get carried by the wind, and leads to an equatorial disk. The angular momentum loss by the stars may lead to a merger. The model of shaping due to this binary interaction is quite popular (Bond and Murdin 2000), (Ciardullo et al. 2005), partly because of the presumed impossibility of a single star to supply the energy necessary to create a magnetic field strong enough for its shaping (Soker 2005). Nevertheless, there is still a lack of observational evidence for the occurrence of close binary systems during the AGB phase. Neither companions (Riera et al. 2003) nor high orbital velocities of the AGB stars (Barnbaum et al. 1995) are detected in a sufficient amount to establish the role of the binarity as predominant (Matt et al. 2000). Evidence for binary interactions may be found in 25–50 per cent of planetary nebulae (Zijlstra 2006), although values of 50–100 per cent have also been suggested (De Marco et al. 2004; De Marco and Moe 2006).

On the other hand, the magnetic field may act as a “squeezer” around the central

star of the PN and thereby give the dust its direction (in the sense of the outflow). Magnetic fields have been detected around AGB stars (Vlemmings et al. 2006) and a few post-AGB stars (Bains et al. 2004) using radio observations of masers (H_2O , SiO , OH). Such observations measure a local value of the strength of field, within masing high-density clumps, which may differ from the global field. The origin of the magnetic field is unknown: a dynamo effect resulting from an interaction between a slow rotating envelope and a fast rotating core has been proposed (Blackman et al. 2001). As magnetic fields are now known to be present in the AGB and the post-AGB phase, their importance should not be ruled out prematurely.

Greaves (2002) found evidence for dust alignment in two carbon-rich objects, NGC 7027 and CRL2688 which are respectively a young and compact bipolar PN and a strongly bipolar proto-planetary nebula (PPN). This was based on polarimetric Scuba 850-micron observations. The data suggests the presence of toroidal collimated magnetic fields, as would be required for the shaping. But the presence of such a field was not conclusively proved, because of the very few detected vectors and limited spatial resolution. We present here new 850-micron and the first 450-micron polarimetry of post-AGB stars, which allows for better resolution and reduces angular smearing. In addition to the objects observed by Greaves (2002), we also observed NGC 6537 and NGC 6302. The sample contains two carbon-rich and two oxygen-rich nebulae. We show the presence of well-aligned toroidal fields in three of the nebulae. The fourth object shows indications for both a toroidal field and one aligned with the polar outflow. We conclude that toroidal fields may be common in bipolar PNe, and could play a role in the shaping of the nebulae.

9.3 Observations

The polarimetric data were obtained on May 10th 2005, with the polarimeter on the Sub-millimeter Common-User Bolometer Array (SCUBA), at the JCMT. The instrument (now decommissioned) is described in Holland et al. (1999). The JCMT beam

size is 15 arcsec at 850 μm and 8 arcsec at 450 μm .

SCUBA contains two arrays of bolometric detectors, covering a field of view of 2.3' in diameter. The 850- μm array has 37 individual detectors, and the 450- μm array has 91 detectors. The two arrays are used simultaneously. The spatial resolution of the detector is 7.5" at 450 μm , and 14" at 850 μm . The gaps between the detectors are covered by moving the telescope in sub-pixel steps, in the so-called jiggle-map mode. The step size needs to be optimised for the wavelength used. The polarimeter (Greaves et al. 2003) measures the linear polarisation by rotating the half-waveplate in 16 steps. We used this in combination with jiggle map mode. A chop-throw of 45 arcsec was used.

Good photometric images cannot be obtained at both wavelengths simultaneously. When the jiggle pattern is optimised in one wave-band, the simultaneous image obtained in the other band is under-sampled. The size of the pixels in the final image is set during the data reduction with the polarimetric package of Starlink. For a jiggle pattern corresponding to a 450 μm measurement, the pixel spacing becomes 3 arcsec and for 850 μm it is 6 arcsec. The reduction of infrared polarimetry is discussed in detail by Hildebrand et al. (2000).

The instrumental polarisation (IP) of each detector has to be removed in order to have a correct polarisation calibration. A new IP calibration, provided on site, was used: this contains a re-measurement of the central detector. For the other detectors, an older IP calibration was used. The IP should not vary too much for detectors close to the center of the array. Tests to see the importance of the instrumental polarisation (by changing its value by the size of the error for example) and if it could affect the polarisation vectors length, showed that in our case, the IP was small (at 850 μm : $\sim 1.20\% \pm 0.25\%$ and at 450 μm : $\sim 3.25\% \pm 0.25\%$) and didn't play any role in modifying the vectors. The resulting polarimetric images were checked for different pixel binning, from 1 \times 1 to 10 \times 10, and we didn't find any significant changes.

The linear polarisation is measured as a percentage polarisation, and a direction. The polarisation is typically caused by the alignment of spinning dust grains, with

their long axis perpendicular to the local magnetic field (Greaves et al. 1999). Thus, the measured angle of polarisation is 90 degrees rotated with respect to the magnetic field. The degree of polarisation does not give direct information on the strength of the magnetic field.

We observed four targets: NGC 6537, CRL 2688, NGC 6302 and NGC 7027. They were observed in jiggle map observing mode at both wave-bands, $450\mu\text{m}$ and $850\mu\text{m}$. For each object, the mean direction and angle of polarisation are listed in Table 1.

The figures below show the direction of the magnetic field, i.e. the vectors are perpendicular to the direction of the grain alignment.

9.4 The results

9.4.1 NGC 6537

NGC 6537 is also known as the Red Spider nebula. It is a bipolar planetary nebula with a very hot central star ($1.5\text{--}2.5\times 10^5\text{K}$). The nebula suffers extinction by circumstellar dust. This extinction is localised mainly in a compact circumstellar shell. An extinction map (Matsuura et al. 2005a) reveals a compact dust shell with a roughly spherical inner radius of about 3 arcsec, with a minimum towards the central star (Matsuura et al. 2005a; Cuesta et al. 1995). The polar outflows (traced by high velocity winds of about 300km/s: Corradi and Schwarz 1993) extend 2 arcminutes along the NE-SW direction. The Scuba $850\text{-}\mu\text{m}$ continuum map (Fig. 9.1) shows elongation perpendicular to the outflow direction, with a major-axis diameter of approximately 20 arcsec. The extinction map is now seen to represent the inner edge of a more extended, and possibly toroidal, structure. The equatorial plane may be oriented a little closer to the EW direction, based on the Scuba map.

The best polarimetric results obtained with SCUBA are obtained at $850\mu\text{m}$. The consistent orientation of the polarisation vectors shows that the magnetic field (here-

after \vec{B}) has a dominant direction along the equatorial plane, approximately perpendicular to the outflow direction. The dust alignment is therefore directed in the same sense as the outflow. The lengths of the 18 different vectors do not show large variations, with a degree of polarisation varying from 8 to 14%, suggesting a consistent magnetic field. Moreover the absence of smaller polarisation vectors toward the center of the nebula indicates that there is no change in geometry of \vec{B} towards the core (Greaves 2002). This supports a location some distance from the star (i.e. in a detached shell), since otherwise averaging of vectors in different directions within the JCMT beam would reduce the detected net polarisation at the central position (beam depolarisation).

These observations indicate the presence of a consistent toroidal magnetic field, located along the equatorial plane of NGC 6537, in a circumstellar torus. Compared to the size of the outflow lobes, the field is located relatively close to the star. The presence of a \vec{B} -field had already been suspected, based on the occurrence of filaments near the central star (Huggins and Manley 2005).

The extinction map obtained by Matsuura et al. (2005a) (Fig. 1-Bottom panel) shows an asymmetry, in that the extinction is higher on the western side (≥ 2 mag versus ≤ 1.6 mag towards the east). This asymmetry is also seen in the Scuba data, with a larger extension and more polarisation vectors on this side. This is a further indication that the magnetic field is located within the detached dust shell.

There is no strong indication for magnetic fields along the spider lobes. There is a slight trend for the vectors to curve, but this is caused by only a few of the vectors and would need confirmation. We cannot state with confidence whether the lobes also carry a magnetic field.

9.4.2 NGC 7027

The $450\mu\text{m}$ jiggle map of the young planetary nebula NGC 7027 (Fig. 9.2) and its near environment covers a field of about 40×36 arcsec². The central star is surrounded by an ionised area of ~ 283 arcsec², which is in turn enclosed by a thin atomic and molecular

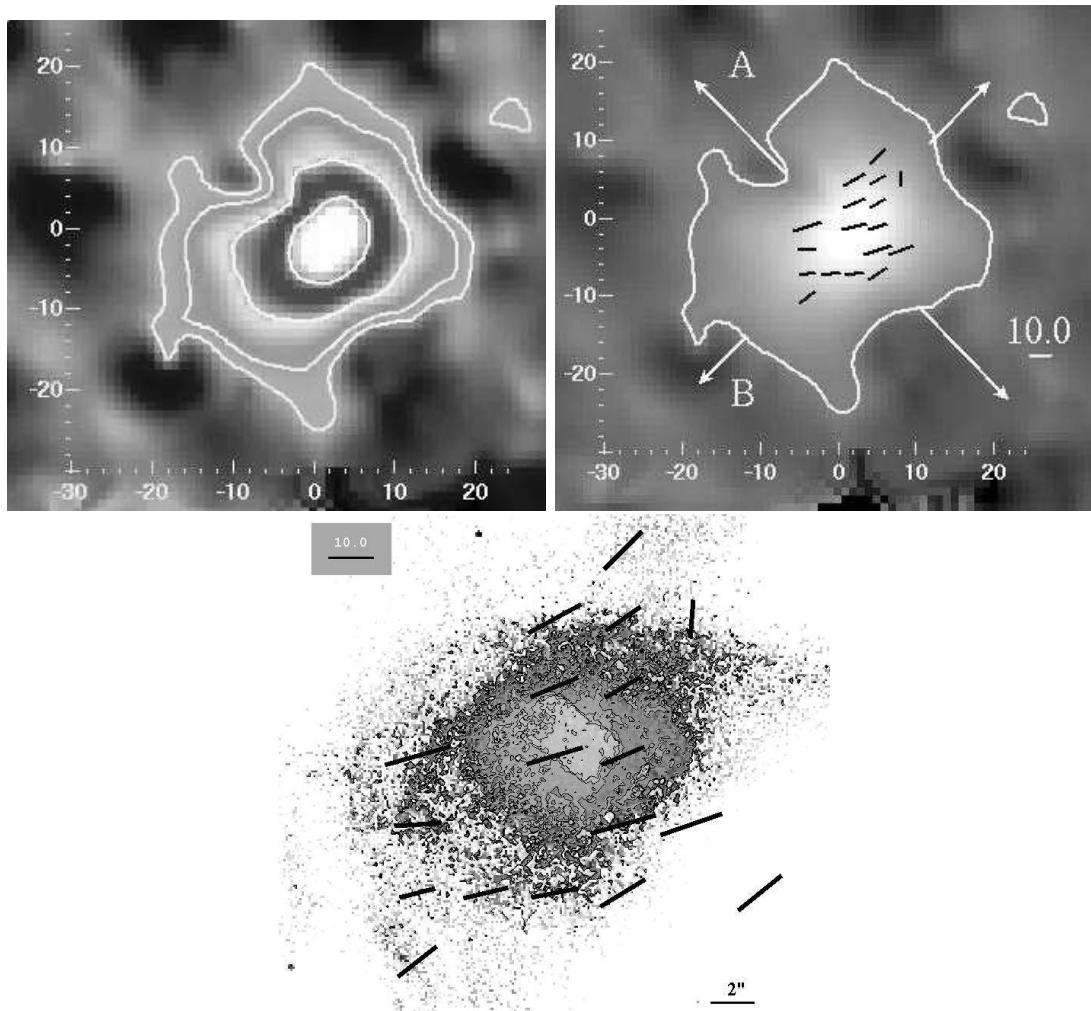


Figure 9.1: Scuba 850 μ m results on NGC 6537. North on the top and East on the left. The axes give the image scale in arcseconds. *Top Left panel:* the 850 μ m continuum map of NGC 6537, with contours at 1%, 2% ,5% and 10% of the peak. *Top Right panel:* Magnetic field orientation. The general outflow direction of the nebula is indicated by A and the equatorial plane by B. The polarisation vector scale indicated on the left (showing the degree of polarisation) is set at 10%. *Bottom panel:* Extinction map presented by Matsuura et al. (2005) obtained with the HST H α (F656N) and H β (F487N) filters. The highest levels of extinction occurs at ~ 4 arcsec from the central star with $E(H\beta - H\alpha) > 2$ mag, coincident with the dust emission in the 850 μ m map. The polarisation vector scale (top left) is set at 10%. The magnetic field which coincides with the area of internal extinction, is mostly aligned along the equatorial plane, indicating a toroidal field. The dust alignment is perpendicular to the vectors displayed here.

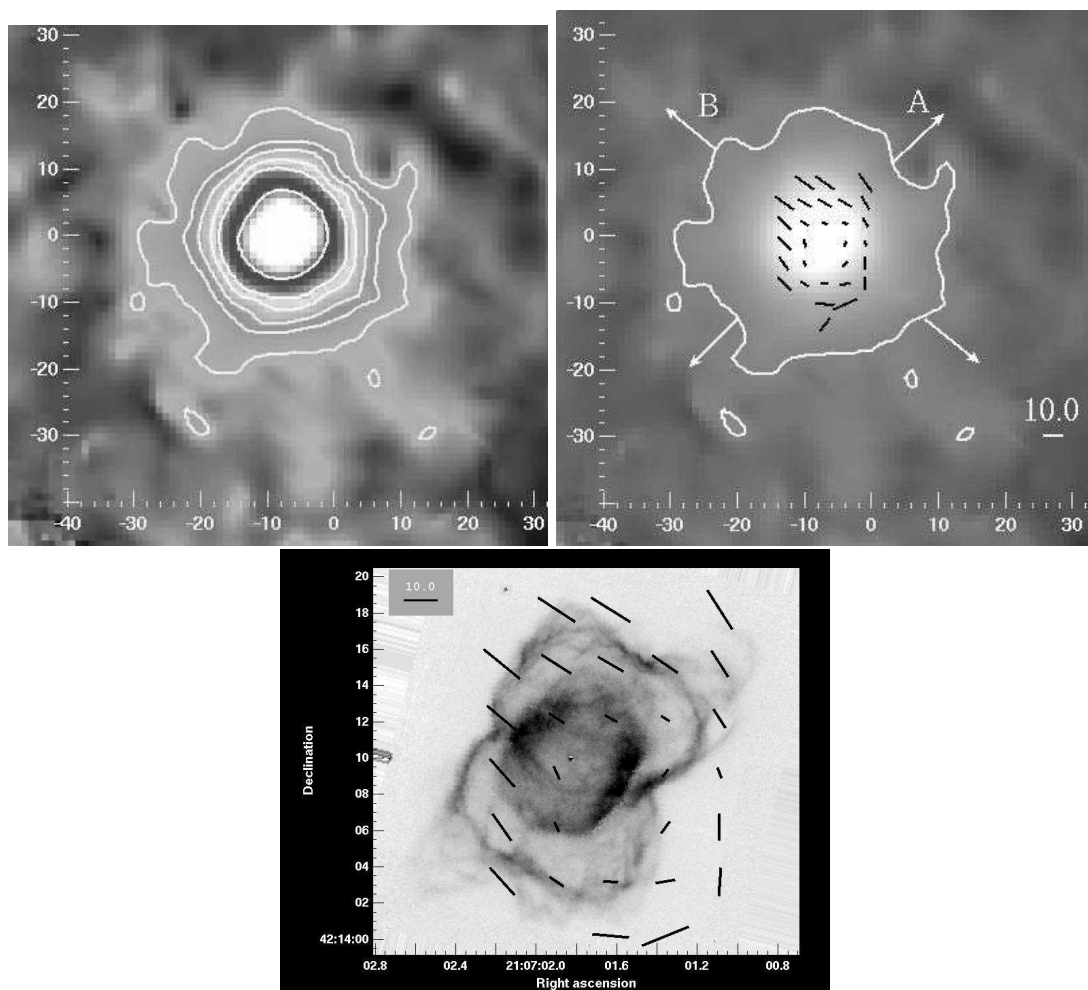


Figure 9.2: Scuba $450\mu\text{m}$ results on NGC 7027. North on the top and East on the left. The axes give the image scale in arcseconds. *Top Left panel:* The $450\mu\text{m}$ continuum map of NGC 7027. Contours are set from 1 to 5% and 10% of the peak. *Top Right panel:* Magnetic field distribution. The general outflow direction is indicated by A and the equatorial plane by B. The polarisation vector scale (showing the degree of polarisation) is set at 10%. *Bottom panel:* The Scuba polarization vectors are shown on an continuum subtracted H_2 (colour-inverted) map of NGC 7027 (North on the top and East on the left). The field is mostly directed along the equatorial plane. The central region shows much reduced polarisation and the field orientation differs on the extreme western side.

layer that is seen for instance in the H_2 emission observed by Cox et al. (2002). A thin dark ring delineates the equatorial plane in optical images. The structure is better seen in the HST image (Fig. 9.2-bottom), which shows both the surrounding molecular layer (in H_2) and the inner ionised region. Latter et al. (2000) shows that the NW lobe is blue-shifted (closer) and the SW lobe is red-shifted.

The dominant direction of the magnetic field coincides with the equatorial plane. But this behaviour is mainly seen on the North-East side while the south-west part seems to be disturbed: the magnetic field may be “broken”. The degree of polarisation is $8.9\% \pm 0.9\%$ towards the NE direction (or lobe) and $7.6\% \pm 1.3\%$ towards the SW. The degree of polarisation is much reduced in the center of the nebula and lacks a coherent direction here. This effect was also noted by Greaves (2002) and may indicate that coherence is lost in the ionised region.

9.4.3 CRL 2688

The proto-planetary nebula CRL 2688 (or Egg Nebula) is a bright carbon-rich bipolar object characterised by two pairs of searchlight beams superposed on a reflection nebula. The origin of the light beams has been suggested to be a very close stellar companion (Sahai et al. 1998; Kastner and Soker 2004), or the presence of dust layers reflecting the light of the central star (Goto et al. 2002). The bipolar reflection nebula shows a dark equatorial lane where a large amount of dust may be present.

The $850\text{-}\mu\text{m}$ image is presented in Fig. 9.3-Top panels. It shows elongation in the direction of the polar outflows. The equatorial extent is less but at the lowest contour the torus is more extended on the eastern side. The extent is $\sim 60'' \times 40''$ although it is not clear precisely where the emission ends. The bright core at $850\mu\text{m}$ shows a FWHM of $16 \times 14 \text{ arcsec}^2$, at a position angle of 25 degrees which is in the same direction as the outflow. We could not measure the core elongation at $450\mu\text{m}$ due to the under-sampling. The spatial resolution is insufficient to separate the two light beams, but the width of the emission suggests that the dust traces the larger lobes which the light

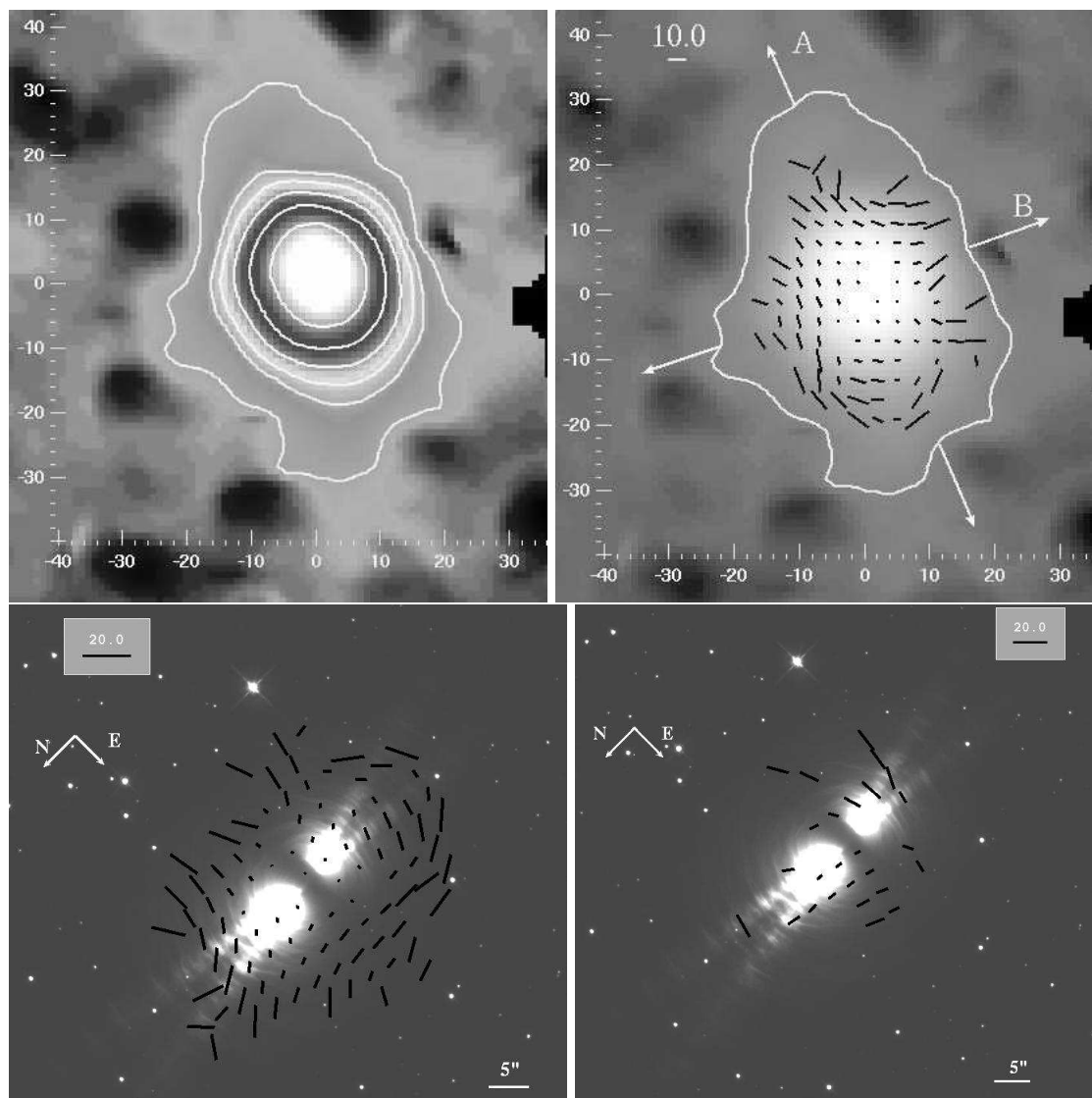


Figure 9.3: Scuba 850 and $450\mu\text{m}$ results on CRL2688. North on the top and East on the left. The axes give the image scale in arcseconds. *Top left panel:* The $850\mu\text{m}$ map of CRL 2688, with contours from 1 to 5% and 10% of the peak. *Top right panel:* The $850\mu\text{m}$ vector polarisation showing the magnetic field orientation. The general outflow direction is indicated by A and the equatorial plane by B. The polarisation vector scale (showing the degree of polarisation) is set at 10%. *Bottom panels:* HST images (WFPC2, filter F606W) with the overlaid magnetic field corresponding to the $850\mu\text{m}$ map (left) and $450\mu\text{m}$ map (right). The dust continuum is elongated along the outflows. The field shows a complicated structure with components along the outflow and along the equatorial plane. The polarisation vector scale (showing the degree of polarisation) is set at 20% for both maps.

beams illuminate, and that these beams themselves are not present in the far-infrared data. (The elongation of the core is in fact along the line of one of the two beams only.)

CRL 2688 presents the highest number of polarisation vectors in our sample. For this nebula, the under-sampled $450\mu\text{m}$ map gives some additional and useful indications (even if we observe a lack of vectors due to this under-sampling). The polarisation vectors cover the full nebular extent (seen at both wavelengths), as they do in NGC 7027. The degree of polarisation is not uniform and strongly decreases near the center. This phenomenon is more visible in the $850\mu\text{m}$ map, which suggests that beam depolarisation may play a role. At $850\mu\text{m}$, the mean value of polarisation of the region containing the bipolar lobes is about 3.2%, the outer region has a mean value of 8.8%, and the region of the dark lane shows a mean degree of polarisation of 1.4%.

If we draw a line passing through the nebula in a longitudinal direction (NNE-SSW Fig. 9.3-Bottom-left panel), we can see distinct behaviours of the magnetic field on either side of this line: on the eastern side, the orientation of \vec{B} is mainly in the direction of this line, while on the western side, the magnetic field appears perpendicular to it.

The $450\text{-}\mu\text{m}$ map (Fig. 9.3-Bottom-right panel) shows the magnetic field at higher resolution, confirming the bimodal distribution. This map is under-sampled and only some positions in the nebula are covered. The map gives a suggestion of a superposition of a toroidal field and one aligned with the polar outflows. The field becomes less ordered towards the tip of the outflow direction, but the emission here is faint and the uncertainties on the polarisation vectors are larger.

The complicated magnetic morphology makes it likely that the dynamics have shaped significant parts of the field, rather than the magnetic field shaping the nebula. The structure may show the superposition of two components over most of the area of the source. The lack of polarisation in the centre suggests that the bright core is not polarised, or its polarisation is averaged out over the JCMT resolution. The outermost field vectors in the longitudinal direction are along the outflow, and this may indicate a field carried along by the outflow. This is most apparent in the north when looking at the outer vectors direction in the figure 3-bottom-left, in the south the outer

vectors point towards the corresponding outflow so we assume that the magnetic field may be carried by this outflow.

The grain alignment, which is perpendicular to the direction of the magnetic field, is in the direction of the outflows on the western side. On the eastern side, the grain alignment is toroidal.

High resolution molecular images in the literature include IRAM CO J=2-1 data (Cox et al. 2000) and HST infrared H₂ images (Sahai et al. 1998). The continuum-subtracted H₂ image in Fig. 4, shows multiple jets, located both in the equatorial plane and towards the polar directions. The CO data show these jets to be the tip of flows originating much closer to the star. These jets all fall within the Scuba 850- μ m core, indicating that indeed structure is present on scales much smaller than the JCMT beam size. Thus, beam dilution and beam-depolarisation of the magnetic field is likely.

We note that the elongation visible in the Scuba image, on the eastern side, is in the same direction as the largest molecular sub-jet E2 in Fig. 9.4, or A1 in Cox et al. (2000) (but the Scuba structure is much larger). The polarisation vectors seem unaffected. On the western side, both the molecular and the Scuba images indicate a smaller extent of the envelope. The polar outflows as seen in the molecular lines do not show the light beams, but instead show relatively well-collimated lobes. The lobes are brighter in the north. The polar lobes in the Scuba image are consistent with this, both in direction and in brightness, but again are much larger than seen in the molecules. The molecular emission shows the wind-blown cavities, while the Scuba emission arises in the surrounding shells.

9.4.4 NGC 6302

This oxygen-rich planetary nebula (Pottasch and Beintema 1999) is a proto-typical butterfly-type nebula. It shows two extended lobes that result from a bipolar outflow, with a dark lane in the center. It has been studied by Meaburn and Walsh (1980), Meaburn et al. (2005), Matsuura et al. (2005b) and Casassus et al. (2000).

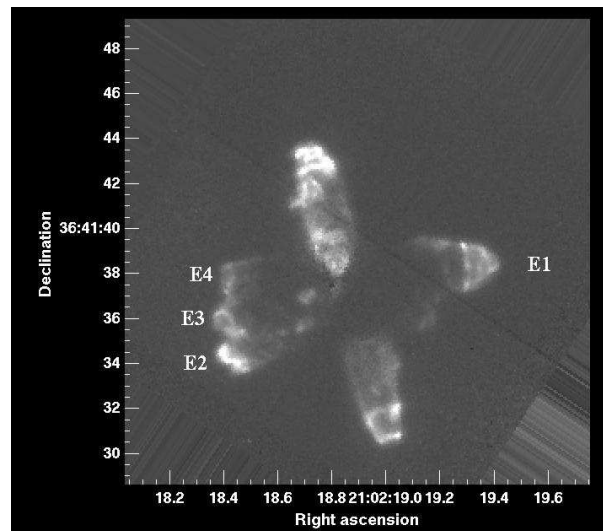


Figure 9.4: Continuum-subtracted H₂ (HST) image showing the jets in CRL 2688. [North at the top and East at the left]. They are named as in Sahai et al (1998). The jets are all located within the compact 850- μ m source, and the some perturbations seen in the Scuba data can be related to the “sub-jets” E2 or A1.

The Scuba observations were optimised for 450- μ m. They show a bright core, of FWHM 14×12 arcsec² (larger than the beam), with the long axis in the north-south direction, with an extension towards the south-southeast (Fig. 9.5). The arcs seen at 25 arcsec are likely part of the diffraction pattern from the very bright core. The polarimetric data obtained at 450 μ m shows only five polarisation vectors. They do not line up with either the dark lane or the outflow. However, they are fairly well aligned with the ellipsoidal radio source in the center of the nebula. The radio nebula shows the inner ionised region, confined by the dense torus: the elongation is perpendicular to the torus.

The difference in position angle of the inner torus with the dark lane is interpreted as a warped disk (Matsuura et al. 2005b). Further from the center the outflows have different position angles, and eventually become east-west in the outer bipolar lobes. The 450- μ m polarisation indicates that the magnetic field may be oriented in the direction

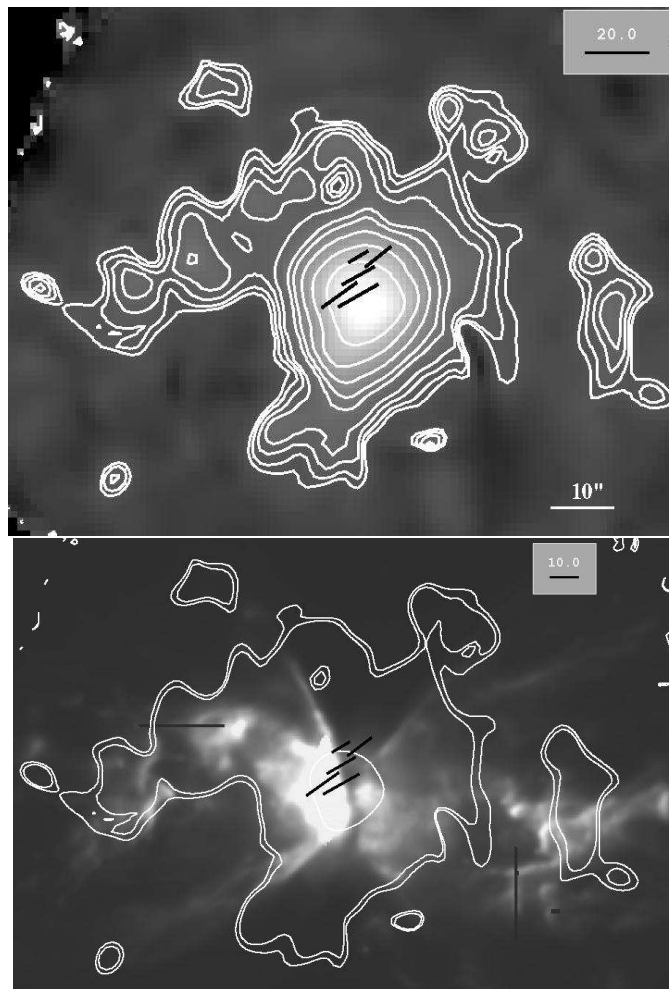


Figure 9.5: Scuba $450\mu\text{m}$ results on NGC 6302. North on the top and East on the left. *Top panel:* The map shows the magnetic field orientation on the planetary nebula with contours from 1 to 5%, 10%, 20% and 25% of the peak. The polarization vector scale (showing the degree of polarisation) is set at 20%. Note that the arcs seen 20 arcsec out are part of the beam side lobes of the very bright core. *Bottom panel:* $450\mu\text{m}$ Scuba map of NGC 6302 overlaid on the F656N band HST image (WFPC2). North on the top and East on the left. The external hexagonal contours do not belong to the star but are representative of the bolometers. The main Eastern outflow seen on the submillimeter image coincides with the one observed with the HST. Note that the arcs seen 25 arcsec out are part of the beam side lobes and the two outer horizontal and vertical features are artefacts from the HST image and not vectors.

Name	Band (μm)	Deg (%)	Angle (deg)
NGC 6537	850	11.2 \pm 2.2	26.5 \pm 5.7
NGC 6302	450	11.4 \pm 1.6	32.7 \pm 4.6
NGC 7027	450	8.2 \pm 0.9	-18.5 \pm 3.7
CRL2688	850	6.8 \pm 1.0	-22.6 \pm 4.5

Table 9.1: Mean values of the polarimetric parameters for the Post-AGB objects, Deg: degree of polarisation, Angle: position angle of the polarisation. These values concern the main band studied for each nebula.

of the inner outflow.

We have no data for magnetic fields elsewhere in the outflows even at 850 μm .

9.5 Discussion and Conclusion

The sub-millimeter observations of the four post-AGB objects reveal new information regarding the distribution of the magnetic fields, the dust emission and the link between the two components.

Extended dust emission was seen for all four nebulae. For CRL 2688, the large polar lobes have been detected. The orientation of its polar lobes is along only one of the two light beams. The equatorial emission is also extended, and shows an asymmetry which is correlated with the appearance of the (much more compact) equatorial jets. These jets originate close to the star and it is unlikely that they are affected by structures at much larger scales. Instead, the jets may affect the dust emission through heating. In NGC 6537, an asymmetry in the dust correlates with differences in the extinction map, suggesting that here the Scuba map shows a true asymmetry in the dust distribution.

The presence of detectable polarisation shows that at least some of the dust grains are not spherical.

9.5.1 Targets

Polarisation is detected for all four nebulae. This in itself suggests that magnetic fields are common for these types of objects. It is thus important to discuss what types of objects were selected.

Firstly, the four targets are all bipolar nebulae. The least pronounced morphology is shown by NGC 7027, but even here the molecular maps clearly show the underlying bipolar structure. We do not have information on the existence of magnetic fields in less bipolar (e.g. elliptical or spherical) nebulae.

Secondly, although three of the nebulae have very hot central stars and ionised cores, all have extended molecular envelopes. It is argued above that the detected fields are located in the molecular or atomic regions. The presence of molecular envelopes around ionising stars indicates very dense nebulae, and therefore very high mass loss rates on the AGB.

Thirdly, the dense nebulae with relatively small ionised regions imply that their stars have evolved to high temperatures before the nebulae have had time to expand significantly. Such fast evolution is characteristic for high-mass central stars. The cooler object (CRL 2688) may have a lower mass, but the fact that it has become a carbon star suggests it still has a relatively higher initial mass ($M_i \geq 3M_\odot$), as lower-mass stars experience insufficient dredge-up to become carbon rich. For NGC 6302, a progenitor mass of 4–5 M_\odot has been suggested, based on the mass of the circumstellar envelope (Matsuura et al. 2005b). The precise initial masses are not well determined, but high mass progenitors appear likely for all four objects.

Thus, the result of the survey can be interpreted that magnetic fields tend to be present for high mass progenitors evolving into bipolar nebulae, and that the fields are detectable while the nebulae still have molecular envelopes.

9.5.2 Field location and orientation

Overall, we see fields aligned with the polar directions and/or toroidal fields in the equatorial plane. Assuming that the dust in the polar flows originates from the dust reservoir in the disk or torus, this suggests that the field also originates there. The alignment with the polar flow is interpreted that the gas carries the field with it.

NGC 6302 is the only source in our sample without evidence for a toroidal field. This nebula has a complicated morphology with a warped disk and the nebula is oriented at 45 degrees with respect to the equatorial dust lane. It is therefore difficult to ascertain the alignment of the field with any particular morphological component. However, alignment with the radio core seems most likely.

The other nebulae show evidence for toroidal field components. We therefore suggest that the initial configuration of the field is toroidal, and is located in the equatorial torus.

The polarisation in all cases appears to be seen in the neutral/molecular regions. Towards the central, ionised regions, the percentage of linear polarisation is much reduced. This may in part be because of the beam averaging over regions of different polarisations, but the ionised regions may also be expected to lose a directional field (non-constancy of \vec{B}). The reason for the absence of a detectable magnetic field in the ionised region can also be explained by the lack of dust (so \vec{B} is not carried). For NGC 6302, the field is aligned with the ionised core but is likely located around rather than within the core.

Polarisation will not be detected if the field is oriented along the line of sight. This is expected for toroidal fields near the tangential points of the torus. This may be present especially in CRL 2688, where two components are found at different locations.

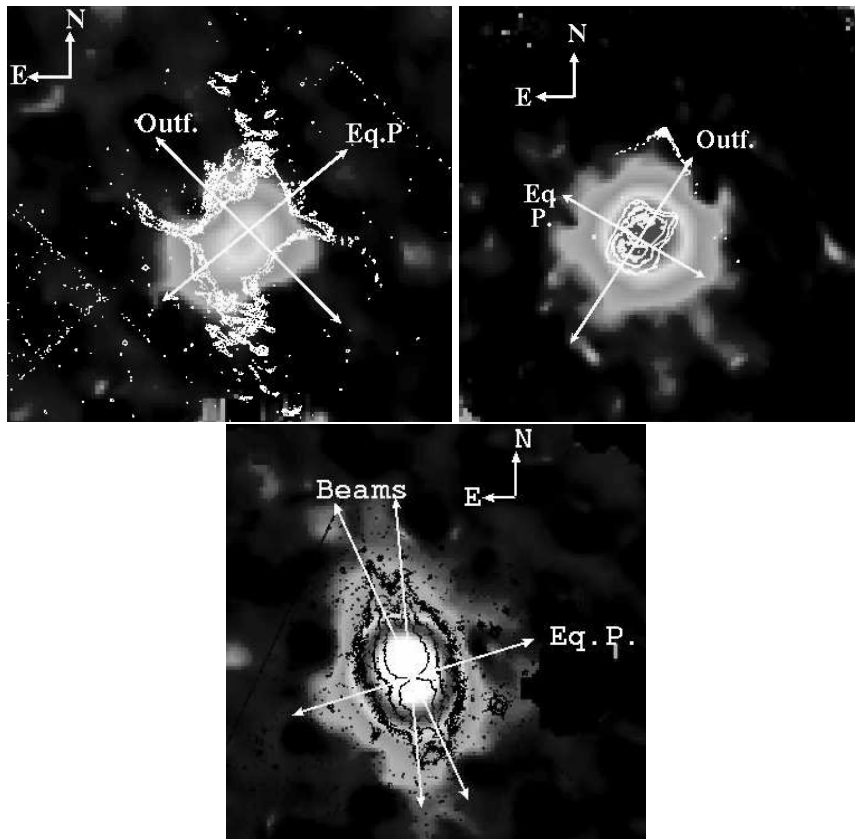


Figure 9.6: Location of the Scuba dust emission, compared to the HST images (contours). We present respectively a) NGC 6537, b) NGC 7027 and c) CRL 2688. NGC 6302 is shown in Fig. 9.5 .

9.5.3 Chemistry

The sample includes two oxygen-rich nebulae (NGC 6537 and NGC 6302, both PNe with hot central stars) and two carbon-rich nebulae (NGC 7027 and CRL 2688: the latter is the cooler post-AGB nebula in our sample). This sample is too small to draw general conclusions. However, we point out the following points of interest, for future study.

- The O-rich PNe both present collimated magnetic fields concentrated near the central star. In both cases, we have an organised magnetic field in the central region, resistant to distortion effects, but do not detect more distant fields.

- The two carbon-rich nebulae show extended fields covering their entire nebula. In both nebulae, the magnetic field is more disorganised than in the two O-rich stars.

The question of whether there is a chemistry-related origin to these behaviours is valid, but cannot be answered with the current sample. Dust chemistry could play a role. First, carbon grains tend to be smaller than silicate grains. Larger grains may be more spherical, which would give less (or no) polarisation. Both oxygen-rich nebulae show evidence for crystalline ice (Molster et al. 2002) (strongest in NGC 6302), indicating coatings on the grains. Second, amorphous carbon grains may be intrinsically non-spherical, build up from graphitic carbon sheets.

For the O-rich nebulae, it is possible that only the hotter dust, above the ice evaporation temperature, leads to non-spherical grains and a polarised signal. Thus, a difference in polarisation does not necessarily imply a difference in magnetic field structure.

Both O-rich nebulae show evidence for weak PAH emission in their central regions. The origins of the PAHs is not clear, but they are seen only in irradiated regions. The continuum radiation from the dust component containing the PAHs is only seen at short wavelengths (warm dust) and contributes very little to the sub-mm flux (Kemper et al. 2002b; Matsuura et al. 2005b). Thus, the polarisation signal is seen in the oxygen-rich grains, not the PAHs.

Iron needles could be considered as carriers of the polarisation: in O-rich stars, some or most of the iron is incorporated in the silicate grains (olivines and pyroxenes: Ferrarotti and Gail 2001), but for a C/O ratio close to and above unity, solid iron and FeSi become more important (e.g., Ferrarotti and Gail 2002). Metallic, non-spherical iron grains may contribute to the NIR opacity in high mass-loss OH/IR stars (Kemper et al. 2002a).

9.5.4 Comparison of less evolved/ more evolved nebulae

The extent of the nebulae shows that the objects differ in age. The nebulae of CRL 2688 (Post-AGB) and NGC 7027 (young PN) are younger than NGC 6537 (PN) and NGC 6302 (PN). (The lobes of the last object extend to over 2 parsec across.)

Our submillimeter polarimetric data show that the magnetic field is better organised for the older nebulae. Assuming an originally toroidal field, later carried by the bipolar flows, the best organised field is expected if one component dominates. The bipolar flows are most massive early in the post-AGB evolution (Bujarrabal et al. 2001). As they diminish, the remaining field may become less confused. However, evolving dust characteristics may also play a role: dust grains become larger in older disks, and may show less polarisation as a result. It is not possible with the current sample to separate evolutionary and chemical effects, but both are expected to occur.

9.5.5 Field strength and origin

The detected polarisation contains information on the direction of the field, but not its strength. A method to obtain the field strength out of fluctuations in polarisation was suggested by Chandrasekhar and Fermi (1953). Applying this method to our data leads to field strengths of the order of mG. This equation assumes that the magnetic field dispersion is caused by Alfvén waves. The applicability to our sources may be in doubt, as the dispersion may be dominated streaming motions.

In neutral-dominated media, Alfvén waves contribute if the collision times between ions and neutrals are shorter than the period of the Alfvén wave. This is the case for waves longer than

$$\lambda_A > \left(\frac{0.3}{\text{pc}}\right) \left(\frac{B}{0.1 \text{ mG}}\right) \left(\frac{10^4}{n}\right)^{3/2} \left(\frac{10^{-7}}{f_i}\right) \quad (9.1)$$

where n is the particle density per cm^3 , and f_i is the fractional ionization (Hildebrand 1996). For our sources, f_i may be high except in the densest regions of the tori. Assuming a typical source size of 0.05 pc, and a field strength of a mG, Alfvén waves

may contribute if $f_i > 10^{-4}$. This is a plausible value for the outflows.

Previous observations of OH Zeeman splitting has shown field strengths in OH/IR stars and post-AGB stars of a few mG at $3 \times 10^{15} - 2 \times 10^{16}$ cm from the stars (Bains et al. 2004, 2003). Much larger values have been inferred from water masers: several Gauss at $\sim 2 \times 10^{14}$ cm (Vlemmings et al. 2005). The difference is consistent with a dipole field, which gives an r^{-3} dependence, and less consistent with a solar-type field r^{-2} . Water masers trace high density clumps and the measured field strengths may not be fully representative of the surrounding areas.

Assuming we look at typical distances of 5 arcsec at 1 kpc, our measurements are at $\sim 5 \times 10^{16}$ cm from the stars. Compared to the OH and water masers, one would expect a field of 1mG or less at this distance. This suggest that the direction changes in the field are due to streaming motions, rather than Alfven waves.

The grains become aligned with the magnetic field with the Davis-Greenstein mechanism. In this mechanism, charged grains align their spin axis along the magnetic field via paramagnetic relaxation (or dissipation). The grains rotate with their angular momenta parallel to the interstellar magnetic field. The time scale for this to occur is (Kruegel 2003, Ch. 11)

$$t_{\text{rel}} \propto B^{-2}$$

and, for fields of the order of a few mG, is typically 10^6 yr. The age of the nebulae is $\sim 10^4$ yr. For this time scale, the alignment of the dust with the magnetic field requires fields in excess of those seen from OH maser emission. The alignment is therefore likely to originate close to the central star, at $r < 10^{15}$ cm, and is maintained while the nebula expands.

9.5.6 Evolution

For OH/IR stars, evidence for dipole fields has been presented by, e.g., Vlemmings et al. (2005). For more evolved stars, in the early post-AGB evolution, the presence of both toroidal (IRAS 20406+2953) and poloidal (OH17.7-2.0) fields are inferred

from OH observations (Bains et al. 2004, 2003). The poloidal fields arise from a stretched dipole. For the even later evolutionary stage studied here, a strong toroidal field component is found, combined with a poloidal field.

A toroidal field can form out of a dipole field by rotation. This already makes it likely that the formation of the torus and the formation of the toroidal field are related. A binary companion can be the source of the required angular momentum. Rotation of the star itself is less likely, as its angular momentum can be expected to be lost early on in the mass loss. A binary companion, on the other hand, can deposit its angular momentum during the time of the peak superwind, at the end of the AGB mass loss.

The fields detected via OH and H₂O masers have been claimed to be strong enough to dominate the dynamics of the nebula (Bains et al. 2004; Vlemmings et al. 2005). Soker (2006) argues that fields of this magnitude cannot be generated by the star itself, and should be attributed to a companion. Based on this, the basic shaping mechanism of the nebula is found in binarity. However, once the strong fields have been generated, they would be a significant factor in the further evolution of the nebula towards the PN phase.

9.5.7 Summary

We present the discovery of magnetic fields in four bipolar post-AGB stars (NGC 6537, NGC 7027, NGC 6302 and CRL 2688). This confirms the earlier work of Greaves (2002) for two of these. The fields are mapped at high resolution (for sub-mm), using either 450 or 850 μ m. The sub-mm emission traces the extended emission. In CRL 2688, we find evidence for the polar lobes which contain the well-known search beams.

All objects show polarisation indicative of grain alignment by magnetic fields. Toroidal fields are found for three objects, and poloidal fields for two (CRL 2688 shows evidence for both). The alignment of the field with nebula is least certain for NGC 6302, where the nebula shows a multipolar structure. Our results suggests that magnetic fields are common in these types of targets: bipolar nebulae with intermediate-

mass progenitors. The fields are long lived as they are observed over different evolutionary stages.

The data also show evidence for elongated grains. The polarisation is stronger and more extended for the carbon-rich nebulae. This may show that amorphous carbon grains are intrinsically non-spherical, e.g. the sheet-like structure of graphite. The oxygen-rich nebulae show polarisation only in their central regions. This is interpreted in that the dust grains in the torii are larger and more spherical.

The poloidal fields in the polar flows suggest that here the field is carried along by the flow and that these flows are not magnetically confined. The toroidal components in the torus may be more important, for the dynamics. As the fields in AGB stars are dipole-like, the toroidal field structure appears to be a later phase of evolution. We suggest that this transition occurs when the equatorial field is wound up through the interaction with a companion. Following Soker (2006), we suggest that the original shaping agent is a binary companion. Once the field has been wound up, it may however become dynamically important for the subsequent nebular evolution.

10

Other detection processes and magnetic field exhibition

We have seen that the analysis of dust polarisation is a good way to determine the global location of the magnetic field over the PNe. Several investigations have been done using this technique (Lazarian 2007), (Falceta-Gonçalves et al. 2008) and (Rao 1999) but in other astrophysical fields the use of the Chandrasekhar-Fermi method is suitable to measure the field strength (Chandrasekhar and Fermi 1953). In the PN field there are still two other ways to measure the field strength: Zeeman splitting and Faraday rotation measurements.

10.1 Spectropolarimetry and radio measurements

The first process to be described is the Zeeman effect. In the presence of a magnetic field B , atomic lines will be split equally and show different transition levels with their $\Delta m_J = 0(\pi)$, $1(\sigma)$ or $-1(-\sigma)$. The latest 3 components are polarised either linearly or circularly, and they are the features intended to be observed to derive the magnetic field strength. But their observation depends on the field's orientation relative to the line of sight (LOS). Thus if the LOS and B are parallel, only the circularly polarised σ components are seen (Fig.10.1, left) and if the LOS and B are perpendicular all 3

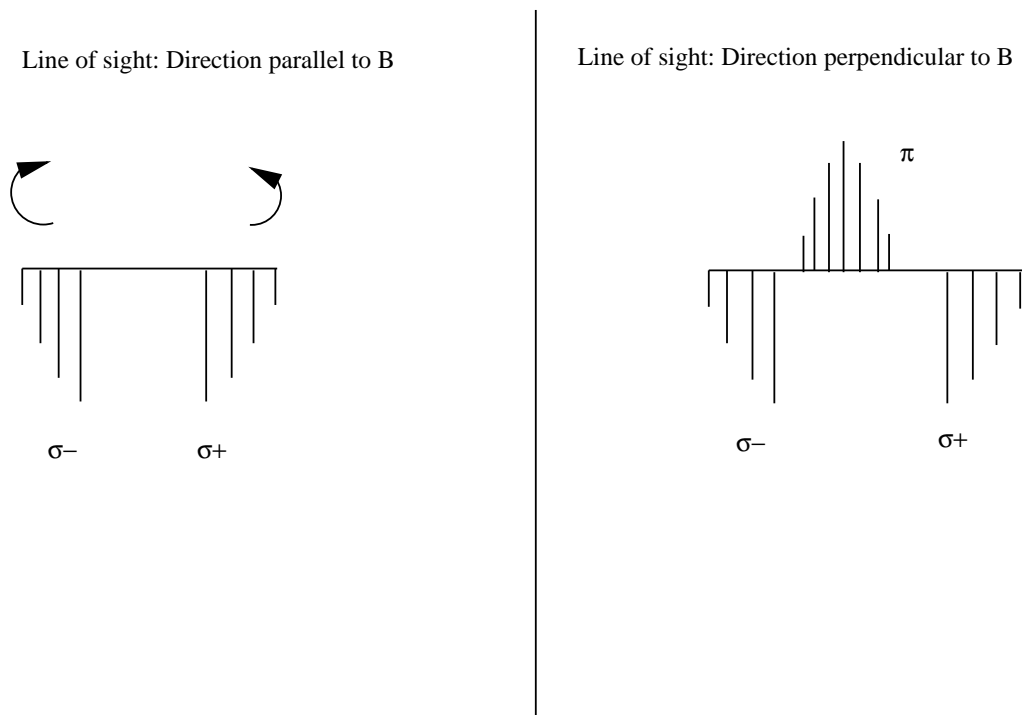


Figure 10.1: Polarization of spectral lines

components are seen with the π component parallel to the field and the σ components perpendicular to it (Fig. 10.1, right). The magnetic field strength can be derived by measuring the separation between the circularly polarised σ components. The angle between B and LOS should also be taken into account.

$$\Delta\lambda = 4.67 \times 10^{-13} \lambda_0^2 z B \cos \theta \quad (10.1)$$

With $\Delta\lambda_z$ the line separation in \AA , λ_0 the wavelength of the line and z the Lande factor.

But due to the weakness of the field, the separation $\delta\lambda_z$ of the lines is not often seen. We must therefore rely on the total circular polarisation given by the Stokes

parameter V . Thus Mathys (1989) and Bagnulo et al. (2002) defined a “weak field approximation”:

$$\frac{V}{I} = -g_{eff}\delta\lambda_z\lambda^2\frac{1}{I}\frac{dI}{d\lambda} < B_{eff} > \quad (10.2)$$

where I is the total intensity, g_{eff} the effective Lande Factor and B_{eff} (Gauss) the effective magnetic field also linked to the mean longitudinal field. The latter is retrieved via a linear regression of the two terms of the equation.

This method has been applied to find $<B_{eff}>$ in the central stars of planetary nebulae by Jordan et al. (2005) and Lee et al. (2007a) using the low resolution FORS1 spectrograph/spectropolarimeter ($R=260-1700$) at the VLT (8m) and the high resolution ($R=60\,000$) ESO Multi-Mode Instrument (EMMI) on the 3.58m New Technology Telescope (NTT) respectively. Magnetic fields in the order of the kG were claimed to be found in the CS of NGC 1360 and LSS1362 (Jordan et al. 2005), and an upper limit of 20 kG in the CS of He 2-64 and MyCn 18 has been established by Lee et al. (2007a). A source of error in this technique lies in the presence of a (hot) companion which would disturb the spectrum of the primary source. In addition, noise may also be taken for a weak magnetic field.

At radio wavelengths, other than the masers detection we discussed earlier, magnetic fields can be detected via Faraday rotation. This process is based on the fact that in the presence of a magnetic field, the polarisation plane will rotate with an angle β proportional to the field’s strength. The method has been applied for the PN Sh 2-216 by Ransom et al. (2008) and a magnetic field of $5\pm 2\ \mu\text{G}$ has been derived but it is likely to be interstellar rather than stellar. The main concern, using this technique, is the presence of a magnetised structure in the line of sight which can lead to a misleading determination of B . Moreover the value obtained for the field is only directional, and does not indicate if the field is located inside or outside the observed target.

10.2 Interstellar magnetic field

The methods described so far have been mainly used to derive magnetic fields inside the planetary nebulae and therefore to look for an “internal” shaping. But the magnetic field could also shape the PNe in an “external” way as the interstellar medium itself is magnetized. As we have seen previously, some PNe with ISM interaction show disruptions, fragmentations, filaments and vortices which may be due to Rayleigh-Taylor instabilities enhanced by interstellar magnetic fields. Figure 8.30 (bottom) shows the location of the different PNe/ISM as a function of the stage of interaction and also in relation to the extinction in the plane. Although we found some WZO2 objects in high extinction zones, we predominantly noticed the presence in this area of nearly all the late stages (WZO3-4, WZO4), which are the most disrupted nebulae. The WZO3 nebula located at a higher latitude may either be a misclassification or located in a locally dense area (see the magnetic maps from Mathewson and Ford (1970)). The regions of interest are the denser (dustier) ones in the Galaxy and populated with dense nebulae (HII regions, SNR). According to Tielens (2005), the magnetic field would increase in those areas as:

$$B \sim n^\alpha \quad (10.3)$$

with $\alpha \sim 0.5$ and n the gas density. Thus at $n \sim 10^4 \text{ cm}^{-3}$, $B \sim 30 \mu\text{G}$. Knowledge of the gas density of the IPHAS nebulae with ISM interaction would therefore provide an estimate of the lower limit of the magnetic field for the disturbed nebulae and of the upper limit for the undisturbed ones. (Ransom et al. (2008) gave a detailed analysis of the magnetic field around the old interacting PN Sh 2-216). By extension, the interstellar magnetic field could be locally traced (probed) in the whole Galactic Plane.

11

Conclusions and Perspectives

11.1 Summary of the investigation

Going down to $2 \times 10^{-17} \text{ erg cm}^{-2} \text{ s}^{-1} \text{ arcsec}^{-2}$ in term of sensitivity, the INT Photometric H α survey has allowed us to discover 233 extended candidate planetary nebulae in the right ascension range 18h to 20h. These objects have been detected visually using 2 degrees squared binned mosaics of 15×15 pixels and 5×5 pixels. Along with these candidate PNe, other stellar populations like emission line stars, SNR and diffuse nebulae have been (re)discovered and have been catalogued in a database specially created to list all the Northern nebulae located between $b \pm 5$. The spectroscopic identification of the IPHAS PNe has not been systematic for all our discoveries. This was mainly due to the allocated time during the follow-up spectroscopy. As such, 18 objects have been confirmed PNe using diagnostic diagrams from Sabbadin et al. (1977) and Riesgo and López (2006). But the lack of spectroscopic data did not slow down our identification of planetary nebulae as we used other tools, like the infrared and radio data linked to our objects as well as their morphological analysis. Thus, the IRAS and MSX surveys were used to classify the IPHAS nebulae in the infrared. The diagnostic diagrams by Pottasch et al. (1988) and Zijlstra et al. (2001) for the IRAS data and the diagram by Ortiz et al. (2005) for the MSX data have allowed us to confirm 10 nebulae as plane-

tary nebulae. The limited number of objects analysed is related firstly to the accuracy on the position between the IR sources and our IPHAS nebulae (which are not compact) and then to the quality criteria inherent to each IR survey, for which we only chose the highest quality data for the bands used. The next classification tool used was the radio identification with the NRAO VLA Sky Survey (Condon et al. 1998) at 1.4 GHz. More IPHAS objects were analysed (60) and this time we defined our own diagnostic diagrams to identify the PNe or at least to probe the likelihood of it being a planetary nebula. These diagrams are based on the brightness temperature, the general PN flux and the evolution of the fraction of PNe/HII regions along with the radio flux. Cross-checking these methods allowed us to identify 1 “very likely” HII region and 12 “very likely” PNe and 38 “probable” PNe. The radio study also gave us the first results regarding the nature of the IPHAS nebulae. Therefore we noticed that, compared to known PNe, the selected IPHAS sources generally have low radio flux and low surface brightness, both consistent with evolved and extended nebulae. Finally, the morphology based classification indicated that 146 sources (nearly 2/3 of the whole sample) can be classified from “very likely” to “probable” PNe due to their shape. This type of classification is, of course, not to be used as a single reference.

The final classification, which concerns 72 objects, is listed in Table 3.10 and is discussed in Section 3.5 for all 233 nebulae. Among the total set of candidate PNe, there are several objects which could also be supernova remnants due to their morphology (generally filamentary), and the presence of young pulsars nearby as well as X-ray sources (see Appendix E).

The identification/classification process has been the first step in our study of the IPHAS PNe, and more information can be derived in order to show the extent and importance of the contribution of the IPHAS to the PN field.

First, our study of the galactic distribution of the new nebulae has revealed that many more objects, hitherto unknown, and particularly those close to the Galactic Plane (near $b=0$ and hence in heavier extinction zones). There is a factor of 4 difference with the number of known PNe in the same sky area. These new nebulae are related

to two “hidden populations” which are the large objects with a size greater than ~ 20 arcsec and the irregular nebulae. We linked the large size nebulae (141 objects) to evolutionary more advanced nebulae and/or which could have derived from massive progenitors. The irregular nebulae are localised, in terms of height above the plane, between the elliptical and bipolar nebulae. They would therefore have as progenitors, (O-rich) AGB stars with intermediate to long periods, with a high mass between $1M_{\odot}$ and $1.5-2 M_{\odot}$ (without reaching the bipolar progenitor mass level). Finally, assuming that $\sim 1200 \pm 200$ planetary nebulae are expected to be present in our area of study, we show that IPHAS contributes quite well towards filling the gap between the actual observations and the expectations. The lack of detection occurs mainly at a low latitude range which implies a higher extinction rate (although IPHAS increases the detection rate in this low latitude range). The missing PNe might not be discovered using optical surveys.

The infrared analysis of the IPHAS sources has revealed that all of them show a systematic $60\mu\text{m}$ excess, due to dust, in comparison to the known PNe located in the same sky area. We therefore suspect that this phenomenon alters the classification of the nebulae as *bona fide* PNe in the Pottasch et al. (1988) study, where they would automatically fall in the left part of their diagnostic diagram (corresponding to HII regions or they would remain unclassified). We used the photoionisation code CLOUDY to determine whether the IRAS colours of the IPHAS nebulae (and particularly those without a clear classification) are consistent or not with a planetary nebula nature. Several models were used varying the nebular radius, the density (hydrogen and electronic), the stellar temperature and the grain nature (graphite and silicate). We concluded that the IPHAS nebulae better fit medium-low density nebulae, with large size (from ~ 0.01 pc in radius) and a tendency for $60\mu\text{m}$ excess or else, dust excess. We therefore showed that the “Pottasch IRAS diagnostic diagram” is incomplete and does not cover all PNe. Based on this initial diagram, we established new boundaries for the identification of planetary nebulae.

One of the important issues in the astronomical field in general is the determination of

distances. In the framework of IPHAS we compared three methods, two statistical and one individual. The first statistical technique is the *surface brightness-radius* relationship based on the relations given by Frew and Parker (2006). We varied this method using four different ways to derive the surface brightness: simple visual determination of the limit of the nebulae, expanding circular adaptive aperture, 1% contour of the nebula, and using the $H\alpha$ flux, corrected from extinction, from the spectroscopy. The three first methods used continuum-subtracted images $H\alpha+[NII]$ IPHAS images. The second, statistical technique is the *Shklovskii method*. Finally, the individual method is based on a new extinction-distance relation developed in the framework of IPHAS (Sales et al, in preparation).

The three methods were tested on the set of IPHAS PNe for which spectroscopic data were available. The results obtained are, in fact, quite disparate. The method using an expanding circular adaptive aperture, and the IPHAS extinction-distance method show non-systematic agreement, although substantial agreement is found within the error margin for 11 objects. We found that neither the size of the nebulae nor their morphology could account for the observed disparity. But we also noted a discrepancy between the methods using the SB-R relation i.e., whether spectroscopy ($H\alpha$) or imaging ($H\alpha+[NII]$) were used to derive the flux. We concluded that the use of the single $H\alpha$ flux would be an important factor in the estimation of the final distance and it should be considered more reliable than the two wavelengths combination. From this work, two ways to accurately derive the surface brightness have been established:

- Spectroscopically: Using an $H\alpha$ integrated spectrum of the whole nebula with integral field spectroscopy.
- Imaging: Using a narrow-band filter in $H\alpha$ and the averaged surface brightness method. A wavelet analysis would sample the images in different areas and levels of brightness.

The “Shklovskii method” appears to be inadequate to derive the distances of our PNe. At the end of this study on distances, we know how to improve our accuracy using the SB-

R relationship, and which methods are unreliable or less reliable. A variation of the nebular extinction is unlikely to be a cause of the discrepancies which could exist with the extinction-distance method (although the error covers the gap), and we consider the photometry (for the A-stars) as precise. The accuracy of the measurement of the nebular extinction is an issue.

Using the distances from the IPHAS extinction curves, we showed that we encounter PNe at close and large galactocentric distances, and they are generally located at lower heights above the plane (< 200 pc). The ionised mass of the IPHAS PNe was also derived.

We continued our study of the 18 IPHAS PNe by looking at their possible recombination and age, as we saw that the survey would more likely target evolved objects. Hence, deriving the recombination time scale as given by Kwok (2000) and the density vs size relation and dynamical age from the R/V_{exp} relation) (Table 7.4), only 1 PN shows a true sign of recombination. We also show that the survey covers PNe with a wide range of ages. But, thank to its sensitivity, IPHAS is more likely to discover first “middle-aged” PNe, comparable to most of the known PNe located in the same sky area. This implies that the new objects were not detected because of their extinction. Also, the survey allowed the discovery of (very) evolved planetary nebulae. In this sky area no known PNe have been observed with the typical characteristics of evolved PNe (large radius and low density, see Fig. 7.3 and 7.4). The non-detection (so far) of the IPHAS nebulae (faintness) is likely to be linked to their advanced evolutionary status. The analysis of the Strömgren radius indicates that most of the planetary nebulae (known or new, in our sky area or outside it) are fully ionised nebulae and then density bounded.

The last investigation carried out on the IPHAS nebulae was the identification of interaction with the interstellar medium. The depth reached by the IPHAS survey combined with the binning detection method allowed us to detect several interacting PNe candidates. The morphology and behaviour of these candidates were compared to the three-dimensional hydrodynamic simulations by Wareing et al. (2007), which list four stages

of interaction depending on the ISM velocity, density and AGB mass loss rates. Each stage can also be linked to an evolutionary status: WZO1 for young candidates, WZO2 stage for middle-aged candidates and WZO3 and WZO4 for old candidates. Table 8.2 lists the 21 nebulae out of 233 for which an interaction other than WZO1 (where the PN is not affected yet by the interaction) was observed. As a result, we observed that most of the IPHAS nebulae showing an ISM interaction belong to stage 2 (17 objects) and show a rather circular morphology. This behaviour is comparable to the known PNe listed by Borkowski et al. (1990) and the ones present in the “IAC Morphological Catalog of Northern Galactic Planetary Nebulae” (Manchado et al. 1996). Only 3 nebulae display a stage 3 interaction and one a stage 4 and these are classified as irregular nebulae. We also observed phase transitions (WZO2 to WZO3 and WZO3 to WZO4). The detection of a stage 4 of interaction is encouraging, as we can now expect more cases in other parts of the Galactic Plane. This is important because we are now able to study PNe at the very end of their life. We also notice the presence of vortexes and perturbations perfectly described by Wareing et al. (2007) in their simulations. The analysis of the size of these interacting nebulae has shown that even if most of the PN-ISM are large (size greater than 100 arcsec) and thus more evolved, the ISM interaction process does not only imply “old” nebulae, as “small-medium size” nebulae (size less than 100 arcsec) are also affected. In terms of location on the Plane, the large nebulae seem to survive at relatively low latitude but they will suffer from the ISM action on their geometry and will display more advanced stages of interaction. Smaller size nebulae at the same latitude range are less affected. When the extinction is maximum i.e. the influence of the ISM (its density) is greater, no PNe-ISM are detected. This can only mean that either they are not detected, so we are not going deep enough in our optical survey, or they have been totally destroyed by the effect of the ISM. Finally we did attempt to identify the central star for each PN-ISM as well as its proper motion.

11.2 Solved problems and future work

The investigation presented in this thesis has demonstrated that the IPHAS survey is a good tool to complete our knowledge about planetary nebulae. In section 1.2, we listed a series of problems which interfere with the study of PNe.

• Thus, we can consider that the “detection problem” has been partially solved or at least a great advance has been made :

- The extinction induced by the ISM is no longer so problematic and nebulae (of different morphologies and sizes) located at low latitude or height are detected.
- Middle-aged and (very) evolved nebulae are observed and constitute the core of the detections.
- From our small sample of newly identified PNe, we notice that they are generally located further in the Galaxy.
- The use of two binning systems greatly helps to identify new nebulae in crowded areas on a large scale.

The general number of objects in the 18h-20h sky area has increased and with it the number of nebulae with ISM interaction. The missing objects have to be found, if possible, using other methods.

Our investigations enabled us to have a new perspective on some physical parameters:

- The size and morphology analysis led to the detection of “hidden populations” (respectively large and irregular nebulae).
- The IR and radio analysis have shown that in the framework of the IPHAS survey we are dealing with generally more evolved, dustier and colder PNe. This gave birth to new diagnostic diagrams.
- The introduction of the IPHAS extinction curves to derive the PNe distances has revealed the (dis)agreement with the distances obtained by other statistical methods.

The origin of the morphology in planetary nebulae was also on our list of unsolved problems. In this thesis we focused on a new shaping agent: the magnetic field. Using SCUBA sub-millimeter polarimetric observations, we were able to detect the presence of magnetic fields (via dust alignment by the latter) i.e. carried/coexistent with the dust in four bipolar PNe (NGC 7027, NGC 6537, CRL 2688 and NGC 6302). All the objects show a toroidal magnetic field which is consistent with their bipolar structure. CRL 2688 also has a poloidal field. We found long-lived magnetic fields which may vary in strength, along with the chemical composition and the evolutionary status of the nebulae. The question of whether the magnetic field governs (alone) the mass flow can only be fully answered by the detection of the field in the PN core and its behaviour with the surrounding plasma. This implies the combination of observations and MHD simulations. In conclusion, magnetic fields can play a role in the shaping of planetary nebulae but with the small amount of data obtained we can only consider that their shaping action is done in conjunction with a binary companion.

The main investigations in the sky area studied here are first the spectroscopic identification of all the nebulae detected in order to strengthen our analysis and then the use of the IPHAS extinction curves for known PNe to identify the point of divergence in the determination of distances. On a larger scale, the search for PNe in the remaining part of the sky is still going on. When this is accomplished, we will be able to obtain an unbiased and general study of planetary nebulae.

The continuation of the sub-mm (dust polarisation), radio (polarisation and Faraday rotation) and optical (spectropolarimetry) observations for more PNe with different morphologies, age and chemistry will give us a better understanding of the effective implication of magnetic fields in the PNe structure (can it be the sole agent in the shaping process?). This will also help us to understand the role of the magnetic field in the physics of PNe.

Appendix A

The IPHAS extended PNe candidates

Table A.1: Full listing of the planetary nebulae candidate in the 18h to 20h region. *Note:* The notation for the morphology is defined as follow: R:Round, B:Bipolar, E:Elliptical, I:Irregular, “:r” is set for “ring”.

IPHAS Name	Morphology	Size (in arcsec)	Name if known
IPHASX J183416.2+021215	I	556	
IPHASX J183438.7+000803	E	8	PN PM 1-242 ¹
IPHASX J183602.4-000226	I	12	PN PM 1-246 ²
IPHASX J183652.8-011536	I	26	
IPHASX J183811.7-010512	I	42	
IPHASX J183911.8+010624	R	6	
IPHASX J184030.3-003820	I	22	
IPHASX J184104.6-014050	I	6	
IPHASX J184137.2+044025	I	35	
IPHASX J184211.4+005031	R	4	
IPHASX J184253.2-022642	I	376	

¹(Preite-Martinez 1988)

²(Preite-Martinez 1988)

Table A.1 – continued .

Name	Morphology	Size (in arcsec)	Name if known
IPHASX J184320.1+042722	I	60	PN G035.4+03.4 ³
IPHASX J184336.6+034640	B	18	
IPHASX J184505.2+001158	R	4	
IPHASX J184540.5-031238	I	34	
IPHASX J184716.3+030929	I	20	
IPHASX J184720.0+021025	I	10	
IPHASX J184745.4+013248	B	46	
IPHASX J184800.6+025420	R	67	
IPHASX J184834.7+063259	I	22	
IPHASX J184836.2+022050	R	6	
IPHASX J184932.7-004437	I	96	
IPHASX J184933.3-003801	I	42	
IPHASX J184938.1+000926	I	14	
IPHASX J185129.8-010752	I	235	
IPHASX J185155.3+084019	I	68	
IPHASX J185208.1-012843	I	326	
IPHASX J185223.1+005322	I	580	
IPHASX J185224.2-004446	R	4	
IPHASX J185225.0+080843	R	20	
IPHASX J185225.5-003326	R	8	
IPHASX J185309.4+075241	E	10	
IPHASX J185312.9-002529	I	20	
IPHASX J185321.8+055641	R	6	
IPHASX J185322.1+083018	R	110	
IPHASX J185342.6-003628	I	14	

³(Acker et al. 1992)

Table A.1 – continued .

Name	Morphology	Size (in arcsec)	Name if known
IPHASX J185525.7-004823	B	12	
IPHASX J185620.8+004856	I	28	
IPHASX J185627.9+005550	I	48	
IPHASX J185640.1-003804	E	12	
IPHASX J185722.5+010929	I	40	
IPHASX J185744.5+105053	E	110	
IPHASX J185759.6+020706	R:r	10	PN G035.5-00.4 ⁴
IPHASX J185815.8+073753	E	8	
IPHASX J185925.8+001734	E	12	
IPHASX J190016.5+103406	I	50	
IPHASX J190115.6+114147	R	30	
IPHASX J190125.5+050857	B	14	
IPHASX J190126.4+051438	I	11	
IPHASX J190143.3-012937	E	8	PHR 1901-0129 ⁵
IPHASX J190155.1+011211	I	140	
IPHASX J190227.3+020815	I	106	
IPHASX J190228.1+020724	I	36	
IPHASX J190319.2+142524	I	14	
IPHASX J190338.5+104227	R	512	
IPHASX J190340.7+094640	I	13	
IPHASX J190346.8+050935	I	52	PN HaTr 12 ⁶
IPHASX J190349.0+045503	I	504	
IPHASX J190356.2+050637	I	92	
IPHASX J190417.9+084916	R	5	

⁴(Acker et al. 1992)

⁵(Parker et al. 2006a)

⁶(Hartl and Tritton 1985)

Table A.1 – continued .

Name	Morphology	Size (in arcsec)	Name if known
IPHASX J190418.6+050635	I	36	
IPHASX J190419.4+152126	R	470	
IPHASX J190432.9+091656	R	7	
IPHASX J190447.9+121844	E:r	10	
IPHASX J190454.0+101801	R	18	
IPHASX J190502.9+034229	E:r	64	
IPHASX J190512.4+161347	R	66	
IPHASX J190543.8+064413	R	14	
IPHASX J190543.8+110018	R	9	
IPHASX J190614.9-013318	B	138	PHR 1906-0133 ⁷
IPHASX J190621.1+030050	I	44	
IPHASX J190631.4-023237	I	20	
IPHASX J190633.6+090720	R:r	14	
IPHASX J190654.9+052216	R	464	
IPHASX J190700.7+043041	R	1090	
IPHASX J190701.9+014646	I	200	
IPHASX J190718.1+044056	E	8	
IPHASX J190757.2+045445	I	31	
IPHASX J190759.4+050519	I	150	
IPHASX J190812.7+143530	I	16	
IPHASX J190816.8+052506	E	8	
IPHASX J190823.6+023302	I	16	
IPHASX J190852.1+031305	I	15	
IPHASX J191001.0+142203	R	6	
IPHASX J191003.4+032224	R	244	

⁷(Parker et al. 2006a)

Table A.1 – continued .

Name	Morphology	Size (in arcsec)	Name if known
IPHASX J191017.4+065258	R	6	
IPHASX J191022.1+110538	R:r	10	
IPHASX J191027.4+034046	R	14	
IPHASX J191037.7+044403	I	96	
IPHASX J191058.9+040350	R:r	11	
IPHASX J191104.7+060845	B	20	
IPHASX J191124.8+002743	B	34	
IPHASX J191255.5+143248	R:r	10	
IPHASX J191344.7+132212	I	48	
IPHASX J191345.6+174752	R	6	
IPHASX J191349.6+121841	I	362	
IPHASX J191421.1+140936	R	47	
IPHASX J191445.1+133219	B	13	
IPHASX J191651.6+065607	I	14	
IPHASX J191707.1+020012	R	72	
IPHASX J191716.4+033447	E	16	
IPHASX J191716.5+181518	R	48	
IPHASX J191725.0+205230	I	108	
IPHASX J191727.0+082036	I	13	
IPHASX J191819.3+141320	I	78	
IPHASX J191840.4+073131	I	36	
IPHASX J192026.4+120222	I	66	
IPHASX J192038.9+160224	I	63	
IPHASX J192043.7+052702	I	25	
IPHASX J192140.4+155354	B	13	
IPHASX J192146.7+172053	R:r	32	

Table A.1 – continued .

Name	Morphology	Size (in arcsec)	Name if known
IPHASX J192150.0+145424	R	320	
IPHASX J192152.0+135223	E	12	
IPHASX J192153.9+143056	E:r	18	
IPHASX J192213.1+161417	I	22	
IPHASX J192221.5+151550	I	44	
IPHASX J192256.9+140700	I	68	DSH J1922.9+1407 ⁸
IPHASX J192320.6+164419	I	78	
IPHASX J192347.8+143642	E	74	
IPHASX J192349.9+143330	I	112	
IPHASX J192410.6+133443	I	824	
IPHASX J192429.6+202433	I	64	
IPHASX J192436.3+154402	E	20	
IPHASX J192458.2+193434	R	29	
IPHASX J192510.8+113353	B	134	
IPHASX J192520.6+092410	I	126	
IPHASX J192535.2+200336	R	38	
IPHASX J192543.2+143546	R	176	
IPHASX J192615.4+191358	R	142	
IPHASX J192619.1+144814	I	14	
IPHASX J192624.7+195045	I	20	
IPHASX J192633.2+235726	I	66	P85b 12 ⁹
IPHASX J192644.3+243836	I	36	
IPHASX J192651.5+224524	I	64	
IPHASX J192717.1+194308	I	400	DSH J1927.2+1943 ¹⁰

⁸(Kronberger et al. 2006)⁹(Petrossian 1985)¹⁰(Kronberger et al. 2006)

Table A.1 – continued .

Name	Morphology	Size (in arcsec)	Name if known
IPHASX J192748.3+203712	I	35	PN PM 1-302 ¹¹
IPHASX J192751.3+140127	R:r	11	
IPHASX J192816.9+231911	I	17	
IPHASX J192837.7+245024	E	12	
IPHASX J192847.1+093439	B	64	
IPHASX J192902.5+244646	R	10	
IPHASX J192950.2+193426	I	96	
IPHASX J193008.9+192137	E:r	188	
IPHASX J193014.2+190105	I	20	
IPHASX J193023.1+181540	R	318	
IPHASX J193056.8+265845	I	23	
IPHASX J193110.7+192904	E:r	20	
IPHASX J193116.8+291232	I	4	
IPHASX J193127.0+115622	E	26	
IPHASX J193305.9+132921	R	67	
IPHASX J193308.9+155354	R	24	
IPHASX J193334.4+175232	I	10	
IPHASX J193517.8+223121	R	44	
IPHASX J193532.1+112115	R	9	
IPHASX J193550.2+162850	I	28	
IPHASX J193617.6+272051	R	9	
IPHASX J193630.3+312810	R	404	
IPHASX J193633.3+153348	R	114	
IPHASX J193637.3+123808	R:r	262	
IPHASX J193718.7+202102	B	62	

¹¹(Preite-Martinez 1988)

Table A.1 – continued .

Name	Morphology	Size (in arcsec)	Name if known
IPHASX J193721.9+233607	I	48	
IPHASX J193740.6+203548	I	31	
IPHASX J193752.1+271119	E	18	
IPHASX J193809.2+205412	R	146	
IPHASX J193827.9+265752	R	7	
IPHASX J193843.4+234949	I	28	
IPHASX J193849.6+313744	R	160	
IPHASX J193912.0+251105	I	38	
IPHASX J194038.5+123129	I	66	
IPHASX J194052.5+301711	I	74	
IPHASX J194204.9+231932	E:r	15	
IPHASX J194226.1+214521	B	24	DSH J1942.4+2145 ¹²
IPHASX J194232.9+150034	R	20	
IPHASX J194240.6+275109	R	74	
IPHASX J194301.3+215424	B	18	
IPHASX J194305.7+272343	I	28	
IPHASX J194332.7+234508	R	14	
IPHASX J194339.9+203213	R	18	
IPHASX J194359.5+170901	B	122	
IPHASX J194408.9+284845	I	21	
IPHASX J194409.1+280600	I	36	
IPHASX J194434.7+255540	I	8	
IPHASX J194510.6+270929	E	9	
IPHASX J194533.8+210751	I	135	
IPHASX J194550.1+313800	I	20	

¹²(Kronberger et al. 2006)

Table A.1 – continued .

Name	Morphology	Size (in arcsec)	Name if known
IPHASX J194556.2+232833	E	58	GM 3-11 ¹³
IPHASX J194610.9+170609	I	14	
IPHASX J194620.6+342337	I	38	
IPHASX J194633.0+231659	R	9	
IPHASX J194638.4+235010	I	272	
IPHASX J194641.5+264820	I	114	
IPHASX J194645.3+262211	R	290	
IPHASX J194727.6+230816	R	37	
IPHASX J194728.9+222823	R	27	
IPHASX J194730.5+250201	R	45	
IPHASX J194745.5+270150	R	207	
IPHASX J194751.9+311818	R	8	
IPHASX J194804.2+254847	I	8	
IPHASX J194810.6+280724	I	149	
IPHASX J194815.0+280730	R	4	
IPHASX J194829.3+245355	I	88	
IPHASX J194843.4+181830	I	81	
IPHASX J194852.7+222516	R	21	
IPHASX J194853.7+181021	R	8	
IPHASX J194905.2+181503	I	26	
IPHASX J194930.9+273028	R	84	
IPHASX J194940.9+261521	B	10	
IPHASX J195011.4+264331	I	17	
IPHASX J195015.9+272859	I	202	
IPHASX J195032.6+272102	I	21	

¹³(Gyul’Budagyan and Magakyan 1977)

Table A.1 – continued .

Name	Morphology	Size (in arcsec)	Name if known
IPHASX J195042.3+255949	I	38	DSH J1950.7+2601 ¹⁴
IPHASX J195057.1+272752	I	94	
IPHASX J195126.5+265838	E	7	
IPHASX J195221.9+315901	E	40	
IPHASX J195248.8+255359	B	10	
IPHASX J195318.5+371005	I	416	
IPHASX J195343.8+202636	I	30	
IPHASX J195357.9+312130	R	212	
IPHASX J195400.7+315551	R	32	
IPHASX J195436.4+313326	R:r	10	
IPHASX J195529.3+294351	I	42	
IPHASX J195627.3+250648	R	24	
IPHASX J195657.6+265714	B	24	
IPHASX J195748.5+304343	I	106	
IPHASX J195759.5+340119	I	44	
IPHASX J195815.1+340143	I	78	
IPHASX J195836.5+292314	B	12	
IPHASX J195919.1+312534	I	6	
IPHASX J195919.6+283827	I	520	
IPHASX J195957.4+395306	I	412	
IPHASX J195958.2+332939	R	60	
IPHASX J200018.7+365934	R	30	GN 19.58.5.03 ¹⁵
IPHASX J200149.5+392944	R	26	

¹⁴(Kronberger et al. 2006)¹⁵(Neckel and Vehrenberg 1985)

Appendix B

Qualitative description of the IPHAS candidate PNe

IPHAS coordinates and Description

183416.223+021215.95: Large curved nebula.

183438.678+000803.00: Well defined elliptical nebula.

183602.400-000226.16: Diffuse and faint nearly-circular nebulosity.

183652.778-011536.81: Diffuse and faint nebulosity. No sign of symmetry.

183811.748-010512.37: Diffuse and faint nebulosity. No sign of symmetry.

183911.810+010624.63: Well defined round nebula.

184030.275-003820.86: Diffuse and faint nebulosity. No sign of symmetry.

184104.600-014050.08: Small nebula with complex morphology and small halo.

184137.235+044025.04: Diffuse and faint nebulosity. No sign of symmetry.

184211.400+005031.63: Well defined round/point-like nebula.

184253.191-022642.51: Large nebulosity: bright part of a former circular nebula interacting with the ISM on the NW direction ?

184320.059+042722.10: Diffuse and faint nebulosity. No sign of symmetry.

184336.580+034640.80: Well defined bipolar nebula .

184505.250+001158.72: Well defined round nebula with halo .

- 184540.555-031238.17:** Diffuse nebulosity with no sign of symmetry.
- 184716.354+030929.13:** Diffuse and faint nebulosity. No sign of symmetry.
- 184720.009+021025.38:** Diffuse and faint nebulosity. No sign of symmetry.
- 184745.400+013248.00:** Well define bipolar nebula.
- 184800.647+025420.70:** Circular nebulosity with two spiral arms around star IRAS 18454+0250.
- 184834.676+063259.30:** Diffuse nebulosity with upper bow shock in the northern direction.
- 184836.250+022050.72:** Well defined and faint round nebula
- 184932.656-004437.57:** Diffuse nebulosity. No sign of symmetry.
- 184933.300-003801.00:** Bow shock nebula with tail .
- 184938.078+000926.88:** Diffuse and faint nebulosity. No sign of symmetry.
- 185129.777-010752.12:** Large diffuse and faint nebulosity. No sign of symmetry.
- 185155.313+084019.08:** Very faint nebulosity. No sign of symmetry.
- 185208.070-012843.08:** Large diffuse nebulosity. No sign of symmetry
- 185223.142+005322.81:** Large quasi-circular nebula with irregular interacting front towards the north.
- 185224.185-004446.66:** Well defined round nebula.
- 185225.044+080843.89:** Faint round nebula.
- 185225.543-003326.48:** Well defined round nebula.
- 185309.450+075241.06:** Well defined elliptical nebula.
- 185312.923-002529.37:** Faint nebulosity. No sign of symmetry.
- 185321.763+055641.24:** Well defined round nebula.
- 185322.127+083018.45:** Well defined semi-circular nebula. The rim may show an ISM interaction in the SW direction. The coordinates are centred on the geometric centre.
- 185342.593-003628.81:** Faint nebulosity. No sign of symmetry.
- 185525.754-004823.38:** Well defined bipolar nebula.
- 185620.761+004856.60:** Faint S-shaped nebulosity.

185627.930+005550.66: Faint nebulosity with no obvious symmetry.

185640.084-003804.00: Faint elliptical nebula.

185722.529+010929.13: Diffuse and faint nebulosity. No sign of symmetry.

185744.505+105053.07: Faint elliptical nebula but showing a bright rim on the SW side.

185759.645+020706.00: Faint round nebula with a ring structure.

185815.852+073753.47: Well defined elliptical nebula.

185925.771+001734.64: Well defined elliptical nebula with a nearly rectangular shape.

190016.482+103406.96: Very faint and diffuse nebulosity around group of stars.

190115.597+114147.65: Faint round nebula.

190125.458+050857.78: Faint bipolar nebula.

190126.412+051438.83: Diffuse and faint nebulosity. No sign of symmetry.

190143.284-012937.15: Small elliptical nebula.

190155.126+011211.68: Faint and diffuse nebulosity. No sign of symmetry.

190227.285+020815.58: Diffuse and faint nebulosity with a SE straight rim ? ISM interaction ?

190228.149+020724.29: Straight nebulosity (also seen in 190227.285+020815.58) treated as independent object.

190319.157+142524.83: Diffuse and faint nebulosity. No sign of symmetry.

190338.530+104227.47: Large well defined semi-circular rim of nebula. The rim may show an ISM interaction in the NW direction. The coordinates are centred on the geometric centre.

190340.715+094640.06: Diffuse nebulosity. No obvious symmetry.

190346.793+050935.71: Diffuse nebulosity with an enhanced rim in the NW direction: ISM interaction ?

190349.023+045503.10: Diffuse and faint nebulosity. No sign of symmetry : SNR?

190356.250+050637.69: Diffuse and faint nebulosity. No sign of symmetry.

190417.986+084916.62: Well defined round nebula.

190418.623+050635.71: Faint and diffuse nebulosity near bright star.

190419.428+152126.59: Faint circular nebula with enhanced rim on the eastern side: ISM interaction?

190432.950+091656.68: Well defined round nebula.

190447.889+121844.58: Faint elliptical structure with a ring shape.

190454.065+101801.00: Faint round/elliptical nebula with a brighter enhancement towards the eastern direction: ISM interaction ?.

190502.989+034229.26: Faint elliptical structure with a ring shape.

190512.452+161347.55: Well defined faint and round nebula with enhanced rim on the western side: ISM interaction?

190543.810+064413.36: Faint round nebula.

190543.843+110018.55: Well defined round nebula.

190614.977-013318.62: Faint bipolar nebula with a brighter eastern side: ISM interaction?

190621.122+030050.24: Diffuse and faint nebulosity. No sign of symmetry.

190631.454-023237.58: Diffuse and faint nebulosity. No sign of symmetry.

190633.643+090720.49: Well defined faint and round nebula with a possible central star also visible.

190654.984+052216.03: Large semi-circular shell: ISM interaction ? or cirrus ?

190700.736+043041.07: Large semi-circular shell with a bright towards the eastern direction: ISM interaction ?

190701.948+014646.06: Diffuse and faint straight nebulosity.

190718.149+044056.11: Well defined elliptical/straight nebula.

190757.194+045445.80: Diffuse and faint nebulosity near bright star.

190759.374+050519.25: Diffuse and faint nebulosity.No sign of symmetry.

190812.756+143530.53: Diffuse and faint nebulosity.No sign of symmetry.

190816.778+052506.00: Well defined nebula but with no obvious symmetry: we classify it as elliptical.

190823.654+023302.00: Diffuse and faint nebulosity.

190852.186+031305.98: Faint and straight nebula with a possible central star.

191001.000+142203.90: Well defined round nebula.
191003.400+032224.00: Faint round nebulosity.
191017.437+065258.48: Well defined round nebula.
191022.104+110538.49: Well defined round nebula with a ring shape.
191027.415+034046.84: Faint round nebula.
191037.726+044403.00: Straight nebulosity .
191058.939+040350.41: Faint round nebula with a ring shape.
191104.751+060845.05: Bipolar nebula with NW and SE outflows .
191124.761+002743.94: Well defined bipolar nebula with opposite bright lobes and possible central star.
191255.483+143248.10: Faint round nebula with a ring shape.
191344.743+132212.36: Diffuse and faint nebulosity. No sign of symmetry.
191345.569+174752.34: Well defined round nebula.
191349.594+121841.73: Diffuse and faint nebulosity. No sign of symmetry.
191421.085+140936.27: Faint round/elliptical nebula with bright NW rim: ISM interaction ?
191445.100+133219.00: Well defined bipolar nebula.
191651.588+065607.00: Small faint nebulosity.
191707.129+020012.14: Faint round nebula.
191716.408+033447.34: Faint elliptical nebula.
191716.561+181518.20: Faint round nebula.
191725.028+205230.05: Straight nebulosity with possible extensions on its two sides.
191727.043+082036.00: Diffuse and compact nebulosity. No obvious symmetry.
191819.310+141320.70: Diffuse straight nebulosity .
191840.443+073131.30: Diffuse and faint nebulosity.
192026.428+120222.98: Diffuse and faint nebulosity.No obvious symmetry.
192038.895+160224.10: Diffuse and faint nebulosity with a bipolar symmetry ?
192043.747+052702.57: Diffuse and faint nebulosity.No obvious symmetry.
192140.402+155354.22: Well defined bipolar nebula with a butterfly shape .

- 192146.723+172053.35:** Well defined round nebula with a ring shape.
- 192150.054+145424.44:** Round nebulosity: independent structure or loop in HII/SNR ?
- 192152.039+135223.19:** Faint elliptical nebula.
- 192153.942+143056.21:** Well defined elliptical nebula with a ring shape. The extreme NW and SE rims are brighter than the rest of the nebula.
- 192213.116+161417.98:** Diffuse and faint nebulosity.No obvious symmetry.
- 192221.545+151550.81:** Well defined nebula with a bow-shock structure: ISM interaction.
- 192256.939+140700.52:** Diffuse and faint nebulosity.No obvious symmetry.
- 192320.640+164419.46:** Diffuse and faint nebulosity.No obvious symmetry.
- 192347.845+143642.99:** Well defined elliptical nebula, with central star ? .
- 192349.947+143330.25:** Irregular nebulosity with an apparently bipolar symmetry and an enhanced eastern side: ISM interaction ?
- 192410.570+133443.12:** Large bright arc: sign of ISM interaction ?
- 192429.557+202433.22:** Diffuse and faint nebulosity. No obvious symmetry.
- 192436.343+154402.00:** Faint elliptical/irregular nebulosity with a brighter SE rim: ISM interaction ?
- 192458.242+193434.94:** Faint round nebula.
- 192510.835+113353.58:** Well defined bipolar nebula.
- 192520.606+092410.76:** Straight/arc nebulosity : ISM interaction ?
- 192535.215+200336.23:** Faint round nebula.
- 192543.221+143546.30:** Faint circular nebula with a bright NE rim: ISM interaction ?
- 192615.422+191358.73:** Large round nebula.
- 192619.123+144814.56:** Diffuse and faint nebulosity. No obvious symmetry.
- 192624.662+195045.34:** Diffuse and faint nebulosity. No obvious symmetry.
- 192633.231+235726.79:** Diffuse and faint nebulosity. No obvious symmetry.
- 192644.309+243836.59:** Diffuse and faint nebulosity. No obvious symmetry.

192651.479+224524.09: Diffuse and faint nebulosity. No obvious symmetry.
192717.136+194308.47: Bright straight nebulosity .
192748.289+203712.37: Diffuse and faint nebulosity. No obvious symmetry.
192751.343+140127.18: Well defined round nebula with a ring shape .
192816.954+231911.22: Diffuse and faint nebulosity. No obvious symmetry.
192837.759+245024.82: Well defined elliptical/bipolar nebula with brighter NE and SW rims.
192847.100+093439.00: Well defined bipolar nebula.
192902.500+244646.30: Well defined round nebula.
192950.224+193426.38: Diffuse and faint nebulosity. No obvious symmetry.
193008.992+192137.49: “Bended” elliptical nebula with ring shape.
193014.182+190105.00: Diffuse and faint nebulosity. No obvious symmetry.
193023.149+181540.94: “Bright” round nebula.
193056.854+265845.87: Diffuse and faint nebulosity. No obvious symmetry.
193110.735+192904.00: Faint elliptical nebula with a ring shape .
193116.853+291232.68: Diffuse and faint nebulosity. No obvious symmetry.
193127.014+115622.93: Faint elliptical nebula .
193305.903+132921.05: Well defined round nebula with bright rim .
193308.903+155354.64: Generally faint round nebula but with brighter rim .
193334.416+175232.83: Small diffuse and faint nebulosity. No obvious symmetry.
193517.767+223121.46: Faint round nebula with possible central star .
193532.110+112115.64: Well defined round nebula .
193550.172+162850.22: Diffuse and faint nebulosity. No obvious symmetry.
193617.561+272051.62: Faint round nebula with possible central star .
193630.281+312810.64: Large semi-circular nebula: ISM interaction ?
193633.347+153348.66: Faint round nebula.
193637.297+123808.36: Large round nebula with a bright NE rim: ISM interaction ?
193718.757+202102.45: Well defined bipolar nebula .
193721.921+233607.09: Diffuse and faint nebulosity. No obvious symmetry.

- 193740.602+203548.72:** Irregular nebula with bow-shock structure inside.
- 193752.094+271119.96:** Faint elliptical nebula.
- 193809.161+205412.05:** Faint round nebula .
- 193827.898+265752.11:** Well defined round nebula.
- 193843.421+234949.58:** Diffuse and faint nebulosity. No obvious symmetry.
- 193849.653+313744.84:** Faint round nebula .
- 193912.000+251105.00:** Irregular nebula with bow-shock structure.
- 194038.557+123129.98:** Diffuse and faint nebulosity. No obvious symmetry.
- 194052.482+301711.13:** Diffuse and faint nebulosity. No obvious symmetry.
- 194204.900+231932.35:** Faint elliptical nebula with ring shape and bright rim on the SE direction: ISM interaction ?
- 194226.150+214521.73:** Well defined bipolar nebula with a possible central star, two outflows (NE and SW direction) and two bright rims (North and South).
- 194232.899+150034.17:** Faint round nebula.
- 194240.579+275109.00:** Faint semi-circular nebula: ISM interaction ?
- 194301.330+215424.90:** Well defined elliptical/bipolar nebula with brighter NE and SW rims.
- 194305.720+272343.30:** Diffuse and faint nebulosity. No obvious symmetry.
- 194332.571+234508.57:** Faint round nebula with with internal loop.
- 194339.948+203213.56:** Faint round/irregular nebulosity.
- 194359.500+170901.00:** Bright bipolar nebula.
- 194408.900+284845.90:** Diffuse and faint nebulosity. No obvious symmetry.
- 194409.130+280600.23:** Diffuse and faint nebulosity. No obvious symmetry.
- 194434.706+255540.16:** Bright irregular nebulosity.
- 194510.651+270929.52:** Elliptical nebula.
- 194533.810+210751.00:** Diffuse and faint nebulosity with a bright “condensation” inside. No obvious symmetry.
- 194550.107+313800.50:** Diffuse and faint nebulosity. No obvious symmetry.
- 194556.236+232833.65:** Faint elliptical/bipolar nebula with two opposite bright rims

on the northern side.

194610.918+170609.00: Faint irregular nebulosity with possible central star.

194620.611+342337.10: Diffuse and faint nebulosity. No obvious symmetry.

194633.002+231659.58: Well defined round nebula with possible spherical halo.

194638.447+235010.65: Large round/irregular nebulosity with possible ring shape.

194641.500+264820.50: Diffuse and faint nebulosity. No obvious symmetry.

194645.310+262211.51: Arc probably sign of pre-existing round nebula: ISM interaction ? Coordinates on geometric centre.

194727.587+230816.56: Faint round nebula with possible central star and enhanced SW rim .

194728.870+222823.81: Faint round nebula.

194730.500+250201.50: Faint round nebula near bright star.

194745.502+270150.69: Large and faint circular nebulosity.

194751.914+311818.12: Small well defined bipolar nebula.

194804.162+254847.70: Small irregular nebulosity with no obvious symmetry.

194810.612+280724.82: Diffuse and faint nebulosity. No obvious symmetry.

194815.014+280730.31: Well defined small nebula with nebular arc (remaining of circular nebula ?) on the western side.

194829.336+245355.30: Faint nebulosity .

194843.409+181830.18: Diffuse and faint nebulosity. No obvious symmetry.

194852.700+222516.92: Round nebula with brighter southern rim: ISM interaction ?

194853.738+181021.10: Well defined round nebula.

194905.200+181503.78: Diffuse and faint nebulosity. No obvious symmetry.

194930.984+273028.27: Faint round nebula.

194940.937+261521.18: Well defined bipolar nebula.

195011.446+264331.80: Faint nebulosity with a bright “condensation” inside. No obvious symmetry.

195015.963+272859.90: Elongated nebulosity: remaining of circular nebula interacting with the ISM ?

- 195032.628+272102.00:** Faint nebulosity .
- 195042.259+255949.97:** Diffuse and faint nebulosity. No obvious symmetry.
- 195057.134+272752.68:** Diffuse and faint nebulosity. No obvious symmetry.
- 195126.520+265838.73:** Well defined round/elliptical nebula.
- 195221.937+315901.70:** Faint elliptical/round nebula .
- 195248.826+255359.65:** Well defined bipolar nebula.
- 195318.494+371005.24:** Large filamentary nebula: SNR?.
- 195343.769+202636.22:** Diffuse and faint nebulosity with a nearly rectangular shape.
- 195357.881+312130.79:** Faint round nebula with a brighter northern rim: ISM interaction ?
- 195400.750+315551.29:** Well visible round nebula.
- 195436.449+313326.39:** Well defined round nebula with ring shape.
- 195529.340+294351.64:** Diffuse and faint nebulosity. No obvious symmetry.
- 195627.338+250648.55:** Very faint round nebula.
- 195657.600+265714.00:** Faint bipolar nebula.
- 195748.478+304343.12:** Diffuse and faint nebulosity with internal “condensation”.
No obvious symmetry.
- 195759.468+340119.54:** Diffuse and faint nebulosity. No obvious symmetry.
- 195815.133+340143.68:** Diffuse and faint nebulosity. No obvious symmetry.
- 195836.475+292314.67:** Small and faint bipolar nebula ?
- 195919.070+312534.06:** Small and bright irregular nebula.
- 195919.636+283827.07:** Large closed nebula (quasi-elliptical) with bright rim on the eastern side: ISM interaction or SNR ?
- 195957.456+395306.60:** Large and faint irregular nebulosity with bow-shock shape.
- 195958.200+332939.90:** Diffuse nebulosity with sharp structure inside .
- 200018.700+365934.00:** Well defined round nebula.
- 200149.462+392944.04:** Possible single faint round nebula .

Appendix C

Spectroscopic observations of candidate PNe located after RA=20h

During the spectroscopy follow-up, during the night and depending of the semester, we were able to observe the whole Northern Galactic plane and obtained spectra for candidate PNe located outside 18h to 20h boundaries (Table C.1 and Fig. C.1). We confirmed 12 nebulae as planetary nebulae. The remaining two objects are still unclear. IPHASX J203128.3+403810, which has a “spiral galaxy” shape has a complicated spectrum and more analysis will be done to see whether we are dealing with a PN or an HII region. IPHASX J231226.4+605813 has a bright CS and we did not see any nebular lines.

It was also possible to derive the distances for some objects (Table C.2 and Fig. C.2) and we can see that due to the lower level of extinction the determination of the distances is somehow easier and more accurate than near the Galactic Centre. Any non-determination is due either to the low $H\beta$ level (introducing too much error) or the unavailability of the extinction curves in the selected area.

Table C.1: List of 14 IPHAS nebulae with spectral data and localised between 20h and 00h in RA.

Name	Morphology	Size (in arcsec)	Name if known	Telescope
IPHASX J200018.7+365933	R	29	GN 19.58.5.03	INT
IPHASX J202946.1+354926	R	16		INT
IPHASX J203128.3+403810	B	32		WHT
IPHASX J203228.7+401712	I	42		INT
IPHASX J205013.7+465518	I	360		WHT
IPHASX J205527.3+390359	B	28	DSH J2055.4+3903	WHT
IPHASX J210205.9+471017	E	67	DSH J2102.1+4710	INT
IPHASX J212151.8+473301	B	28		INT
IPHASX J212201.3+550427	B	52	DSH J2122.0+5504	WHT
IPHASX J221118.2+552844	B	76		INT
IPHASX J231226.4+605813	R	54		INT
IPHASX J231303.4+591739	R	100	PN WeSb 6	WHT
IPHASX J233841.2+614145	E	60		INT
IPHASX J234403.8+603242	R	24		INT

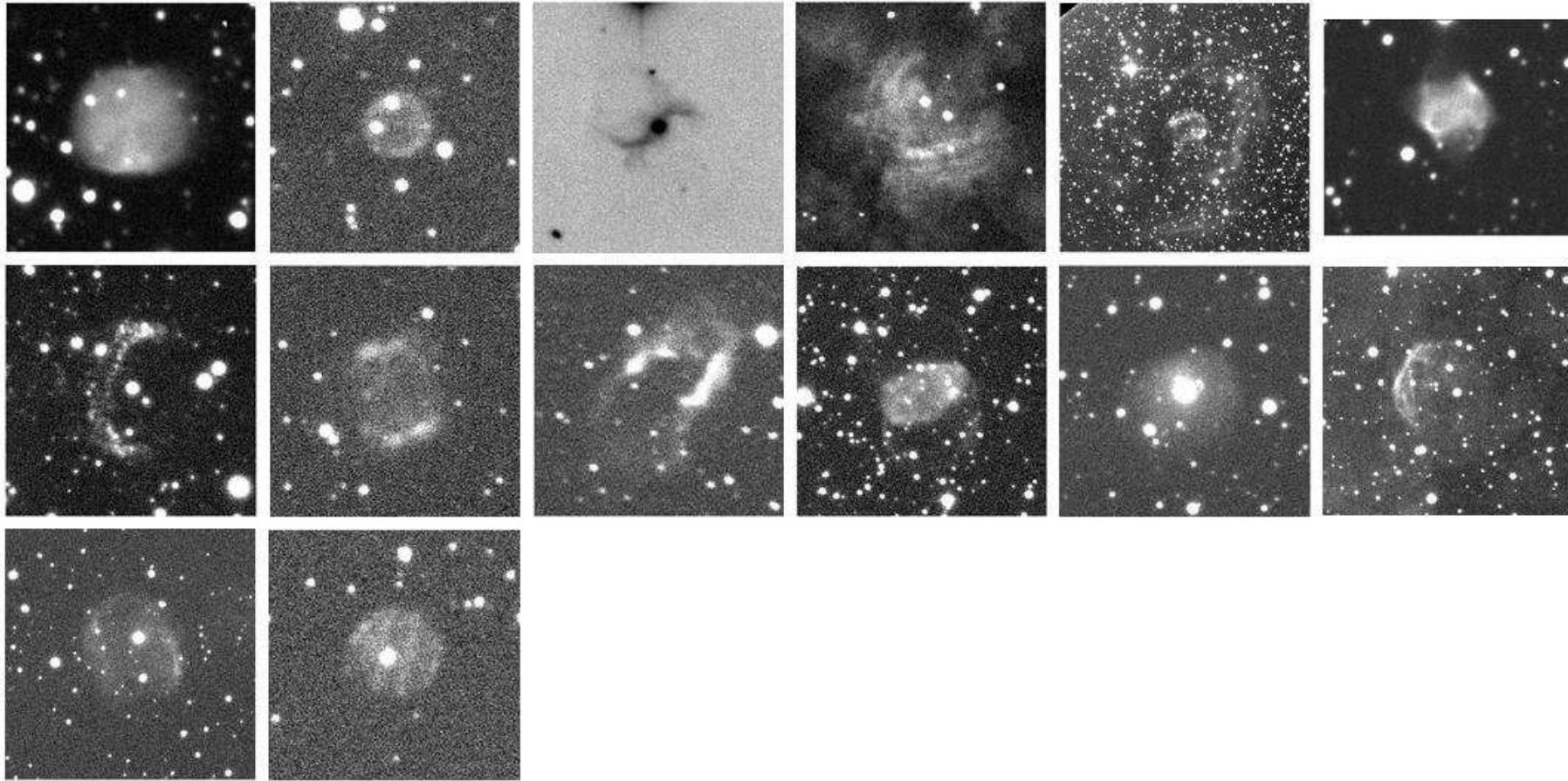


Figure C.1: $H\alpha$ IPHAS images of the nebulae with spectra in the 20h-7h region. From Top to Bottom and from Left to Right the nebulae are listed by ascending RA, see TableC.1. North on the top and East on the left.

Table C.2: Distances and extinction for some of the nebulae outside the 18h-20h boundary. “*” indicates that there is no available lower incertitude.

Name	cH β	Av	Distance (kpc)
IPHASX J203128.3+403810	1.78	3.61	1.3 ^{-0.6} _{+0.3}
IPHASX J205013.7+465518	1.06	2.10	3.2 ⁻¹ ₊₁
IPHASX J205527.3+390359	0.25	0.47	0.7 ^{-*} _{+0.6}
IPHASX J212151.8+473301	1.61	3.23	0.8 ^{-*} _{+0.9}
IPHASX J212201.3+550427	1.70	3.43	1.7 ^{-0.5} ₊₃
IPHASX J221118.2+552844	0.91	1.78	2.7 ⁻¹ ₊₁
IPHASX J231303.4+591739	0.51	0.98	0.8 ^{-0.5} _{+0.5}
IPHASX J234403.8+603242	1.26	2.51	0.8 ^{-0.2} _{+0.4}

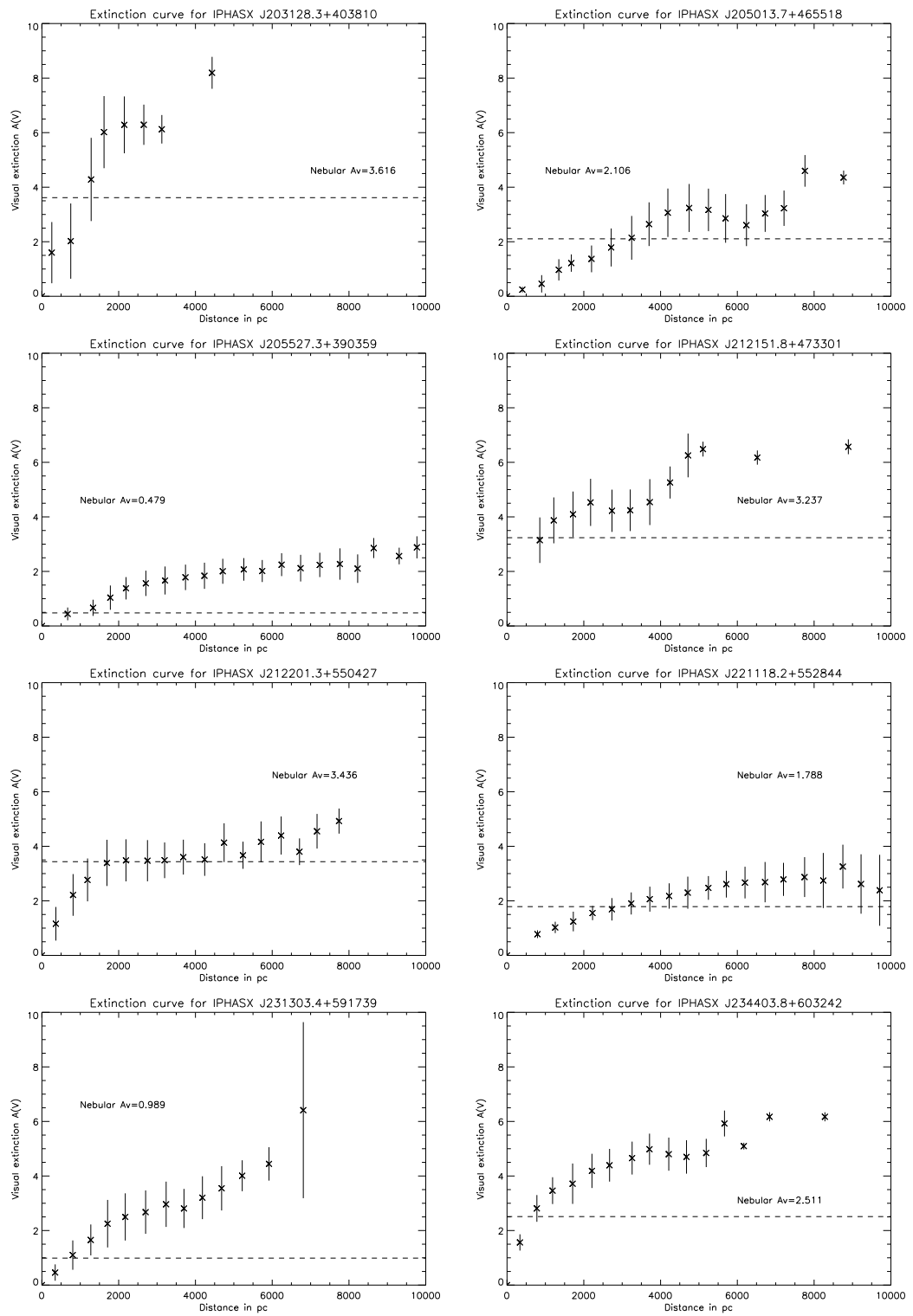


Figure C.2: Extinction curves of the main sequence stars in the direction of each of the nebulae allowing to retrieve their distances.

Appendix D

Spectra for each models obtained with CLOUDY

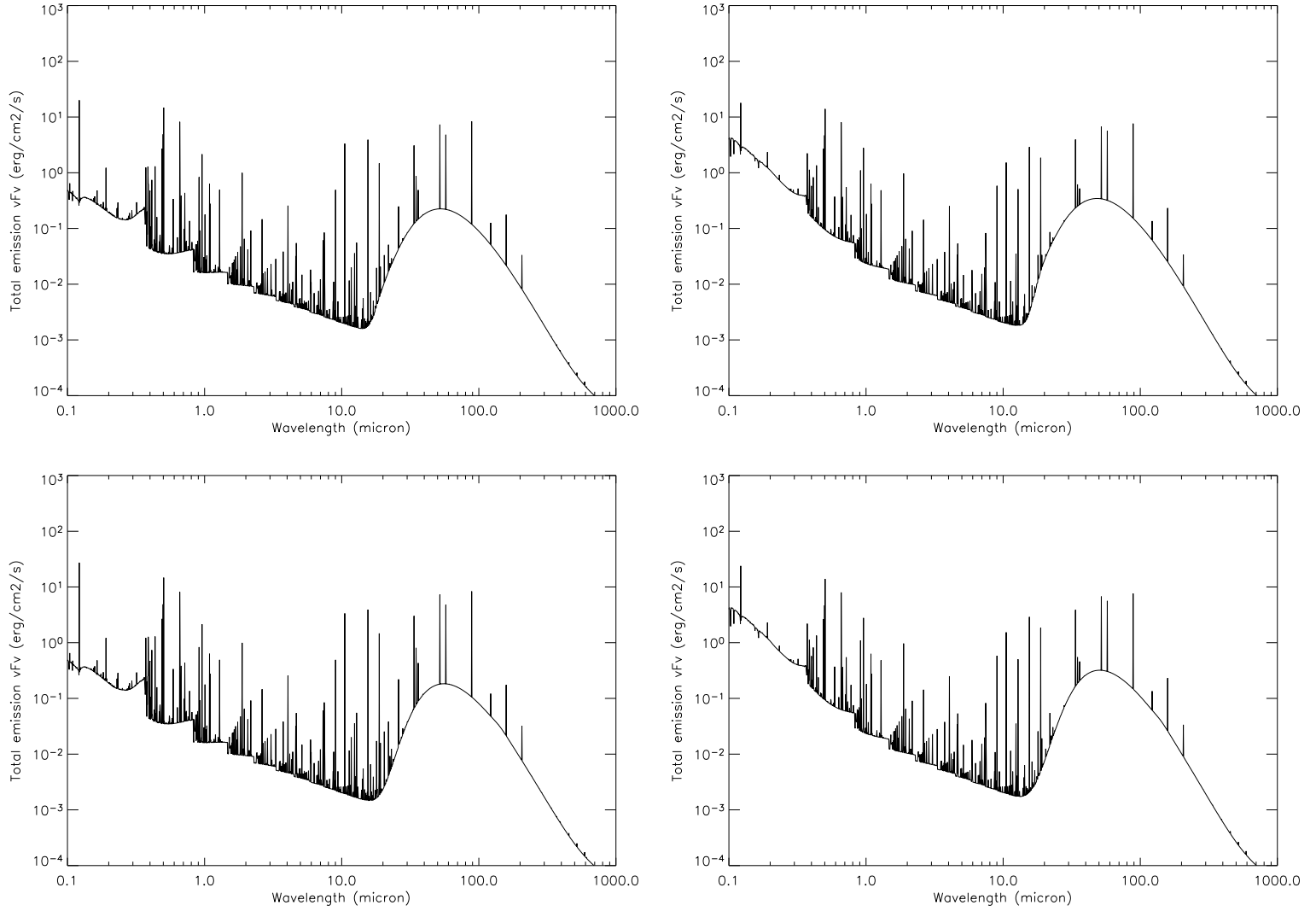


Figure D.1: CLOUDY model A for a density of 100 cm^{-3} : From left to right and top to bottom: Silicate & $T_{eff}=1e5 \text{ K}$, Silicate & $T_{eff}=5e4 \text{ K}$, Graphite & $T_{eff}=1e5 \text{ K}$ and Graphite & $T_{eff}=5e4 \text{ K}$.

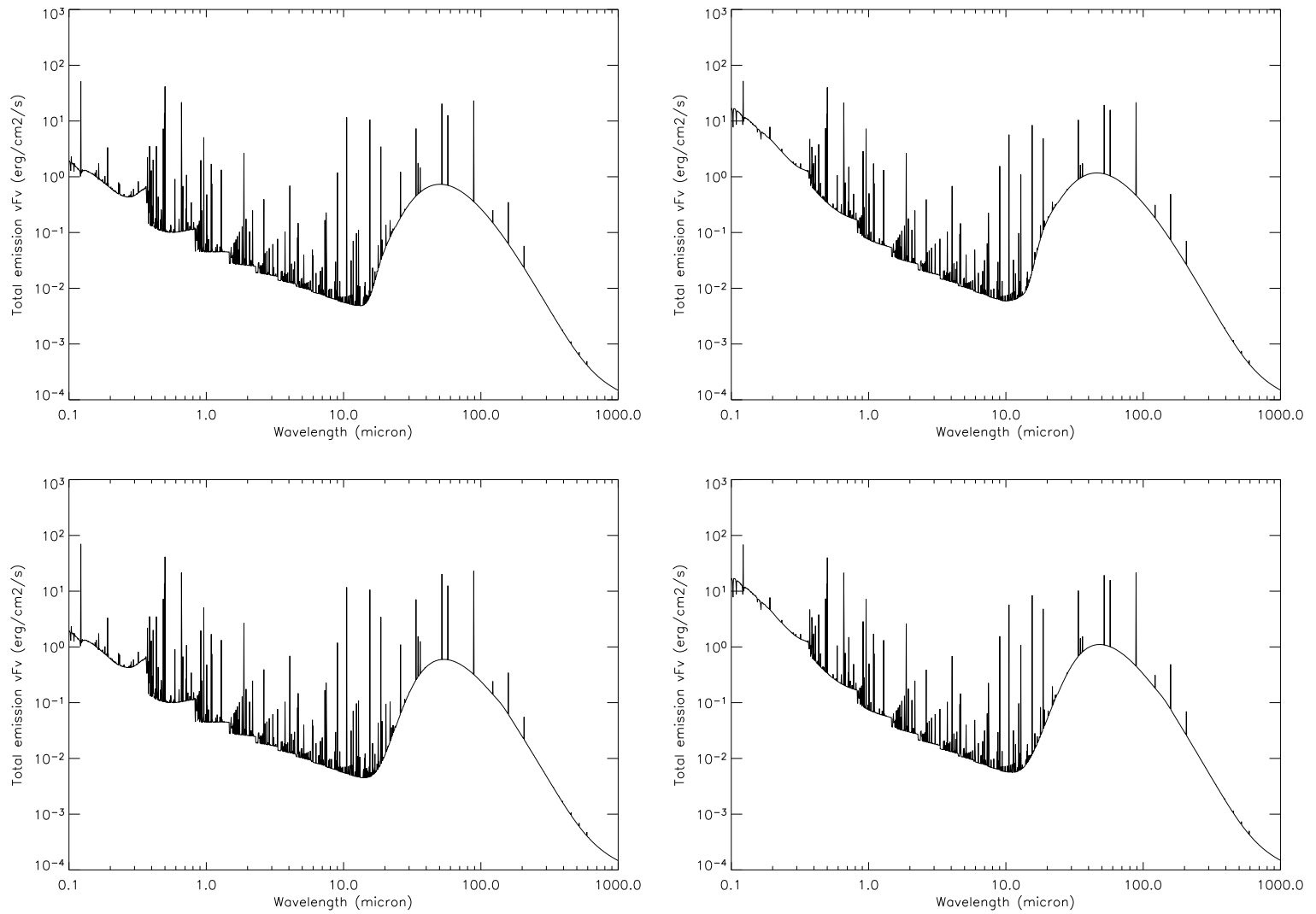


Figure D.2: CLOUDY model B for a density of 100 cm⁻³: From left to right and top to bottom: Silicate & $T_{eff}=1e5$ K, Silicate & $T_{eff}=5e4$ K, Graphite & $T_{eff}=1e5$ K and Graphite & $T_{eff}=5e4$ K.

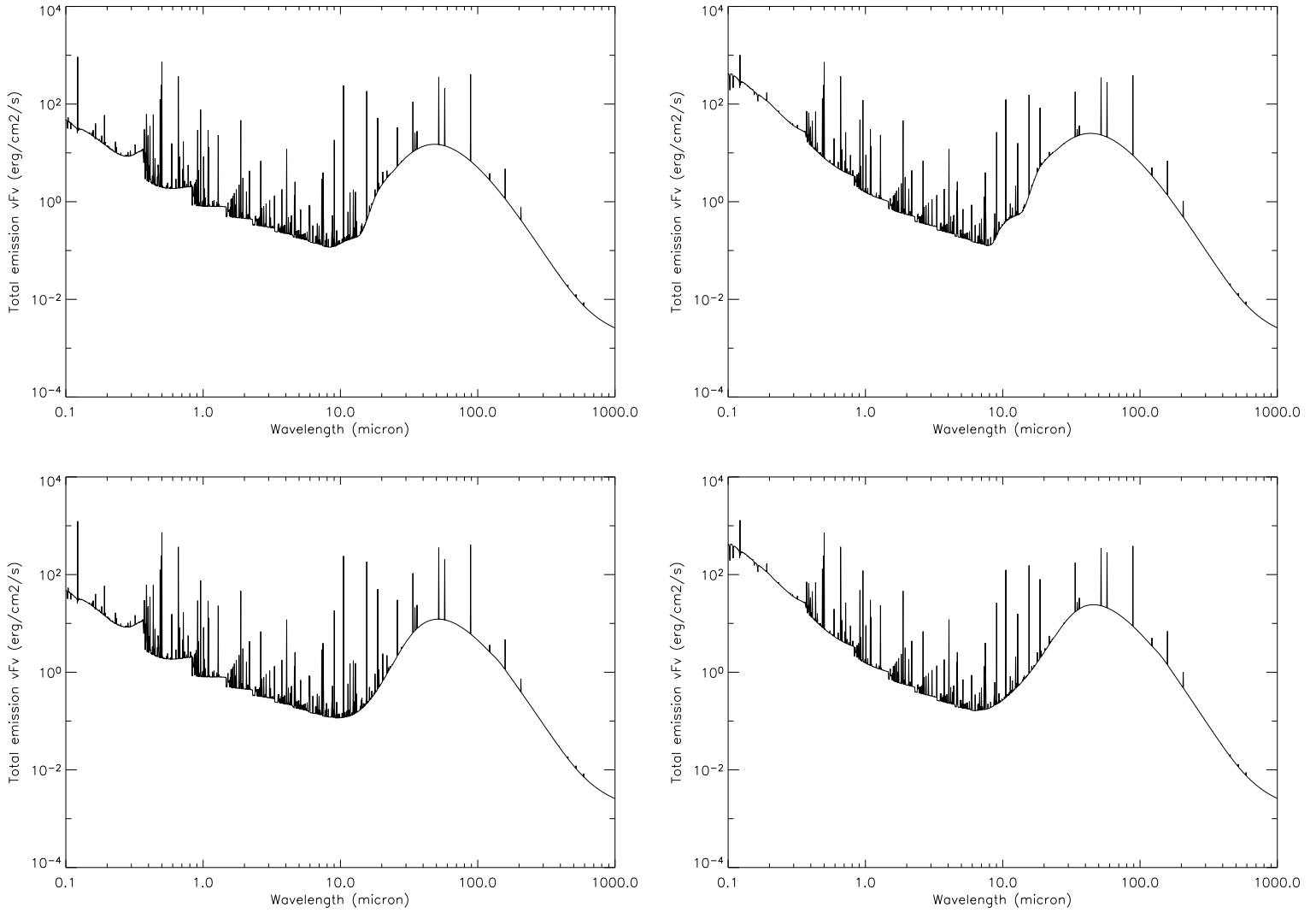


Figure D.3: CLOUDY model C for a density of 100 cm^{-3} : From left to right and top to bottom: Silicate & $T_{\text{eff}}=1e5 \text{ K}$, Silicate & $T_{\text{eff}}=5e4 \text{ K}$, Graphite & $T_{\text{eff}}=1e5 \text{ K}$ and Graphite & $T_{\text{eff}}=5e4 \text{ K}$.

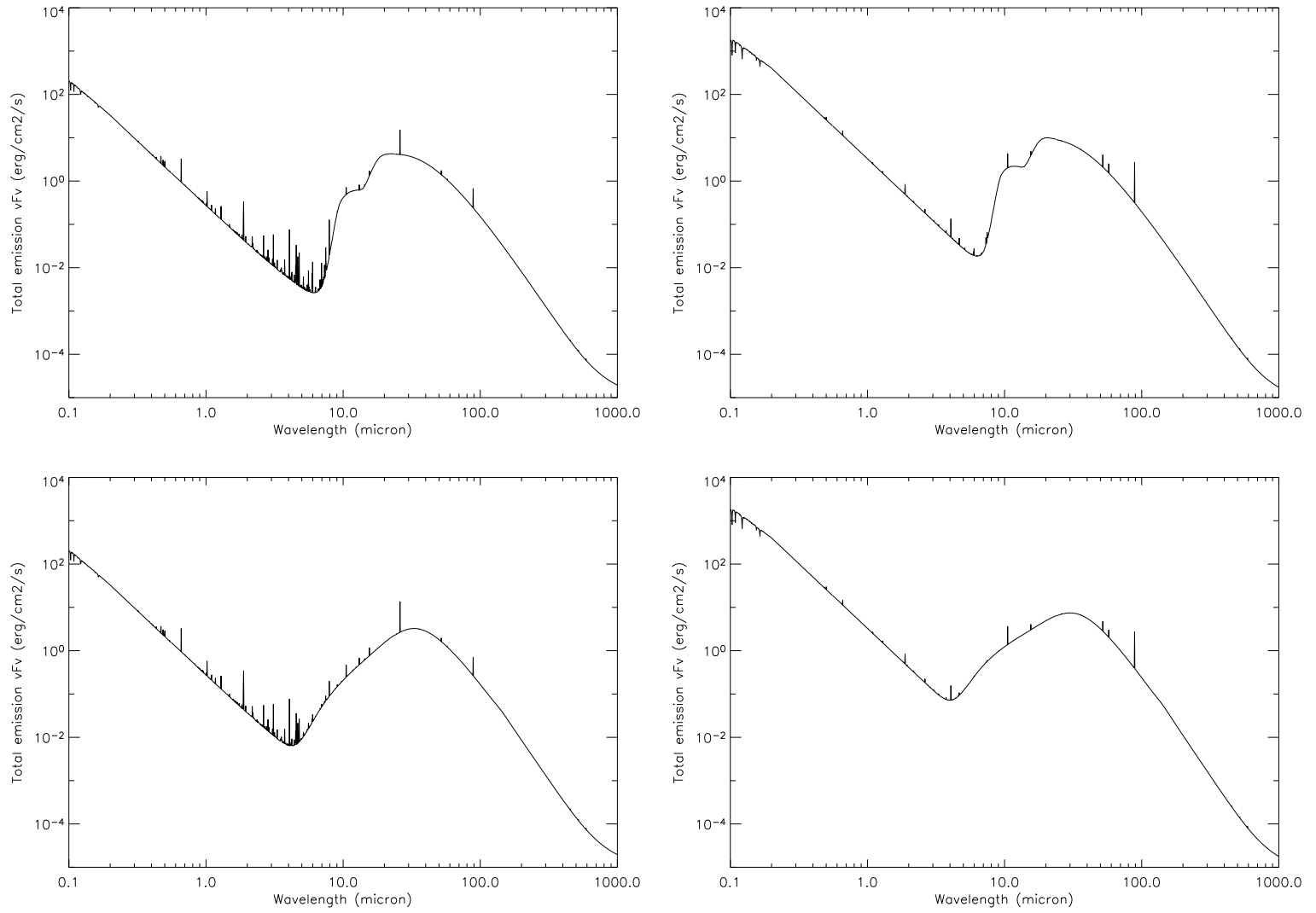


Figure D.4: CLOUDY model D for a density of 100 cm^{-3} : From left to right and top to bottom: Silicate & $T_{eff}=1e5$ K, Silicate & $T_{eff}=5e4$ K, Graphite & $T_{eff}=1e5$ K and Graphite & $T_{eff}=5e4$ K.

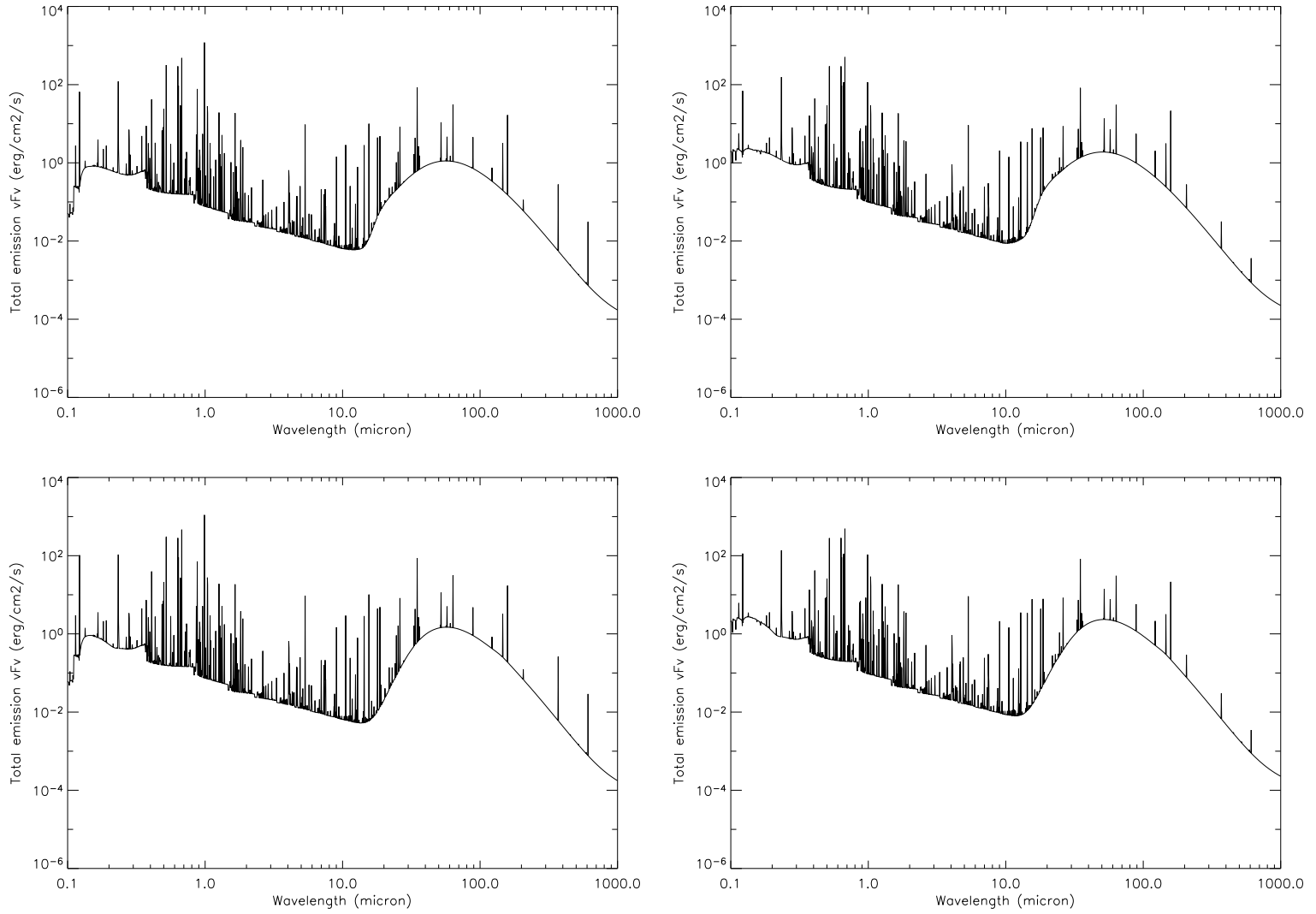


Figure D.5: CLOUDY model A for a density of 1000 cm^{-3} : From left to right and top to bottom: Silicate & $T_{eff}=1e5 \text{ K}$, Silicate & $T_{eff}=5e4 \text{ K}$, Graphite & $T_{eff}=1e5 \text{ K}$ and Graphite & $T_{eff}=5e4 \text{ K}$.

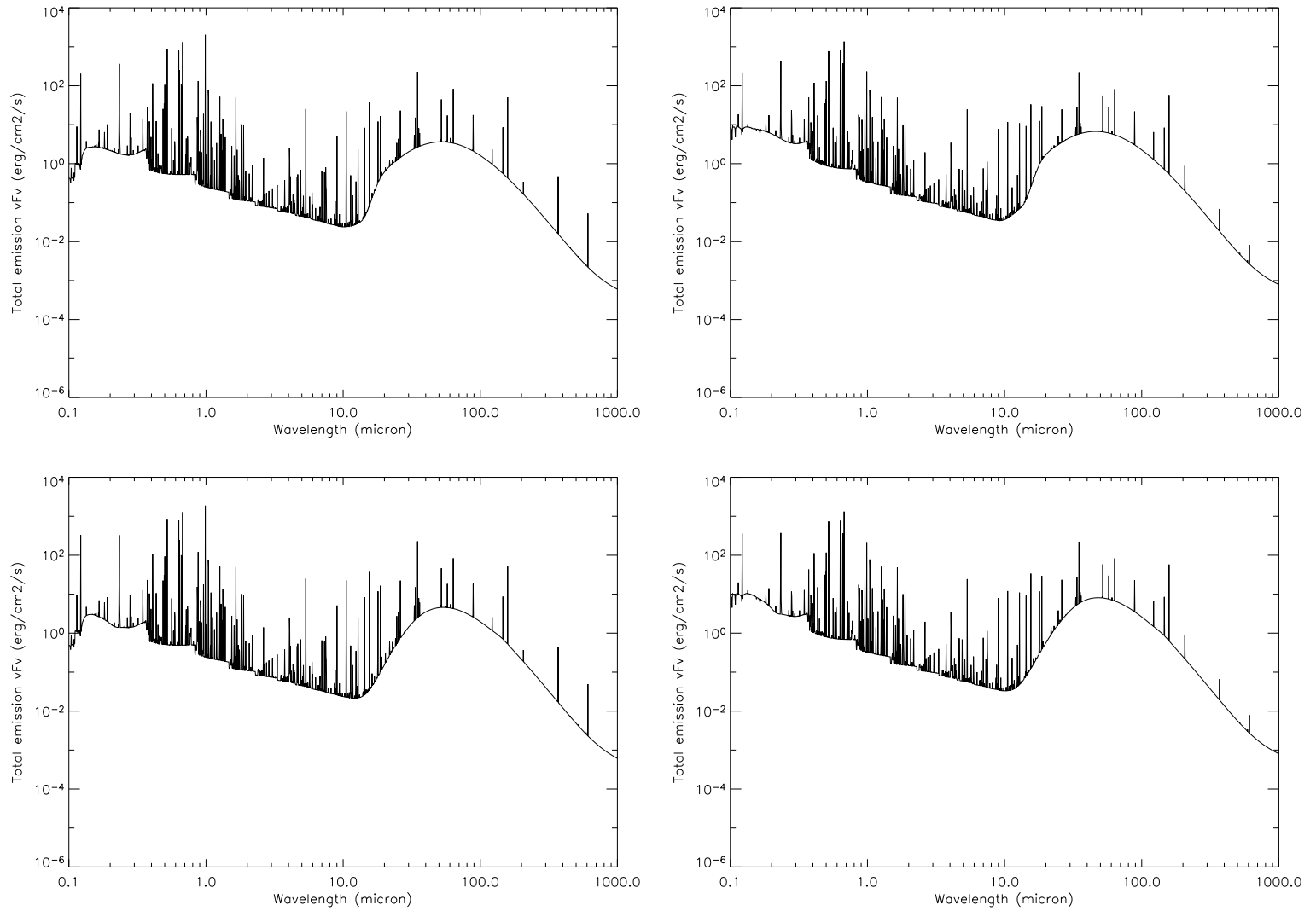


Figure D.6: CLOUDY model B for a density of 1000 cm^{-3} : From left to right and top to bottom: Silicate & $T_{eff}=1e5 \text{ K}$, Silicate & $T_{eff}=5e4 \text{ K}$, Graphite & $T_{eff}=1e5 \text{ K}$ and Graphite & $T_{eff}=5e4 \text{ K}$.

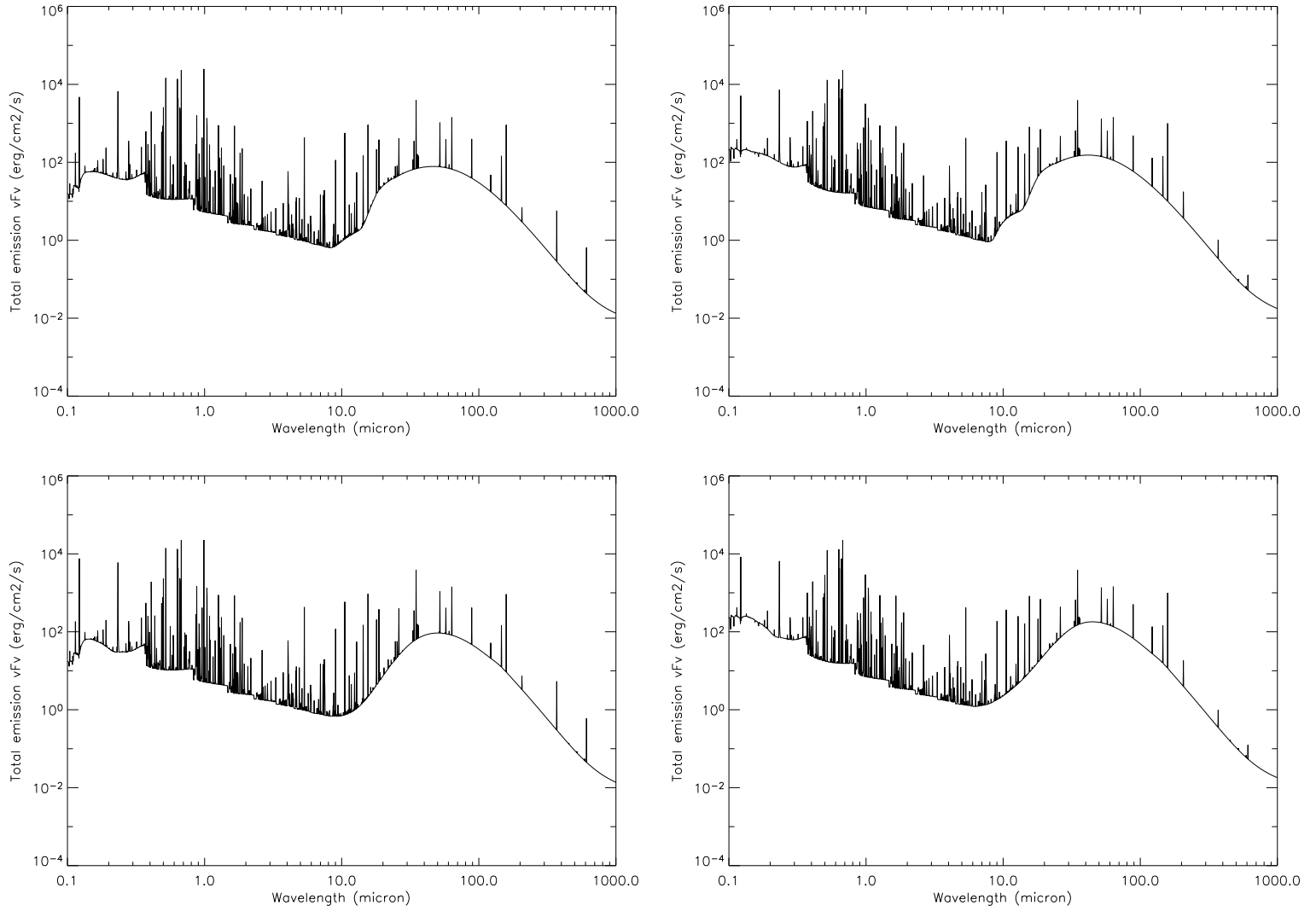


Figure D.7: CLOUDY model C for a density of 1000 cm^{-3} : From left to right and top to bottom: Silicate & $T_{eff}=1e5 \text{ K}$, Silicate & $T_{eff}=5e4 \text{ K}$, Graphite & $T_{eff}=1e5 \text{ K}$ and Graphite & $T_{eff}=5e4 \text{ K}$.

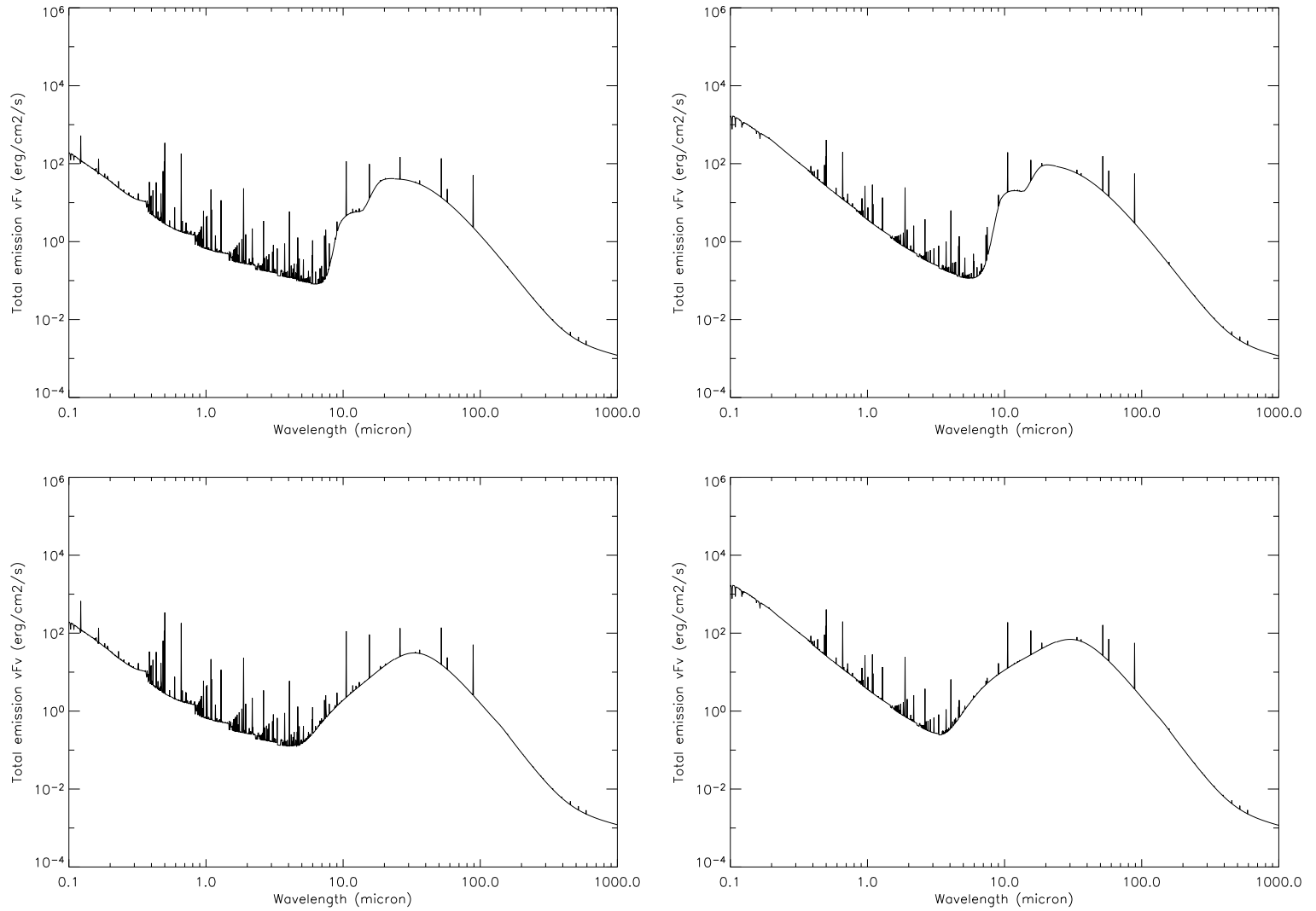


Figure D.8: CLOUDY model D for a density of 1000 cm^{-3} : From left to right and top to bottom: Silicate & $T_{eff}=1e5$ K, Silicate & $T_{eff}=5e4$ K, Graphite & $T_{eff}=1e5$ K and Graphite & $T_{eff}=5e4$ K.

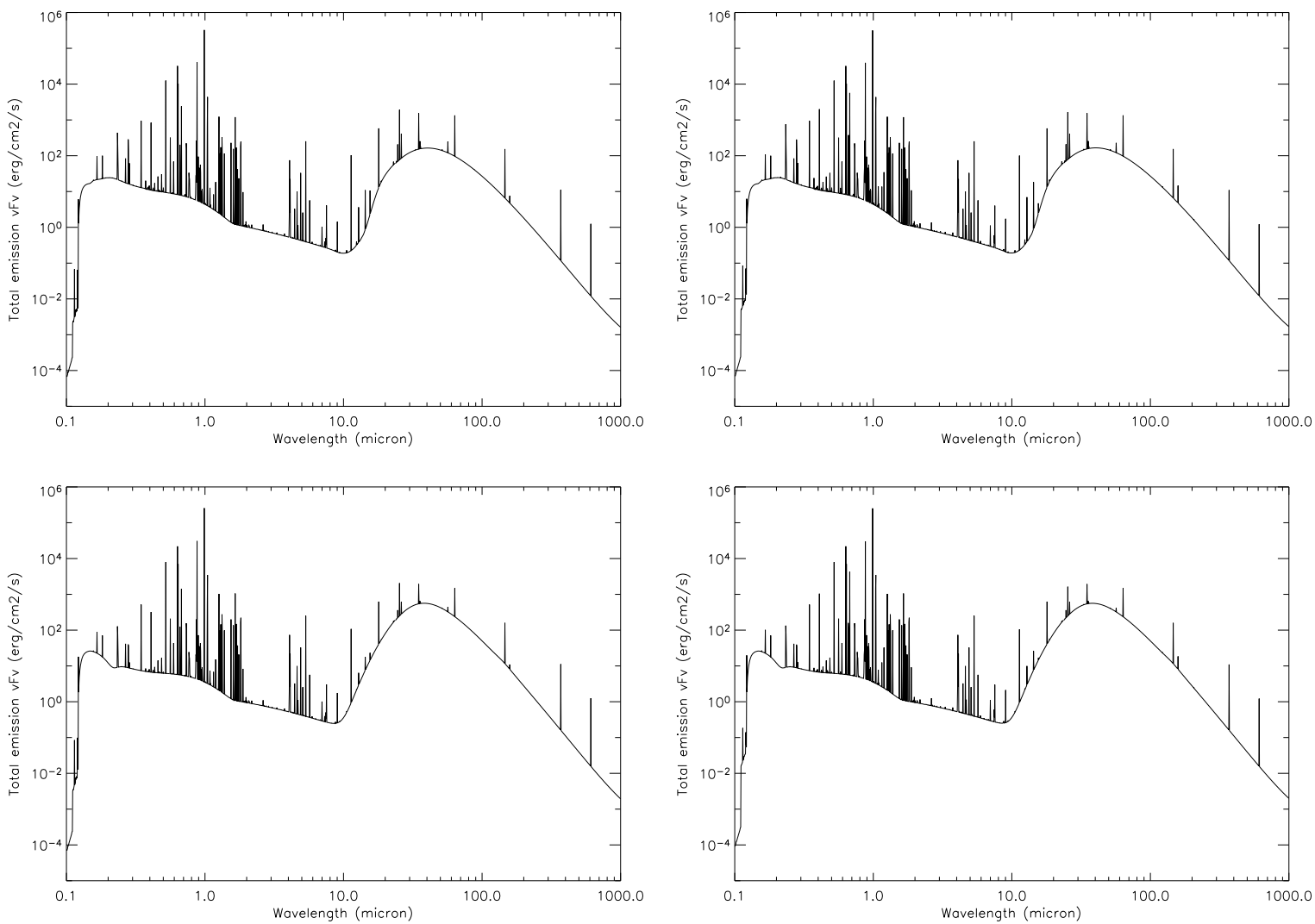


Figure D.9: CLOUDY model A for a density of 10000 cm^{-3} : From left to right and top to bottom: Silicate & $T_{eff}=1e5 \text{ K}$, Silicate & $T_{eff}=5e4 \text{ K}$, Graphite & $T_{eff}=1e5 \text{ K}$ and Graphite & $T_{eff}=5e4 \text{ K}$.

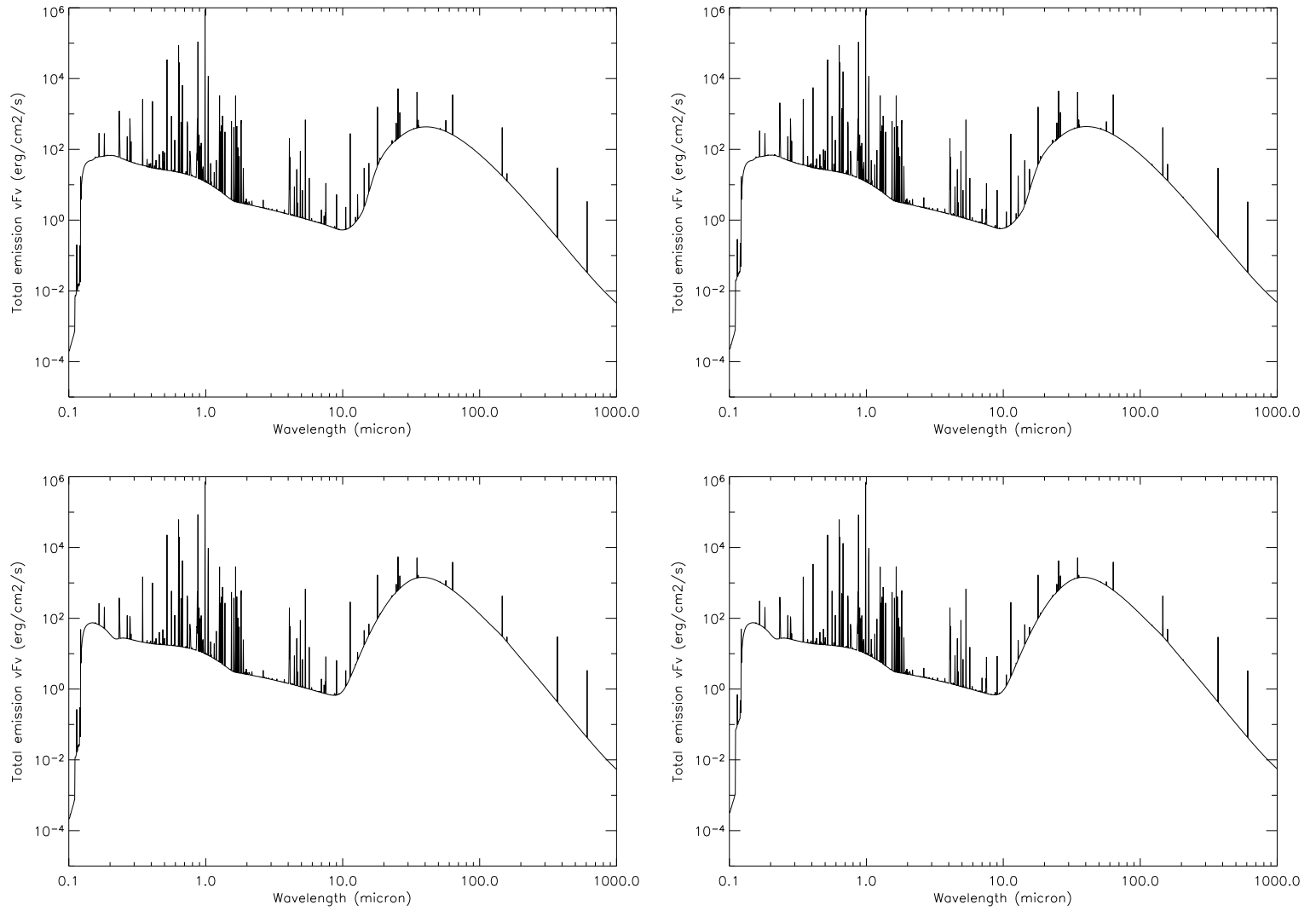


Figure D.10: CLOUDY model B for a density of 10000 cm⁻³: From left to right and top to bottom: Silicate & $T_{eff}=1e5$ K, Silicate & $T_{eff}=5e4$ K, Graphite & $T_{eff}=1e5$ K and Graphite & $T_{eff}=5e4$ K.

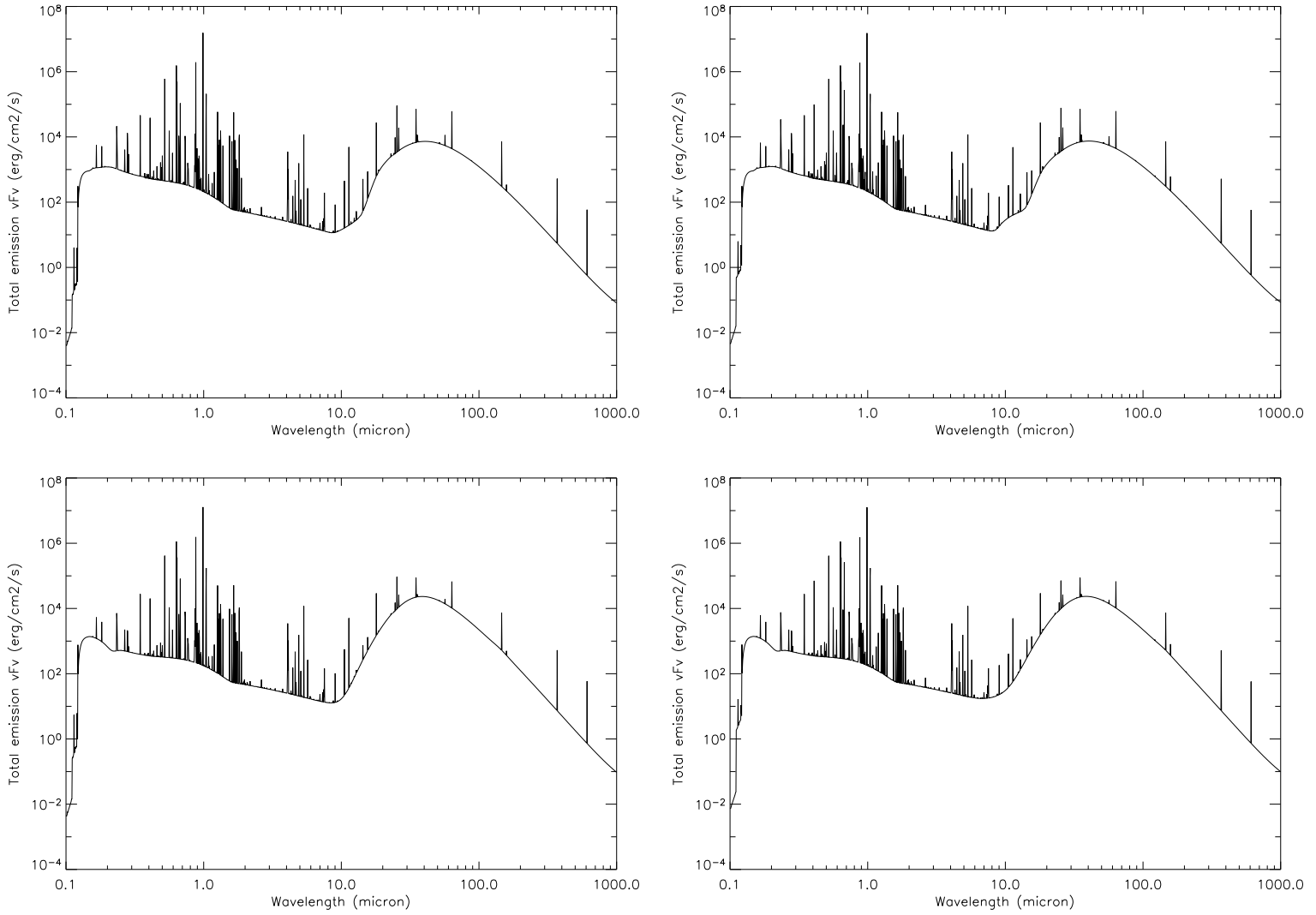


Figure D.11: CLOUDY model C for a density of 10000 cm^{-3} : From left to right and top to bottom: Silicate & $T_{eff}=1e5 \text{ K}$, Silicate & $T_{eff}=5e4 \text{ K}$, Graphite & $T_{eff}=1e5 \text{ K}$ and Graphite & $T_{eff}=5e4 \text{ K}$.

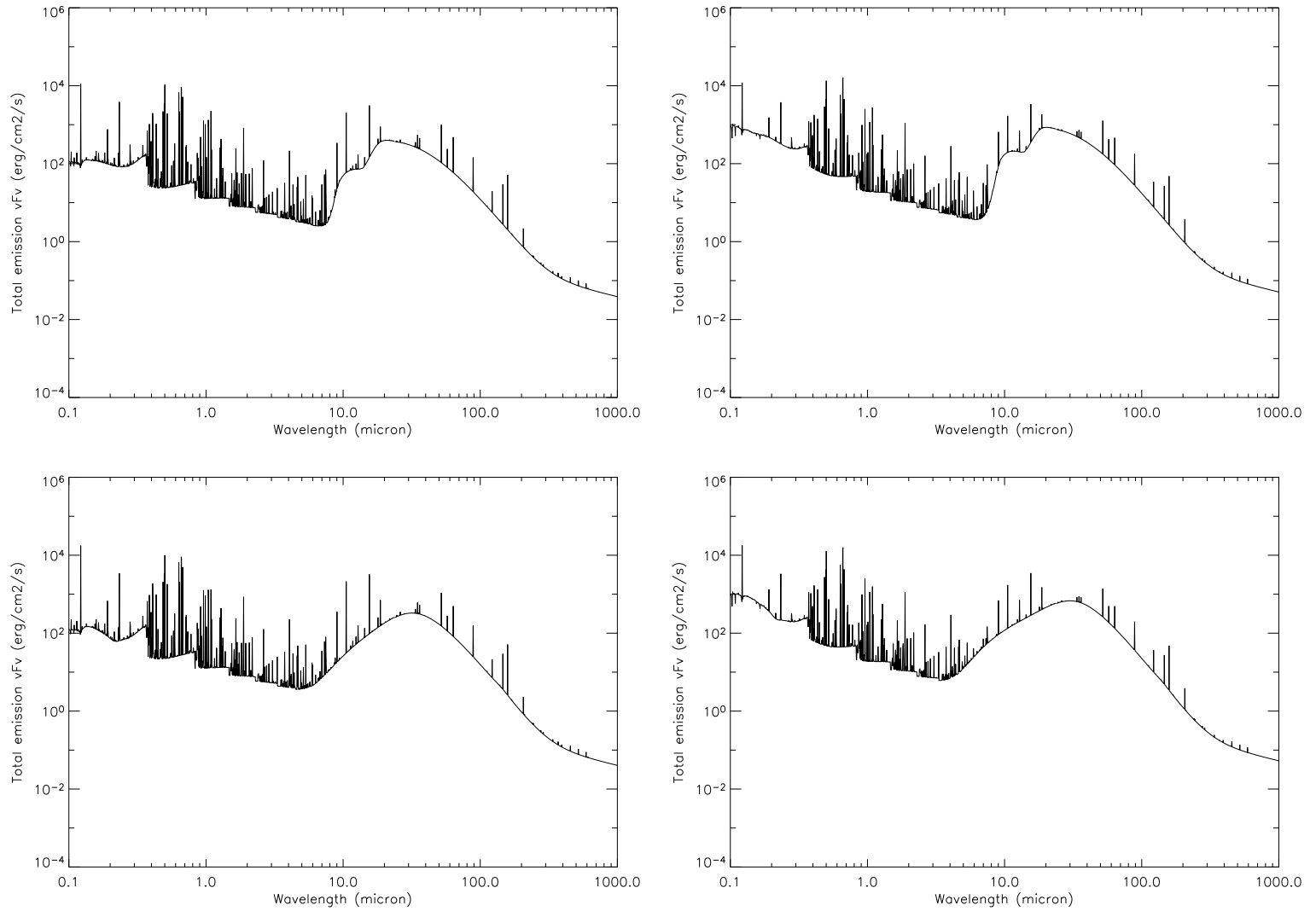


Figure D.12: CLOUDY model D for a density of 10000 cm⁻³: From left to right and top to bottom: Silicate & $T_{eff}=1e5$ K, Silicate & $T_{eff}=5e4$ K, Graphite & $T_{eff}=1e5$ K and Graphite & $T_{eff}=5e4$ K.

Appendix E

The case of the Supernovae Remnants

Throughout this thesis, we have mentioned several times the possibility for some objects to be SNRs rather than Planetary Nebulae. This claim was based, in the first instance, on morphological criteria (filamentary structure), and most of the candidates were observed to have a “medium-small” size (less than 20 arcmin). These dimensions are characteristic of rather young objects and we expect with IPHAS to discover more of these new outbursts. The other tools used to classify some nebulae as potential SNRs are the following:

- The presence of X-ray source(s) on the morphologically identified objects.
- The presence in the area of a young pulsar i.e. with an age lower than 10^6 years. The pulsars coordinates were obtained in the ATNF Pulsar Database¹ (Manchester et al. 2005), and we cross-correlated this list with the IPHAS mosaics.

So, in addition to the 17 known SNR found (Table E.1), we derived:

- Five nebulae with ROSAT X-Ray data from the bright sources (Voges et al. 1999) and faint sources catalogues (Voges et al. 2000) (these sources are not always on the nebula location) (Table E.2).
- Twelve pulsars showing a nebula in their surrounding regions. We also added 4 ob-

¹<http://www.atnf.csiro.au/research/pulsar/psrcat/>

Table E.1: The 17 known SNRs in the 18h-20h region.* This small SNR is linked to the pulsar PSR B1951+32 (or PSR J1952+3252) of age: $1.07e+05$ yrs.

Ra	Dec	Approx. Diameter (arcsec)	Name
18 51 24.534	-00 09 50.11	1258	SNR 032.8-00.1
18 51 32.804	-01 31 03.39	1286	SNR 031.5-00.6
18 52 09.684	+00 33 16.30	976	SNR 033.6+00.1
18 55 32.262	+01 28 46.32	1450	SNR 034.7-00.7
18 55 57.498	+01 21 51.85	2279	SNR 034.7-00.4
19 06 08.879	+10 30 10.37	2026	SNR 043.9+01.6
19 23 31.421	+14 07 24.09	1460	SNR 049.5-00.4
19 23 37.885	+14 06 47.71	1663	SNR 049.2-00.7
19 29 59.779	+18 46 58.81	2036	SNR 053.9+00.3
19 31 20.362	+19 23 36.13	4006	SNR 055.0+00.3
19 32 32.447	+19 14 56.79	4844	SNR 054.4-00.3
19 38 22.405	+17 15 39.72	1458	SNR 053.6-02.2
19 38 38.919	+24 23 07.92	2592	SNR 059.8+01.2
19 42 36.230	+23 37 28.19	4810	[TWG92]059.5+0.1
19 52 58.063	+32 52 45.83	80	SNR 69.0+2.7*
19 53 51.051	+32 42 44.22	5772	SNR 068.8+02.6
19 59 55.372	+32 34 41.24	10330	SNR 069.4+01.2

jects outside our initial search boundaries (Table E.3). One can see that the association of a pulsar to a candidate SNR is quite difficult as we are in a zone where SNR are quite numerous and also because it may have moved quite far from its original location. But the pulsar's youth is a guarantee that it is not linked to a large degree-scale SNR.

We underline that all the objects have not been classified as PN candidates.

Table E.2: SNR candidates with X-ray emission nearby and/or adequate morphology.* *Caveat: HII regions around.*

Ra	Dec	~Diameter (arcsec)	X-ray source	Offset (arcsec)	Count/s	Comments
19 25 43.22	+14 35 46.3	176	1RXS J192547.8+143612	71	1.56e-02	Inside nebula (round shell)
19 59 19.64	+28 38 27.1	520	1RXS J195944.9+284314	439	1.54e-02	Outside nebula
19 53 18.49	+37 10 05.2	416	1RXS J195313.0+372529	926	2.62e-02	Outside nebula (+filamentary structure)
18 52 23.14	+00 53 22.8	580	1RXS J185224.3+004148	695	6.25e-02	Outside nebula (+ sharp and filamentary structure)*
19 07 00.72	+04 30 41.1	1090	1RXS J190709.4+043100	131	3.95e-02	Inside semi circular area(also PN candidate)

Table E.3: Young Pulsars close to nebulae found within IPHAS. Notes: (1)(or wider: at 776'' on 19:04:57.065 +06:08:29.37 ?), (2)(or wider at 2858'' on 19:07:02.258 +03:00:30.52 ?)

Ra	Dec	Age (years)	Offset with nebular source (")	Comments on nebula
06 31 27.54	+10 37 02.2	4.36e+04	240''	circular structure
18 49 10.25	-00 40 20.00	9.56e+05	1200''	new SNR or known HII?
18 55 26.63	+03 07 20.2	7.4e+05	1039''	Centered on 18:55:16.083 +03:12:41.31
19 01 57.85	+05 10 34.00	3.13e+05	1800''	Centered on 19:03:49.02 +04:55:03.1
19 05 06.84	+06 16 16.7	1.16e+05	214''	Centered on 19:04:54.888 +06:13:34.15 (1)
19 07 14.54	+03 45 10.6	4.63e+05	2852''	Centered on 19:08:10.592 +03:52:38.42 (2)
19 13 50.82	+04 46 06.00	9.18e+04	780 ''	Centered on 19:14:03.09 +05:00:33.2,+filaments, 13' diameter
19 18 23.63	+14 45 06.00	8.81e+04	940 ''	Link to nebulosity centered at 19:18:41.298 +14:44:57.68
19 30 30.13	+18 52 14.1	2.89e+03	1116 ''	SNR 053.9+00.3 or independent small nebula at 19:29:40.234 +18:48:39.46 ?
20 02 04.42	+32 17 18.31	1.05e+05	1098 ''	Centered on 20:02:14.758 +32:13:33.99
20 21 04.50	+36 51 27.00	1.72e+04	1000 ''	Centered on 20:21:24.398 +36:54:17.68 or HII DWB 16
23 37 05.77	+61 51 01.69	4.09e+04	852 ''	SNR 114.3+00.3 or small structure at 23:37:26.914 +61:51:05.78

References

- A. Acker, J. Marcout, F. Ochsenbein, B. Stenholm, and R. Tylenda. *Strasbourg - ESO catalogue of galactic planetary nebulae. Part 1; Part 2*. Garching: European Southern Observatory, 1992, 1992.
- A. Acker, J. Marcout, and F. Ochsenbein. *First Supplement to the SECGPN*. Observatoire de Strasbourg, 1996.
- C. Alard. Image subtraction using a space-varying kernel. *A&AS*, 144:363–370, June 2000.
- C. Alard and R. H. Lupton. A Method for Optimal Image Subtraction. *ApJ*, 503: 325–+, August 1998. doi: 10.1086/305984.
- L. H. Aller and S. J. Czyzak. Chemical compositions of planetary nebulae. *ApJS*, 51: 211–247, February 1983. doi: 10.1086/190846.
- S. Bagnulo, T. Szeifert, G. A. Wade, J. D. Landstreet, and G. Mathys. Measuring magnetic fields of early-type stars with FORS1 at the VLT. *A&A*, 389:191–201, July 2002. doi: 10.1051/0004-6361:20020606.
- I. Bains, T. M. Gledhill, J. A. Yates, and A. M. S. Richards. MERLIN polarimetry of the OH masers in OH17.7-2.0. *MNRAS*, 338:287–302, January 2003. doi: 10.1046/j.1365-8711.2003.06071.x.
- I. Bains, T. M. Gledhill, A. M. S. Richards, and J. A. Yates. The Magnetic Field and Maser Structure in the Proto-Planetary Nebula IRAS 20406+2953. In *ASP Conf. Ser. 313: Asymmetrical Planetary Nebulae III: Winds, Structure and the Thunderbird*, pages 186–+, 2004.
- B. Balick. The evolution of planetary nebulae. I - Structures, ionizations, and morphological sequences. *AJ*, 94:671–678, September 1987. doi: 10.1086/114504.
- B. Balick and A. Frank. Shapes and Shaping of Planetary Nebulae. *ARA&A*, 40: 439–486, 2002. doi: 10.1146/annurev.astro.40.060401.093849.

- T. Barker. The ionization structure of planetary nebulae. IV - NGC 6853. *ApJ*, 284: 589–596, September 1984. doi: 10.1086/162441.
- C. Barnbaum, M. Morris, and C. Kahane. Evidence for Rapid Rotation of the Carbon Star V Hydrae. *ApJ*, 450:862–+, September 1995. doi: 10.1086/176190.
- C. A. Beichman, G. Neugebauer, H. J. Habing, P. E. Clegg, and T. J. Chester, editors. *Infrared astronomical satellite (IRAS) catalogs and atlases. Volume 1: Explanatory supplement*, volume 1, 1988.
- E. G. Blackman, A. Frank, J. A. Markiel, J. H. Thomas, and H. M. Van Horn. Dynamos in asymptotic-giant-branch stars as the origin of magnetic fields shaping planetary nebulae. *Nature*, 409:485–487, January 2001.
- H. Bond and P. Murdin. Binary Stars in Planetary Nebulae. *Encyclopedia of Astronomy and Astrophysics*, November 2000. doi: 10.1888/0333750888/2382.
- K. J. Borkowski, C. L. Sarazin, and N. Soker. Interaction of planetary nebulae with the interstellar medium. *ApJ*, 360:173–183, September 1990. doi: 10.1086/169106.
- D. Buckley and S. E. Schneider. The Ionized Masses of Planetary Nebulae. *ApJ*, 446: 279–+, June 1995. doi: 10.1086/175787.
- V. Bujarrabal, A. Castro-Carrizo, J. Alcolea, and C. Sánchez Contreras. Mass, linear momentum and kinetic energy of bipolar flows in protoplanetary nebulae. *A&A*, 377:868–897, October 2001. doi: 10.1051/0004-6361:20011090.
- J. H. Cahn, J. B. Kaler, and L. Stanghellini. A catalogue of absolute fluxes and distances of planetary nebulae. *A&AS*, 94:399–452, September 1992.
- J. A. Cardelli, G. C. Clayton, and J. S. Mathis. The relationship between infrared, optical, and ultraviolet extinction. *ApJ*, 345:245–256, October 1989. doi: 10.1086/167900.
- S. Casassus, P. F. Roche, and M. J. Barlow. The coronal line regions of planetary nebulae NGC 6302 and 6537: 3–13 μ m grating and echelle spectroscopy. *MNRAS*, 314:657–671, June 2000.
- S. J. Chan, T. Henning, and K. Schreyer. A catalogue of massive young stellar objects. *A&AS*, 115:285–+, February 1996.
- S. Chandrasekhar and E. Fermi. Magnetic Fields in Spiral Arms. *ApJ*, 118:113–+, July 1953.
- C. Charbonnel. Post-AGB Stars and PNe: Crucial Probes of Stellar Nucleosynthesis. In R. Szczerba, G. Stasinska, and S. K. Gorny, editors, *Planetary Nebulae as As-*

- tronomical Tools*, volume 804 of *American Institute of Physics Conference Series*, pages 117–123, November 2005. doi: 10.1063/1.2146246.
- R. Ciardullo, S. Sigurdsson, J. J. Feldmeier, and G. H. Jacoby. Close Binaries as the Progenitors of the Brightest Planetary Nebulae. *ApJ*, 629:499–506, August 2005. doi: 10.1086/431353.
- J. J. Condon and D. L. Kaplan. Planetary Nebulae in the NRAO VLA Sky Survey. *ApJS*, 117:361–+, July 1998. doi: 10.1086/313128.
- J. J. Condon, W. D. Cotton, E. W. Greisen, Q. F. Yin, R. A. Perley, G. B. Taylor, and J. J. Broderick. The NRAO VLA Sky Survey. *AJ*, 115:1693–1716, May 1998. doi: 10.1086/300337.
- R. L. M. Corradi and H. E. Schwarz. The kinematics of the high velocity bipolar nebulae NGC 6537 and HB 5. *A&A*, 269:462–468, March 1993.
- R. L. M. Corradi and H. E. Schwarz. Morphological populations of planetary nebulae: which progenitors? I. Comparative properties of bipolar nebulae. *A&A*, 293:871–888, January 1995.
- P. Cox, R. Lucas, P. J. Huggins, T. Forveille, R. Bachiller, S. Guilloteau, J. P. Maillard, and A. Omont. Multiple molecular outflows in AFGL 2688. *A&A*, 353:L25–L28, January 2000.
- P. Cox, P. J. Huggins, J.-P. Maillard, E. Habart, C. Morisset, R. Bachiller, and T. Forveille. High resolution near-infrared spectro-imaging of NGC 7027. *A&A*, 384:603–619, March 2002. doi: 10.1051/0004-6361:20011780.
- K. M. Cudworth. New proper motions, statistical parallaxes, and kinematics of planetary nebulae. *AJ*, 79:1384–1395, December 1974.
- L. Cuesta, J. P. Phillips, and A. Mampaso. The outflow structure of NGC 6537. *A&A*, 304:475–+, December 1995.
- S. Curiel. Radio Continuum Observations of Herbig-Haro Objects. In S. Lizano and J. M. Torrelles, editors, *Revista Mexicana de Astronomia y Astrofisica Conference Series*, volume 1 of *Revista Mexicana de Astronomia y Astrofisica Conference Series*, pages 59–+, April 1995.
- R. M. Cutri, M. F. Skrutskie, S. van Dyk, C. A. Beichman, J. M. Carpenter, T. Chester, L. Cambresy, T. Evans, J. Fowler, J. Gizis, E. Howard, J. Huchra, T. Jarrett, E. L. Kopan, J. D. Kirkpatrick, R. M. Light, K. A. Marsh, H. McCallon, S. Schneider, R. Stiening, M. Sykes, M. Weinberg, W. A. Wheaton,

- S. Wheelock, and N. Zacarias. *2MASS All Sky Catalog of point sources*. The IRSA 2MASS All-Sky Point Source Catalog, NASA/IPAC Infrared Science Archive. <http://irsa.ipac.caltech.edu/applications/Gator/>, June 2003.
- E. Daltabuit, S. Dodorico, and F. Sabbadin. A spectroscopic survey of supernova remnant candidates in the 6000-6800 Å spectral region - General discussion. *A&A*, 52:93–98, October 1976.
- O. De Marco. Binary central stars of planetary nebula. *ArXiv Astrophysics e-prints*, May 2006.
- O. De Marco and M. Moe. Common Envelope Evolution through Planetary Nebula Eyes. In R. Szczerba, G. Stasińska, and S. K. Gorny, editors, *Planetary Nebulae as Astronomical Tools*, volume 804 of *American Institute of Physics Conference Series*, pages 169–172, November 2005. doi: 10.1063/1.2146264.
- O. De Marco and M. Moe. Common envelope evolution through planetary nebula eyes. *ApJ*, *in press*, November 2006.
- O. De Marco, H. E. Bond, D. Harmer, and A. J. Fleming. Indications of a Large Fraction of Spectroscopic Binaries among Nuclei of Planetary Nebulae. *ApJL*, 602: L93–L96, February 2004. doi: 10.1086/382156.
- B. Dennison, J. H. Simonetti, and G. A. Topasna. An imaging survey of northern galactic H-alpha emission with arcminute resolution. *Publications of the Astronomical Society of Australia*, 15:147–48, April 1998.
- R. Dgani and N. Soker. Instabilities in Moving Planetary Nebulae. *ApJ*, 495:337–+, March 1998. doi: 10.1086/305257.
- J. M. Dickey and F. J. Lockman. H I in the Galaxy. *ARA&A*, 28:215–261, 1990. doi: 10.1146/annurev.aa.28.090190.001243.
- M. A. Dopita. Optical emission from shock waves. I - Abundances in N49. *ApJ*, 209: 395–401, October 1976.
- J. E. Drew, R. Greimel, M. J. Irwin, A. Aungwerojwit, M. J. Barlow, R. L. M. Corradi, J. J. Drake, B. T. Gänsicke, P. Groot, A. Hales, E. C. Hopewell, J. Irwin, C. Knigge, P. Leisy, D. J. Lennon, A. Mampaso, M. R. W. Mashed, M. Matsuura, L. Morales-Rueda, R. A. H. Morris, Q. A. Parker, S. Phillipps, P. Rodriguez-Gil, G. Roelofs, I. Skillen, J. L. Sokoloski, D. Steeghs, Y. C. Unruh, K. Viironen, J. S. Vink, N. A. Walton, A. Witham, N. Wright, A. A. Zijlstra, and A. Zurita. The INT Photometric H α Survey of the Northern Galactic Plane (IPHAS). *MNRAS*, 362:753–776,

- September 2005. doi: 10.1111/j.1365-2966.2005.09330.x.
- J. E. Drew, R. Greimel, M. J. Irwin, and S. E. Sale. Early-A stars from IPHAS, and their distribution in and around the Cyg OB2 association. *MNRAS*, 386:1761–1773, June 2008. doi: 10.1111/j.1365-2966.2008.13147.x.
- J. P. Emerson. IRAS Observations. In A. K. Dupree and M. T. V. T. Lago, editors, *NATO ASIC Proc. 241: Formation and Evolution of Low Mass Stars*, pages 193–+, 1988.
- D. Falceta-Gonçalves, A. Lazarian, and G. Kowal. Studies of Regular and Random Magnetic Fields in the ISM: Statistics of Polarization Vectors and the Chandrasekhar-Fermi Technique. *ApJ*, 679:537–551, May 2008. doi: 10.1086/587479.
- G. J. Ferland, K. T. Korista, D. A. Verner, J. W. Ferguson, J. B. Kingdon, and E. M. Verner. CLOUDY 90: Numerical Simulation of Plasmas and Their Spectra. *PASP*, 110:761–778, July 1998.
- A. S. Ferrarotti and H.-P. Gail. Mineral formation in stellar winds. II. Effects of Mg/Si abundance variations on dust composition in AGB stars. *A&A*, 371:133–151, May 2001. doi: 10.1051/0004-6361:20010316.
- A. S. Ferrarotti and H.-P. Gail. Mineral formation in stellar winds. III. Dust formation in S stars. *A&A*, 382:256–281, January 2002. doi: 10.1051/0004-6361:20011580.
- Katia M. Ferrière. The interstellar environment of our galaxy. *Rev. Mod. Phys.*, 73(4): 1031–1066, Dec 2001. doi: 10.1103/RevModPhys.73.1031.
- E. L. Fitzpatrick. Correcting for the Effects of Interstellar Extinction. *PASP*, 111: 63–75, January 1999.
- D. J. Frew and Q. A. Parker. Towards a New Distance Scale and Luminosity Function for Nearby Planetary Nebulae. In M. J. Barlow and R. H. Méndez, editors, *Planetary Nebulae in our Galaxy and Beyond*, volume 234 of *IAU Symposium*, pages 49–54, 2006. doi: 10.1017/S1743921306002742.
- D. R. Garnett and H. L. Dinerstein. Spatially Resolved O II Recombination Line Observations of the Ring Nebula, NGC 6720. *ApJ*, 558:145–156, September 2001. doi: 10.1086/322452.
- J. E. Gaustad, P. R. McCullough, W. Rosing, and D. Van Buren. A Robotic Wide-Angle H α Survey of the Southern Sky. *PASP*, 113:1326–1348, November 2001.
- Y. P. Georgelin and Y. M. Georgelin. Régions H II de l’hémisphère austral. *A&AS*, 3:

- 1–+, November 1970.
- K. Gesicki and A. A. Zijlstra. Central Stars of Planetary Nebulae. In R. Napiwotzki and M. R. Burleigh, editors, *15th European Workshop on White Dwarfs*, volume 372 of *Astronomical Society of the Pacific Conference Series*, pages 41–+, September 2007.
- F. C. Gillett, F. J. Low, and W. A. Stein. Infrared Observations of the Planetary Nebula NGC 7027. *ApJL*, 149:L97+, September 1967. doi: 10.1086/180066.
- E. A. Gonzalez-Solares, N. A. Walton, R. Greimel, J. E. Drew, M. J. Irwin, S. E. Sale, K. Andrews, A. Aungwerojwit, M. J. Barlow, E. van den Besselaar, R. L. M. Corradi, B. T. Gaensicke, P. J. Groot, A. S. Hales, E. C. Hopewell, H. Hu, J. Irwin, C. Knigge, E. Lagadec, P. Leisy, J. R. Lewis, A. Mampaso, M. Matsuura, B. Moont, L. Morales-Rueda, R. A. H. Morris, T. Naylor, Q. A. Parker, P. Prema, S. Pyrzas, G. T. Rixon, P. Rodriguez-Gil, G. Roelofs, L. Sabin, I. Skillen, J. Suso, R. Tata, K. Viironen, J. S. Vink, A. Witham, N. J. Wright, A. A. Zijlstra, A. Zurita, J. Drake, J. Fabregat, D. J. Lennon, P. W. Lucas, E. L. Martin, D. Steeghs, and Y. C. Unruh. Initial Data Release from the INT Photometric H-alpha Survey of the Northern Galactic Plane (IPHAS). *ArXiv e-prints*, 712, December 2007.
- S. K. Gorny, G. Stasinska, and R. Tylenda. Planetary nebulae morphologies, central star masses and nebular properties. *A&A*, 318:256–268, February 1997.
- M. Goto, N. Kobayashi, H. Terada, and A. T. Tokunaga. Imaging and Spatially Resolved Spectroscopy of AFGL 2688 in the Thermal Infrared Region. *ApJ*, 572:276–287, June 2002. doi: 10.1086/340194.
- J. S. Greaves. Toroidal magnetic fields around planetary nebulae. *A&A*, 392:L1–L4, September 2002. doi: 10.1051/0004-6361:20021002.
- J. S. Greaves, W. S. Holland, N. R. Minchin, A. G. Murray, and J. A. Stevens. Submillimetre polarization and constraints on dust grain alignment. *A&A*, 344:668–674, April 1999.
- J. S. Greaves, W. S. Holland, T. Jenness, A. Chrysostomou, D. S. Berry, A. G. Murray, M. Tamura, E. I. Robson, P. A. R. Ade, R. Nartallo, J. A. Stevens, M. Momose, J.-I. Morino, G. Moriarty-Schieven, F. Gannaway, and C. V. Haynes. A submillimetre imaging polarimeter at the James Clerk Maxwell Telescope. *MNRAS*, 340:353–361, April 2003. doi: 10.1046/j.1365-8711.2003.06230.x.
- M. A. Guerrero. Planetary Nebulae and Their Central Stars in the X-ray and EUV Regions. In M. J. Barlow and R. H. Méndez, editors, *Planetary Nebulae in our*

- Galaxy and Beyond*, volume 234 of *IAU Symposium*, pages 153–160, 2006. doi: 10.1017/S1743921306002900.
- C. S. Gum. A survey of southern HII regions. *MmRAS*, 67:155–177, 1955.
- A. Gutierrez-Moreno. Planetary Nebulae and Symbiotic Stars. In V. M. Blanco and M. M. Phillips, editors, *Progress and Opportunities in Southern Hemisphere Optical Astronomy. The CTIO 25th Anniversary Symposium*, volume 1 of *Astronomical Society of the Pacific Conference Series*, pages 12–+, 1988.
- A. Gutierrez-Moreno, H. Moreno, and G. Cortes. A Diagnostic Diagram for Planetary Nebulae and Symbiotic Stars. *PASP*, 107:462–+, May 1995.
- A. L. Gyul’Budagyan and T. Y. Magakyan. New interesting nebulous objects. *Astronomicheskij Tsirkulyar*, 953:1–2, 1977.
- L. M. Haffner, R. J. Reynolds, S. L. Tufte, G. J. Madsen, K. P. Jaehnig, and J. W. Percival. The Wisconsin H α Mapper Northern Sky Survey. *ApJS*, 149:405–422, December 2003. doi: 10.1086/378850.
- J. P. Harrington, D. J. Monk, and R. E. S. Clegg. Thermal infrared emission by dust in the planetary nebula NGC 3918 - A model analysis of IRAS observations. *MNRAS*, 231:577–595, April 1988.
- H. Hartl and S. B. Tritton. New planetary nebulae of low surface brightness detected on UK-Schmidt plates. *A&A*, 145:41–44, April 1985.
- R. H. Hildebrand. Problems in Far-Infrared Polarimetry. In W. G. Roberge and D. C. B. Whittet, editors, *ASP Conf. Ser. 97: Polarimetry of the Interstellar Medium*, pages 254–+, 1996.
- R. H. Hildebrand, J. A. Davidson, J. L. Dotson, C. D. Dowell, G. Novak, and J. E. Vailancourt. A Primer on Far-Infrared Polarimetry. *PASP*, 112:1215–1235, September 2000.
- W. S. Holland, E. I. Robson, W. K. Gear, C. R. Cunningham, J. F. Lightfoot, T. Jenness, R. J. Ivison, J. A. Stevens, P. A. R. Ade, M. J. Griffin, W. D. Duncan, J. A. Murphy, and D. A. Naylor. SCUBA: a common-user submillimetre camera operating on the James Clerk Maxwell Telescope. *MNRAS*, 303:659–672, March 1999.
- P. J. Huggins and S. P. Manley. Filaments as Possible Signatures of Magnetic Field Structure in Planetary Nebulae. *PASP*, 117:665–675, July 2005. doi: 10.1086/430576.
- I. Iben, Jr. and A. V. Tutukov. Binary stars and planetary nebulae. In S. Torres-

- Peimbert, editor, *Planetary Nebulae*, volume 131 of *IAU Symposium*, pages 505–522, 1989.
- M. Irwin and J. Lewis. INT WFS pipeline processing. *New Astronomy Review*, 45: 105–110, January 2001a.
- M. Irwin and J. Lewis. INT WFS pipeline processing. *New Astronomy Review*, 45: 105–110, January 2001b.
- H. M. Johnson. Symmetric Galactic Nebulae. *ApJ*, 121:604–+, May 1955.
- H. M. Johnson. Symmetric Galactic Nebulae. II. *ApJ*, 124:90–+, July 1956.
- S. Jordan, K. Werner, and S. J. O’Toole. Discovery of magnetic fields in central stars of planetary nebulae. *A&A*, 432:273–279, March 2005. doi: 10.1051/0004-6361:20041993.
- M. Jura and S. G. Kleinmann. Short- and intermediate-period oxygen-rich Miras. *ApJS*, 79:105–121, March 1992a. doi: 10.1086/191646.
- M. Jura and S. G. Kleinmann. Oxygen-rich semiregular and irregular variables. *ApJS*, 83:329–349, December 1992b. doi: 10.1086/191740.
- J. B. Kaler. A catalog of relative emission line intensities observed in planetary and diffuse nebulae. *ApJS*, 31:517–688, August 1976.
- J. B. Kaler and J. H. Lutz. Dust-distances to planetary nebulae. *PASP*, 97:700–706, August 1985.
- J. B. Kaler, R. A. Shaw, and K. B. Kwitter. Large planetary nebulae and their significance to the late stages of stellar evolution. *ApJ*, 359:392–418, August 1990. doi: 10.1086/169073.
- J. H. Kastner. X-ray Emission from Planetary Nebulae and their Central Stars: a Status Report. *ArXiv e-prints*, 709, September 2007.
- J. H. Kastner and N. Soker. The Egg Nebula (AFGL 2688): Deepening Enigma. In *ASP Conf. Ser. 313: Asymmetrical Planetary Nebulae III: Winds, Structure and the Thunderbird*, pages 57–+, 2004.
- F. Kemper, A. de Koter, L. B. F. M. Waters, J. Bouwman, and A. G. G. M. Tielens. Dust and the spectral energy distribution of the OH/IR star OH 127.8+0.0: Evidence for circumstellar metallic iron. *A&A*, 384:585–593, March 2002a. doi: 10.1051/0004-6361:20020036.
- F. Kemper, F. J. Molster, C. Jäger, and L. B. F. M. Waters. The mineral composition and

- spatial distribution of the dust ejecta of NGC 6302. *A&A*, 394:679–690, November 2002b. doi: 10.1051/0004-6361:20021119.
- R. C. Kennicutt, Jr. The integrated spectra of nearby galaxies - General properties and emission-line spectra. *ApJ*, 388:310–327, April 1992. doi: 10.1086/171154.
- R. C. Kennicutt, Jr., F. Bresolin, H. French, and P. Martin. An Empirical Test and Calibration of H II Region Diagnostics. *ApJ*, 537:589–612, July 2000. doi: 10.1086/309075.
- F. Kerber, R. P. Mignani, R. L. Smart, and A. Wicenec. Galactic planetary nebulae and their central stars. II. Proper motions. *A&A*, 479:155–160, February 2008. doi: 10.1051/0004-6361:20078199.
- T. D. Kinman, M. W. Feast, and B. M. Lasker. New planetary nebulae in the Galactic bulge. *AJ*, 95:804–820, March 1988. doi: 10.1086/114679.
- C. R. Kitchin. Book Review: Allen's astrophysical quantities / Arthur N. Cox (ed.) Springer-Verlag, ISBN 0-387-98746-0. *Astronomy Now (ISSN 0951-9726)*, Vol. 18, No. 4, p. 24 (2004), 18(4):040000–+, April 2004.
- J. Koeppen, A. Acker, and B. Stenholm. Spectrophotometric survey of southern planetary nebulae. II - Chemical compositions. *A&A*, 248:197–208, August 1991.
- M. Kronberger, P. Teutsch, B. Alessi, M. Steine, L. Ferrero, K. Graczewski, M. Juchert, D. Patchick, D. Riddle, J. Saloranta, M. Schoenball, and C. Watson. New galactic open cluster candidates from DSS and 2MASS imagery. *A&A*, 447:921–928, March 2006. doi: 10.1051/0004-6361:20054057.
- E. Kruegel. *The physics of interstellar dust*. IoP Series in astronomy and astrophysics (IoP: Bristol, UK), 2003.
- S. Kwok. *The Origin and Evolution of Planetary Nebulae*. The origin and evolution of planetary nebulae / Sun Kwok. Cambridge ; New York : Cambridge University Press, 2000. (Cambridge astrophysics series ; 33), June 2000.
- S. Kwok, C. R. Purton, and P. M. Fitzgerald. On the origin of planetary nebulae. *ApJL*, 219:L125–L127, February 1978a. doi: 10.1086/182621.
- S. Kwok, C. R. Purton, and P. M. Fitzgerald. On the origin of planetary nebulae. *ApJL*, 219:L125–L127, February 1978b. doi: 10.1086/182621.
- A. U. Landolt. UBVRI photometric standard stars in the magnitude range 11.5-16.0 around the celestial equator. *AJ*, 104:340–371, July 1992. doi: 10.1086/116242.
- W. B. Latter, A. Dayal, J. H. Biegging, C. Meakin, J. L. Hora, D. M. Kelly, and

- A. G. G. M. Tielens. Revealing the Photodissociation Region: HST/NICMOS Imaging of NGC 7027. *ApJ*, 539:783–797, August 2000. doi: 10.1086/309252.
- A. Lazarian. Tracing magnetic fields with aligned grains. *Journal of Quantitative Spectroscopy and Radiative Transfer*, 106:225–256, July 2007. doi: 10.1016/j.jqsrt.2007.01.038.
- T. Le Bertre, M. Matsuura, J. M. Winters, H. Murakami, I. Yamamura, M. Freund, and M. Tanaka. Galactic mass-losing AGB stars probed with the IRTS. I. *A&A*, 376:997–1010, September 2001. doi: 10.1051/0004-6361:20011033.
- T.-H. Lee, L. Stanghellini, L. Ferrario, and D. Wickramasinghe. High-Resolution Spectra of Bright Central Stars of Bipolar Planetary Nebulae and the Question of Magnetic Shaping. *AJ*, 133:987–999, March 2007a. doi: 10.1086/510743.
- T.-H. Lee, L. Stanghellini, L. Ferrario, and D. T. Wickramasinghe. High Resolution Echelle Spectroscopy of Central Stars of Bipolar Planetary Nebulae: Disclosing the Shaping Mechanisms of Asymmetric Planetary Nebulae. In R. Napiwotzki and M. R. Burleigh, editors, *15th European Workshop on White Dwarfs*, volume 372 of *Astronomical Society of the Pacific Conference Series*, pages 173–+, September 2007b.
- A. Leene and S. R. Pottasch. Observations of extended planetary nebulae. I - NGC 7293 - The Helix nebula. *A&A*, 173:145–154, February 1987.
- M. H. Liller and W. Liller. Observed Angular Motions in Planetary Nebulae. In D. E. Osterbrock and C. R. O’dell, editors, *Planetary Nebulae*, volume 34 of *IAU Symposium*, pages 38–+, 1968.
- F. Lykou, O. Chesneau, E. Lagadec, and A. Zijlstra. A disc in the heart of the Ant nebula. *ArXiv e-prints*, 710, October 2007.
- W. J. Maciel and S. R. Pottasch. Distances of planetary nebulae. *A&A*, 88:1–2, August 1980.
- A. Mampaso, K. Viironen, R. L. M. Corradi, J. E. Drew, R. Greimel, and L. Sabin. A Search for New Planetary Nebulae Located at Large Galactocentric Distances. In A. Vallenari, R. Tantalò, L. Portinari, and A. Moretti, editors, *From Stars to Galaxies: Building the Pieces to Build Up the Universe*, volume 374 of *Astronomical Society of the Pacific Conference Series*, pages 199–+, December 2007.
- A. Manchado, M. A. Guerrero, L. Stanghellini, and M. Serra-Ricart. *The IAC morphological catalog of northern Galactic planetary nebulae*. The IAC morphological

- catalog of northern Galactic planetary nebulae, Publisher: La Laguna, Spain: Instituto de Astrofísica de Canarias (IAC), 1996, Foreword by Stuart R. Pottasch, ISBN: 8492180609, 1996.
- A. Manchado, E. Villaver, L. Stanghellini, and M. A. Guerrero. The Morphological and Structural Classification of Planetary Nebulae. In J. H. Kastner, N. Soker, and S. Rappaport, editors, *ASP Conf. Ser. 199: Asymmetrical Planetary Nebulae II: From Origins to Microstructures*, pages 17–+, 2000.
- R. N. Manchester, G. B. Hobbs, A. Teoh, and M. Hobbs. The Australia Telescope National Facility Pulsar Catalogue. *AJ*, 129:1993–2006, April 2005. doi: 10.1086/428488.
- C. R. Masson. The structure of NGC 7027 and a determination of its distance by measurement of proper motions. *ApJ*, 336:294–303, January 1989. doi: 10.1086/167011.
- D. S. Mathewson and V. L. Ford. Polarization observations of 1800 stars. *MmRAS*, 74: 139–+, 1970.
- G. Mathys. The Observation of Magnetic Fields in Nondegenerate Stars. *Fundamentals of Cosmic Physics*, 13:143–308, 1989.
- M. Matsuura, A. A. Zijlstra, M. D. Gray, F. J. Molster, and L. B. F. M. Waters. The symmetric dust shell and the central star of the bipolar planetary nebula NGC6537. *MNRAS*, 363:628–640, October 2005a. doi: 10.1111/j.1365-2966.2005.09464.x.
- M. Matsuura, A. A. Zijlstra, F. J. Molster, L. B. F. M. Waters, H. Nomura, R. Sahai, and M. G. Hoare. The dark lane of the planetary nebula NGC 6302. *MNRAS*, 359: 383–400, May 2005b. doi: 10.1111/j.1365-2966.2005.08903.x.
- S. Matt, B. Balick, R. Winglee, and A. Goodson. Bipolarity Without Binarity: AGB Winds, Dipole Magnetic Fields, and Disk Formation. , 32:743–+, May 2000.
- J. Meaburn and J. A. López. Optical Evidence for Dense Neutral Globules in the Dumbbell Planetary Nebula - NGC6853 M27. *MNRAS*, 263:890–+, August 1993.
- J. Meaburn and J. R. Walsh. Complex flows in the outer regions of NGC 6302. II. *MNRAS*, 193:631–640, November 1980.
- J. Meaburn, J. A. López, W. Steffen, M. F. Graham, and A. J. Holloway. The Hubble-Type Outflows from the High-Excitation, Polypolar Planetary Nebula NGC 6302. *AJ*, 130:2303–2311, November 2005. doi: 10.1086/496978.
- J. Meaburn, J. A. López, and M. G. Richer. Optical line profiles of the Helix planetary

- nebula (NGC 7293) to large radii. *MNRAS*, 384:497–503, February 2008. doi: 10.1111/j.1365-2966.2007.12710.x.
- D. Middlemass. A model for the planetary nebula NGC 7027. *MNRAS*, 244:294–309, May 1990.
- J. D. Mill. Midcourse Space Experiment (MSX): an overview of the instruments and data collection plans. In I. Kadar and V. Libby, editors, *Proc. SPIE Vol. 2232, p. 200-216, Signal Processing, Sensor Fusion, and Target Recognition III, Ivan Kadar; Vibeke Libby; Eds.*, volume 2232 of *Presented at the Society of Photo-Optical Instrumentation Engineers (SPIE) Conference*, pages 200–216, June 1994.
- G. E. Miller and J. M. Scalo. The initial mass function and stellar birthrate in the solar neighborhood. *ApJS*, 41:513–547, November 1979. doi: 10.1086/190629.
- F. J. Molster, L. B. F. M. Waters, A. G. G. M. Tielens, and M. J. Barlow. Crystalline silicate dust around evolved stars. I. The sample stars. *A&A*, 382:184–221, January 2002. doi: 10.1051/0004-6361:20011550.
- D. G. Monet, S. E. Levine, B. Canzian, H. D. Ables, A. R. Bird, C. C. Dahn, H. H. Guetter, H. C. Harris, A. A. Henden, S. K. Leggett, H. F. Levison, C. B. Luginbuhl, J. Martini, A. K. B. Monet, J. A. Munn, J. R. Pier, A. R. Rhodes, B. Riepe, S. Sell, R. C. Stone, F. J. Vrba, R. L. Walker, G. Westerhout, R. J. Brucato, I. N. Reid, W. Schoening, M. Hartley, M. A. Read, and S. B. Tritton. The USNO-B Catalog. *AJ*, 125:984–993, February 2003. doi: 10.1086/345888.
- C. Morisset, G. Stasińska, and M. Peña. NEBU_3D: A Fast Pseudo-3D Photoionization Code for Aspherical Planetary Nebulae and HII Regions. In R. Szczerba, G. Stasińska, and S. K. Gorny, editors, *Planetary Nebulae as Astronomical Tools*, volume 804 of *American Institute of Physics Conference Series*, pages 44–47, November 2005. doi: 10.1063/1.2146223.
- T. Neckel and H. Vehrenberg. *Atlas galaktischer Nebel I. RA 0h00m-12h00m, Dekl. +90 deg. - -33 deg.* Duesseldorf: Treugesell-Verlag, 1985, 1985.
- C. R. O’Dell, B. Balick, A. R. Hajian, W. J. Henney, and A. Burkert. Knots in Nearby Planetary Nebulae. *AJ*, 123:3329–3347, June 2002. doi: 10.1086/340726.
- R. Ortiz, S. Lorenz-Martins, W. J. Maciel, and E. M. Rangel. Evolution from AGB to planetary nebula in the MSX survey. *A&A*, 431:565–574, February 2005. doi: 10.1051/0004-6361:20040401.
- D. E. Osterbrock. *Astrophysics of gaseous nebulae*. Research supported by the Re-

- search Corp., Wisconsin Alumni Research Foundation, John Simon Guggenheim Memorial Foundation, Institute for Advanced Studies, and National Science Foundation. San Francisco, W. H. Freeman and Co., 1974. 263 p., 1974.
- S. Palmerini and M. Busso. Nucleosynthesis in AGB stars. *Memorie della Societa Astronomica Italiana*, 78:499–+, 2007.
- J. M. Paredes, M. Ribó, and J. Martí. A search for microquasar candidates at low galactic latitudes. *A&A*, 394:193–203, October 2002. doi: 10.1051/0004-6361:20021086.
- Q. A. Parker, S. Phillipps, and D. H. Morgan. The AAO/UKST H-alpha Survey. In A. R. Taylor, T. L. Landecker, and G. Joncas, editors, *ASP Conf. Ser. 168: New Perspectives on the Interstellar Medium*, pages 126–+, 1999.
- Q. A. Parker, S. Phillipps, M. J. Pierce, M. Hartley, N. C. Hambly, M. A. Read, H. T. MacGillivray, S. B. Tritton, C. P. Cass, R. D. Cannon, M. Cohen, J. E. Drew, D. J. Frew, E. Hopewell, S. Mader, D. F. Malin, M. R. W. Masheder, D. H. Morgan, R. A. H. Morris, D. Russeil, K. S. Russell, and R. N. F. Walker. The AAO/UKST SuperCOSMOS H α survey. *MNRAS*, 362:689–710, September 2005. doi: 10.1111/j.1365-2966.2005.09350.x.
- Q. A. Parker, A. Acker, D. J. Frew, M. Hartley, A. E. J. Peyaud, F. Ochsenbein, S. Phillipps, D. Russeil, S. F. Beaulieu, M. Cohen, J. Köppen, B. Miszalski, D. H. Morgan, R. A. H. Morris, M. J. Pierce, and A. E. Vaughan. The Macquarie/AAO/Strasbourg H α Planetary Nebula Catalogue: MASH. *MNRAS*, 373: 79–94, November 2006a. doi: 10.1111/j.1365-2966.2006.10950.x.
- Q. A. Parker, A. Acker, D. J. Frew, and W. A. Reid. Milky Way and Magellanic Cloud Surveys for Planetary Nebulae. In M. J. Barlow and R. H. Méndez, editors, *Planetary Nebulae in our Galaxy and Beyond*, volume 234 of *IAU Symposium*, pages 1–8, 2006b. doi: 10.1017/S1743921306002675.
- M. Peimbert. Planetary nebulae. *Reports of Progress in Physics*, 53:1559–1619, 1990.
- M. Peimbert. Chemical abundances in planetary nebulae. In Y. Terzian, editor, *Planetary Nebulae*, volume 76 of *IAU Symposium*, pages 215–223, 1978.
- M. Peimbert and S. Torres-Peimbert. Type I planetary nebulae. In D. R. Flower, editor, *Planetary Nebulae*, volume 103 of *IAU Symposium*, pages 233–241, 1983.
- L. Perek and L. Kohoutek. Catalogue of galactic planetary nebulae. In *Acad. Publ. House of the Czech. Acad. Sci., 1-276 (1967)*, pages 1–276, 1967.
- M. Perinotto. Chemical abundances in planetary nebulae - Basic data and correlations

- between elements. *ApJS*, 76:687–713, June 1991. doi: 10.1086/191578.
- H. G. Perkins, D. J. King, and S. M. Scarrott. Optical Polarization in the Bipolar Nebula S106 - Evidence for a Central Illuminating Source. *MNRAS*, 196:7P–+, July 1981.
- V. M. Petrossian. New Nebulous Objects. *Astrofizika*, 22:423–+, 1985.
- J. P. Phillips. The relation between elemental abundances and morphology in planetary nebulae. *MNRAS*, 340:883–892, April 2003. doi: 10.1046/j.1365-8711.2003.06346.x.
- J. P. Phillips. Stellar evolution and the planetary nebula formation rate. In S. Torres-Peimbert, editor, *Planetary Nebulae*, volume 131 of *IAU Symposium*, pages 425–442, 1989.
- J. P. Phillips. The determination of progenitor masses for planetary nebulae. *MNRAS*, 326:1041–1048, September 2001a. doi: 10.1046/j.1365-8711.2001.04715.x.
- J. P. Phillips. Bipolar Nebulae: The Missing Population. *PASP*, 113:846–850, July 2001b.
- J. P. Phillips. The Distances of Planetary Nebulae: A Scale Based upon Nearby Sources. *ApJS*, 139:199–217, March 2002. doi: 10.1086/338028.
- J. P. Phillips. The Use of Line Excitation Mapping to Investigate Planetary Nebula Morphologies. *Revista Mexicana de Astronomia y Astrofisica*, 40:193–208, October 2004.
- M. J. Pierce, D. J. Frew, Q. A. Parker, and J. Köppen. PFP 1: A Large Planetary Nebula Caught in the First Stages of ISM Interaction. *Publications of the Astronomical Society of Australia*, 21:334–343, September 2004. doi: 10.1071/AS04039.
- S. R. Pottasch, editor. *Planetary nebulae - A study of late stages of stellar evolution*, volume 107 of *Astrophysics and Space Science Library*, 1984.
- S. R. Pottasch and D. A. Beintema. The ISO spectrum of the planetary nebula NGC 6302. II. Nebular abundances. *A&A*, 347:975–982, July 1999.
- S. R. Pottasch and A. A. Zijlstra. Shklovsky distances to galactic bulge planetary nebulae. *A&A*, 256:251–254, March 1992.
- S. R. Pottasch, R. Olling, C. Bignell, and A. A. Zijlstra. Planetary nebulae near the galactic center. I - Method of discovery and preliminary results. *A&A*, 205:248–256, October 1988.

- S. R. Pottasch, D. A. Beintema, and W. A. Feibelman. Abundance in the planetary nebulae NGC 6537 and He2-111. *A&A*, 363:767–778, November 2000.
- A. Preite-Martinez. Possible new planetary nebulae in the IRAS Point Source Catalogue. *A&AS*, 76:317–330, December 1988.
- S. D. Price, M. P. Egan, S. J. Carey, D. R. Mizuno, and T. A. Kuchar. Midcourse Space Experiment Survey of the Galactic Plane. *AJ*, 121:2819–2842, May 2001. doi: 10.1086/320404.
- C. Quireza, H. J. Rocha-Pinto, and W. J. Maciel. Bayesian posterior classification of planetary nebulae according to the Peimbert types. *ArXiv e-prints*, 709, September 2007.
- R. Ransom, B. Uyaniker, R. Kothes, and T. Landecker. Probing the Magnetized Interstellar Medium Surrounding the Planetary Nebula Sh 2-216. *ArXiv e-prints*, 806, June 2008.
- R. P. Rao. *Measurement of magnetic fields from linear polarization of dust emission*. PhD thesis, AA(UNIVERSITY OF ILLINOIS AT URBANA-CHAMPAIGN), May 1999.
- M. A. Ratag. *A study of galactic bulge planetary nebulae*. Groningen: Rijksuniversiteit, 1991, 1991.
- M. A. Ratag, S. R. Pottasch, A. A. Zijlstra, and J. Menzies. Planetary nebulae near the Galactic center. II - The second VLA measurements. *A&A*, 233:181–189, July 1990.
- T. Rauch. A grid of synthetic ionizing spectra for very hot compact stars from NLTE model atmospheres. *A&A*, 403:709–714, May 2003. doi: 10.1051/0004-6361:20030412.
- T. Rauch, E. Furlan, F. Kerber, and M. Roth. Survey of Large Planetary Nebulae in Decay. In J. H. Kastner, N. Soker, and S. Rappaport, editors, *Asymmetrical Planetary Nebulae II: From Origins to Microstructures*, volume 199 of *Astronomical Society of the Pacific Conference Series*, pages 341–+, 2000.
- T. Rauch, K. Werner, M. Ziegler, J. W. Kruk, and C. M. Oliveira. Spectral Analysis of Central Stars of Planetary Nebulae. *ArXiv e-prints*, 709, September 2007.
- C. Reimers, E. A. Dorfi, and S. Höfner. Shaping of Planetary Nebulae by Dust Driven AGB Winds. *Ap&SS*, 272:205–212, 2000.
- A. Riera, P. García-Lario, A. Manchado, O. Suárez, A. García-Hernández, and M. A.

- Guerrero. GLMP 621: a Binary Planetary Nebula. In *Revista Mexicana de Astronomía y Astrofísica Conference Series*, pages 97–99, September 2003.
- H. Riesgo and J. A. López. Revised Diagnostic Diagrams for Planetary Nebulae. *Revista Mexicana de Astronomía y Astrofísica*, 42:47–51, April 2006.
- G. J. Robinson, N. K. Reay, and P. D. Atherton. Measurements of expansion velocities in planetary nebulae. *MNRAS*, 199:649–657, May 1982.
- A. W. Rodgers, C. T. Campbell, and J. B. Whiteoak. A catalogue of H α -emission regions in the southern Milky Way. *MNRAS*, 121:103–+, 1960.
- F. Sabbadin and S. D’Odorico. Spectroscopic observations of the supernova remnant candidates 3C 400.2 and S91. *A&A*, 49:119–123, May 1976a.
- F. Sabbadin and S. D’Odorico. Spectroscopic observations of the supernova remnant candidates 3C 400.2 and S91. *A&A*, 49:119–123, May 1976b.
- F. Sabbadin, S. Minello, and A. Bianchini. Sharpless 176: a large, nearby planetary nebula. *A&A*, 60:147–149, August 1977.
- L. Sabin, A.A. Zijlstra, and J.S. Greaves. Magnetic fields in planetary nebulae and post-AGB nebulae. *MNRAS*, 376:378–386, March 2007. doi: 10.1111/j.1365-2966.2007.11445.x.
- R. Sahai, D. C. Hines, J. H. Kastner, D. A. Weintraub, J. T. Trauger, M. J. Rieke, R. I. Thompson, and G. Schneider. The Structure of the Prototype Bipolar Protoplanetary Nebula CRL 2688 (Egg Nebula): Broadband, Polarimetric, and H 2 Line Imaging with NICMOS on the Hubble Space Telescope. *ApJL*, 492:L163+, January 1998. doi: 10.1086/311108.
- R. Sahai, M. Morris, C. Sánchez Contreras, and M. Claussen. Preplanetary Nebulae: An HST Imaging Survey and a New Morphological Classification System. *ArXiv e-prints*, 707, July 2007.
- H. E. Saraph and M. J. Seaton. Electron densities in planetary nebulae. *MNRAS*, 148:367–381, 1970.
- D. J. Schlegel, D. P. Finkbeiner, and M. Davis. Maps of Dust Infrared Emission for Use in Estimation of Reddening and Cosmic Microwave Background Radiation Foregrounds. *ApJ*, 500:525–+, June 1998. doi: 10.1086/305772.
- H. M. Schmid. Identification of the emission bands at 6830, 7088 Å. *A&A*, 211:L31–L34, March 1989.
- S. E. Schneider and D. Buckley. The Distances of Planetary Nebulae and the Galactic

- Bulge. *ApJ*, 459:606–+, March 1996. doi: 10.1086/176925.
- S. E. Schneider, Y. Terzian, A. Purgathofer, and M. Perinotto. Radial velocities of planetary nebulae. *ApJS*, 52:399–423, August 1983. doi: 10.1086/190874.
- H. E. Schwarz. Symbiotics: Spectroscopy Programmes at ESO. In V. M. Blanco and M. M. Phillips, editors, *Progress and Opportunities in Southern Hemisphere Optical Astronomy. The CTIO 25th Anniversary Symposium*, volume 1 of *Astronomical Society of the Pacific Conference Series*, pages 355–+, 1988.
- S. Sharpless. A Catalogue of H II Regions. *ApJS*, 4:257–+, December 1959a.
- S. Sharpless. A Catalogue of Emission Nebulae Near the Galactic Plane. *ApJ*, 118:362–+, November 1953.
- S. Sharpless. A Catalogue of H II Regions. *ApJS*, 4:257–+, December 1959b.
- R. A. Shaw and R. J. Dufour. Software for the Analysis of Emission Line Nebulae. *PASP*, 107:896–+, September 1995.
- I. S. Shklovskii. . *Soviet Astronomy*, 33:315–+, December 1956.
- N. Siódmiak and R. Tylenda. An analysis of the observed radio emission from planetary nebulae. *A&A*, 373:1032–1042, July 2001. doi: 10.1051/0004-6361:20010664.
- J. P. Sivan. A new look at the interstellar hydrogen through a very-wide-field photographic H α survey of the whole Milky Way. *A&AS*, 16:163–172, 1974.
- J. A. Smith, D. L. Tucker, S. Kent, M. W. Richmond, M. Fukugita, T. Ichikawa, S. i. Ichikawa, A. M. Jorgensen, A. Uomoto, J. E. Gunn, M. Hamabe, M. Watanabe, A. Tolea, A. Henden, J. Annis, J. R. Pier, T. A. McKay, J. Brinkmann, B. Chen, J. Holtzman, K. Shimasaku, and D. G. York. The u'g'r'i'z' Standard-Star System. *AJ*, 123:2121–2144, April 2002. doi: 10.1086/339311.
- N. Soker. Binary Progenitor Models for Bipolar Planetary Nebulae. *ApJ*, 496:833–+, March 1998. doi: 10.1086/305407.
- N. Soker. Can We Ignore Magnetic Fields in Studies of PN Formation, Shaping and Interaction with the ISM? In R. Szczerba, G. Stasinska, and S. K. Gorny, editors, *AIP Conf. Proc. 804: Planetary Nebulae as Astronomical Tools*, pages 89–94, November 2005. doi: 10.1063/1.2146238.
- N. Soker. Why Magnetic Fields Cannot Be the Main Agent Shaping Planetary Nebulae. *PASP*, 118:260–269, February 2006. doi: 10.1086/498829.
- N. Soker and E. Subag. A Possible Hidden Population of Spherical Planetary Nebulae.

- AJ*, 130:2717–2724, December 2005. doi: 10.1086/497295.
- N. Soker, K. J. Borkowski, and C. L. Sarazin. Interaction of planetary nebulae with the interstellar medium - Theory. *AJ*, 102:1381–1392, October 1991. doi: 10.1086/115963.
- L. Stanghellini, R. L. M. Corradi, and H. E. Schwarz. The correlations between planetary nebula morphology and central star evolution. *A&A*, 279:521–528, November 1993.
- L. Stanghellini, E. Villaver, A. Manchado, and M. A. Guerrero. The Correlations between Planetary Nebula Morphology and Central Star Evolution: Analysis of the Northern Galactic Sample. *ApJ*, 576:285–293, September 2002. doi: 10.1086/341340.
- B. Strömgren. The Physical State of Interstellar Hydrogen. *ApJ*, 89:526–+, May 1939.
- R. Szczerba, N. Siódmiak, G. Stasińska, and J. Borkowski. An evolutionary catalogue of galactic post-AGB and related objects. *A&A*, 469:799–806, July 2007. doi: 10.1051/0004-6361:20067035.
- A. G. G. M. Tielens. *The Physics and Chemistry of the Interstellar Medium*. The Physics and Chemistry of the Interstellar Medium, by A. G. G. M. Tielens, pp. . ISBN 0521826349. Cambridge, UK: Cambridge University Press, 2005., September 2005.
- Y. G. Tsamis, J. R. Walsh, D. Péquignot, M. J. Barlow, I. J. Danziger, and X.-W. Liu. Integral field spectroscopy of planetary nebulae: mapping the line diagnostics and hydrogen-poor zones with VLT FLAMES. *MNRAS*, 386:22–46, May 2008. doi: 10.1111/j.1365-2966.2008.13051.x.
- R. W. Tweedy and K. B. Kwitter. An Atlas of Ancient Planetary Nebulae and Their Interaction with the Interstellar Medium. *ApJS*, 107:255–+, November 1996. doi: 10.1086/192364.
- R. Tylenda. Planetary nebulae with massive nuclei. I - Time-dependent photoionization models. *A&A*, 126:299–306, October 1983.
- G. C. van de Steene and A. A. Zijlstra. On an alternative statistical distance scale for planetary nebulae. *A&A*, 293:541–549, January 1995.
- P. A. M. van Hoof, G. C. van Steene, D. A. Beintema, P. G. Martin, S. R. Pottasch, and G. J. Ferland. Properties of the dust emission of the planetary nebula NGC 6445. In P. Cox and M. Kessler, editors, *The Universe as Seen by ISO*, volume 427 of *ESA*

- Special Publication*, pages 417–+, March 1999.
- E. Vassiliadis and P. R. Wood. Evolution of low- and intermediate-mass stars to the end of the asymptotic giant branch with mass loss. *ApJ*, 413:641–657, August 1993. doi: 10.1086/173033.
- K. Viironen, L. Sabin, E. R. Rodríguez-Flores, A. Mampaso, R. L. M. Corradi, and R. Greimel. New Planetary Nebulae found by the IPHAS Survey. In M. J. Barlow and R. H. Méndez, editors, *Planetary Nebulae in our Galaxy and Beyond*, volume 234 of *IAU Symposium*, pages 533–534, 2006. doi: 10.1017/S1743921306004108.
- E. Villaver, A. Manchado, and G. García-Segura. The Formation of Asymmetries in Multiple Shell Planetary Nebulae Due to Interaction with the ISM. In J. H. Kastner, N. Soker, and S. Rappaport, editors, *Asymmetrical Planetary Nebulae II: From Origins to Microstructures*, volume 199 of *Astronomical Society of the Pacific Conference Series*, pages 321–+, 2000.
- E. Villaver, G. García-Segura, and A. Manchado. Ram Pressure Stripping in Planetary Nebulae. *ApJL*, 585:L49–L53, March 2003. doi: 10.1086/373941.
- W. H. T. Vlemmings, H. J. van Langevelde, and P. J. Diamond. The magnetic field around late-type stars revealed by the circumstellar H₂O masers. *A&A*, 434:1029–1038, May 2005. doi: 10.1051/0004-6361:20042488.
- W. H. T. Vlemmings, P. J. Diamond, and H. Imai. A magnetically collimated jet from an evolved star. *Nature*, 440:58–60, March 2006. doi: 10.1038/nature04466.
- W. Voges, B. Aschenbach, T. Boller, H. Bräuninger, U. Briel, W. Burkert, K. Dennerl, J. Englhauser, R. Gruber, F. Haberl, G. Hartner, G. Hasinger, M. Kürster, E. Pfeffermann, W. Pietsch, P. Predehl, C. Rosso, J. H. M. M. Schmitt, J. Trümper, and H. U. Zimmermann. The ROSAT all-sky survey bright source catalogue. *A&A*, 349:389–405, September 1999.
- W. Voges, B. Aschenbach, T. Boller, H. Brauning, U. Briel, W. Burkert, K. Dennerl, J. Englhauser, R. Gruber, F. Haberl, G. Hartner, G. Hasinger, E. Pfeffermann, W. Pietsch, P. Predehl, J. Schmitt, J. Trumper, and U. Zimmermann. ROSAT all-sky survey faint source catalogue. *IAU Circ.*, 7432:1–+, May 2000.
- C. J. Wareing, T. J. O’Brien, A. A. Zijlstra, K. B. Kwitter, J. Irwin, N. Wright, R. Greimel, and J. E. Drew. The shaping of planetary nebula Sh2-188 through interaction with the interstellar medium. *MNRAS*, 366:387–396, February 2006. doi: 10.1111/j.1365-2966.2005.09875.x.

- C. J. Wareing, A. A. Zijlstra, and T. J. O'Brien. The interaction of planetary nebulae and their AGB progenitors with the interstellar medium. *ArXiv e-prints*, 709, September 2007.
- R. Weinberger. A catalogue of expansion velocities of Galactic planetary nebulae. *A&AS*, 78:301–324, May 1989.
- A. R. Witham, C. Knigge, J. E. Drew, R. Greimel, D. Steeghs, B. T. Gänsicke, P. J. Groot, and A. Mampaso. The IPHAS catalogue of H α emission-line sources in the northern Galactic plane. *MNRAS*, 384:1277–1288, March 2008. doi: 10.1111/j.1365-2966.2007.12774.x.
- C. Y. Zhang. A statistical distance scale for Galactic planetary nebulae. *ApJS*, 98: 659–678, June 1995. doi: 10.1086/192173.
- Y. Zhang, X.-W. Liu, R. Wesson, P. J. Storey, Y. Liu, and I. J. Danziger. Electron temperatures and densities of planetary nebulae determined from the nebular hydrogen recombination spectrum and temperature and density variations. *MNRAS*, 351: 935–955, July 2004. doi: 10.1111/j.1365-2966.2004.07838.x.
- A. Zijlstra, S. Pottasch, and C. Bignell. Mis-classified planetary nebulae. *A&AS*, 82: 273–277, February 1990.
- A. A. Zijlstra. Binary central stars of planetary nebulae. In R. Szczerba and J. Mikolajewska, editors, *Symbiotic stars*, 2006.
- A. A. Zijlstra. Binary Central Stars of Planetary Nebulae. *Baltic Astronomy*, 16:79–86, 2007.
- A. A. Zijlstra and S. R. Pottasch. On the scale height of planetary nebulae. *A&A*, 243: 478–482, March 1991.
- A. A. Zijlstra, S. R. Pottasch, and C. Bignell. A catalogue of VLA radio continuum observations of planetary nebulae with the Very Large Array. *A&AS*, 79:329–357, September 1989.
- A. A. Zijlstra, J. M. Chapman, P. te Lintel Hekkert, L. Likkell, F. Comeron, R. P. Norris, F. J. Molster, and R. J. Cohen. Bipolar outflows in OH/IR stars. *MNRAS*, 322:280–308, April 2001.